AL-TR-90-026 AD:

(2)

Final Report
for the period
05 Aug 1986 to
15 Dec 1989

Model Studies of CBES Decomposition (FN_3/BiF Chemical Laser)

October 1990

Authors:
D.J. Benard
B.K. Winker

Rockwell International Space Center
1049 Camino Dos Rios
Thousand Oaks CA 91360

F04611-86-C-0072
SC5467.FR

Approved for Public Release

Prepared for the: **Astronautics Laboratory (AFSC)**
Air Force Space Technology Center
Space Systems Division
Air Force Systems Command
Edwards AFB CA 93523-5000

NOTICE

When U. S. Government drawings, specifications, or other data are used for any purpose other than a definitely related Government procurement operation, the fact that the Government may have formulated, furnished, or in any way supplied the said drawings, specifications, or other data, is not to be regarded by implication or otherwise, or in any way licensing the holder or any other person or corporation, or conveying any rights or permission to manufacture, use or sell any patented invention that may be related thereto.

FOREWORD

This final report was submitted by Rockwell International Space Center, Thousand Oaks CA on completion of contract F04611-86-C-0072 with the Astronautics Laboratory (AFSC), Edwards AFB CA. AL Project Managers were Capt Steve Thompson and Lt Robert Mantz.

This report has been reviewed and is approved for release and distribution in accordance with the distribution statement on the cover and on the DD Form 1473.

ROBERT A. MANTZ, LT, USAF
Project Manager

STEPHEN L. RODGERS
Chief, Applied Research in Energy Storage Office

FOR THE DIRECTOR

ROBERT C. CORLEY
Director, Astronautical Sciences Division

REPORT DOCUMENTATION PAGE

FORM APPROVED
OMB No. 0704-0188

1a. REPORT SECURITY CLASSIFICATION UNCLASSIFIED	1b. RESTRICTIVE MARKINGS
2a. SECURITY CLASSIFICATION AUTHORITY	3. DISTRIBUTION/AVAILABILITY OF REPORT Approved for public release; distribution is unlimited
2b. CLASSIFICATION/DOWNGRADING SCHEDULE	
4. PERFORMING ORGANIZATION REPORT NUMBER(S) SC5467.FR	5. MONITORING ORGANIZATION REPORT NUMBER(S) AL-TR-90-026
6a. NAME OF PERFORMING ORGANIZATION ROCKWELL INTERNATIONAL Science Center 6b. OFFICE SYMBOL (If Applicable)	7a. NAME OF MONITORING ORGANIZATION Astronautics Laboratory (AFSC)
6c. ADDRESS (City, State, and ZIP Code) 1049 Camino Dos Rios Thousand Oaks, CA 91360	7b. ADDRESS (City, State and ZIP Code) AL/LSX Edwards AFB CA 93523-5000
8a. NAME OF FUNDING/SPONSORING ORGANIZATION Air Force Weapons Laboratory 8b. OFFICE SYMBOL (If Applicable)	9. PROCUREMENT INSTRUMENT IDENTIFICATION NUMBER F04611-86-C-0072
8c. ADDRESS (City, State and ZIP Code) Kirtland AFB New Mexico 87117	10. SOURCE OF FUNDING NOS. PROGRAM ELEMENT NO.: 62302F PROJECT NO.: 5730 TASK NO.: 00WM WORK UNIT ACCESSION NO.: 342420

11. TITLE (Include Security Classification)
MODEL STUDIES OF CBES DECOMPOSITION (FN_3/BiF CHEMICAL LASER)

12. PERSONAL AUTHOR(S)
Benard, D.J. and Winker, B.K.

13a. TYPE OF REPORT	13b. TIME COVERED	14. DATE OF REPORT (Year, Month, Day)	15. PAGE COUNT
Final Report	FROM 86/08/05 TO 89/12/15	9010	106

16. SUPPLEMENTARY NOTATION

17. COSATI CODES			18. SUBJECT TERMS (Continue on reverse if necessary and identify by block number)
FIELD	GROUP	SUB-GROUP	
7	04		Fluorine azide, nitrogen fluoride, bismuth fluoride, trimethylbismuthine, sulphur hexafluoride, HF/DF/CO_2 pulsed laser initiation, thermal dissociation, electronic excitation, metastable states, quenching and self-annihilation, transfer and pooling, stimulated emission, optical gain, kinetic modelling, high energy lasers.
21	09		

19. ABSTRACT (Continue on reverse if necessary and identify by block number)
Mixtures of FN_3, $Bi(CH_3)_3$ and a sensitizing agent were subjected to pulsed infrared laser excitation to thermally dissociate the reagents into NF(a) and Bi-atoms, which in turn produced BiF(A) upon subsequent reaction. The mechanism, rate, yield and scalability of NF(a) and BiF(A) generation were investigated. Liberation of NF(a) from FN_3 was shown to occur by dissociation over a 0.5 eV barrier with a high branching ratio. The primary loss of NF(a) was due to self-annihilation at a rate of 3×10^{-12} cm^3/s. Production of BiF(A) was subject to a kinetic bottleneck caused by slow dissociation of the $Bi(CH_3)_3$, however, subsequent pumping of BiF(A) by NF(a) occurred at a rate of 4×10^{-11} cm^3/s thereafter. The peak yields of NF(a) and BiF(A) were $3 \times 10^{16}/cm^3$ and $1 \times 10^{13}/cm^3$, respectively, and measurements of optical transmission through the reacting medium revealed that BiF(X) concentrations were low enough to support lasing at visible wavelength.

20. DISTRIBUTION/AVAILABILITY OF ABSTRACT	21. ABSTRACT SECURITY CLASSIFICATION
UNCLASSIFIED/UNLIMITED ☐ SAME AS RPT. ☒ DTIC USERS ☐	UNCLASSIFIED

22a. NAME OF RESPONSIBLE INDIVIDUAL	22b. TELEPHONE NUMBER (Include Area Code)	22c. OFFICE SYMBOL
2Lt Robert A. Mantz	805-275-5945	LSXC

DD FORM 1473, JUN 86 Previous editions are obsolete.

TABLE OF CONTENTS

	Page
INTRODUCTION	1
PRODUCTION OF BiF(A)	3
Generation of FN_3	4
Release of NF(a)	4
Reaction with $Bi(CH_3)_3$	9
Synthesis of BiH_3	14
Intracavity Spectroscopy	15
MEASUREMENT OF BiF(X)	23
Intracavity Scattering	23
Cavity Ringdown Method	25
Calibration of Sensitivity	28
Extent of Inversion	34
Scaling Predictions	38
CONCLUSIONS AND RECOMMENDATIONS	43
REFERENCES	45
APPENDIX	49

LIST OF FIGURES

Figure		Page
1	Block diagram of experimental apparatus used to study excitation of NF(a) and BiF(A) by thermal dissociation of FN_3	3
2	Schematic diagram of on-line FN_3 generator.	5
3	Computed time profiles of the temperature rise (above 300 K) and concentrations of FN_3 and NF(a). The dashed line represents an approximation to the time profile of the CO_2 laser.	7
4	Energy levels and kinetic processes relevant to the reaction of $Bi(CH_3)_3$ with NF(a).	10
5	Construction of reactor used to pulse heat mixtures of FN_3, $Bi(CH_3)_3$ and SF_6 by a CO_2 laser.	11
6	Comparison of BiF(A-X, $v' = 0$ to $v'' = 0$) spectra (a) without an optical cavity, (b) with an optical cavity formed by 95% reflecting mirrors, and (c) with an optical cavity formed by 99.9% reflecting mirrors and use of a KrF laser to aid the dissociation of $Bi(CH_3)_3$.	16
7	Comparison of $Bi(^2D)$ time profiles with (bottom) and without (top) use of a KrF laser to assist the dissociation of $Bi(CH_3)_3$.	18
8	Computed time profiles of cavity output based on the measured BiF(A) time profile and assuming either zero gain or loss or a peak gain of 0.05%/cm in the limits of fast recycling or bottlenecked removal of BiF(X)	21
9	Fractional enhancement of cavity output due to intracavity gain as a function of peak gain.	21
10	Schematic diagram of reactor modification used to eliminate intracavity scattering	24
11	Schematic diagram of cavity ringdown experiment	27
12	Timing diagram of cavity ringdown experiment	27
13	Spectrum of dye laser as measured by the OMA	28
14	Determination of empty cavity decay time	32
15	Determination of linewidth of dye laser	32

LIST OF FIGURES

Figure		Page
16	Plot of response function $\Delta S/S$ assuming ($\Delta\nu$ = 1.13 GHz) vs intracavity single pass absorption	33
17	Expanded section of OMA data showing the absorption of one etalon mode by BiF	35
18	Determination of temperature from emission data	36
19	Calculated gain vs temperature at [NF(a)] ~ $6 \times 10^{15}/cm^3$	40
20	Calculated gain vs [NF(a)] at a temperature of 1200 K	42

LIST OF TABLES

Table		Page
1	Comparison of Model to Data for CO_2 Laser Dissociation of FN_3	8
2	Calculated Gain/Loss Coefficients for Selected BiF(A-X) Transitions	38

INTRODUCTION

This contract investigated the use of fluorine azide (FN_3) as both an advanced high energy density propellant and as a fuel for an advanced high energy visible wavelength chemical laser. The work on the propellant application (which included development of a safe lab-scale generator of FN_3) performed for the Air Force Astronautics Laboratory has been covered in a parallel final report.[1] This report addresses the work on the laser application which also utilized the FN_3 generator and was performed for the Air Force Weapons Laboratory and the Strategic Defense Initiative Office under the administration of the Air Force Astronautics Laboratory. The proposed laser operates by producing the electronically excited NF(a) metastable species upon thermal dissociation of FN_3 and utilizing subsequent energy transfer reactions to pump the BiF(A-X) laser transitions near 450 nm. The work was done in four major blocks which include:

1. Production of FN_3,
2. Conversion of FN_3 to NF(a),
3. Excitation of BiF(A) by NF(a),
4. Measurement of BiF(X),

The methods used and results obtained from the first three blocks of effort are fully detailed and analyzed in prior publications that are reproduced in the appendix section of this report.[1-3] This work, which is summarized the next section of this report, addresses the physical and chemical processes involved in the pumping of the laser transition. The following section describes in detail our investigation of the state of inversion and the potential for generation of adequate gain to sustain laser action.

In the course of performing this work knowledge was gained concerning the mechanism of reaction and a number of key kinetic rate constants. Also efficient production of electronically excited species was demonstrated at densities large enough to power a high energy laser system. Finally, the BiF(X) ground state concentration was found to be consistent with a model based on population by radiative cascade from BiF(A) and removal by NF(a) at a near gas kinetic rate. These results support the development of an NF/BiF chemical laser that is operable at visible wavelengths.

PRODUCTION OF BiF(A)

Figure 1 shows in block form the method used to carry out the experiments. The FN_3 (diluted in He) was mixed with a sensitizer (HF, DF or SF_6) and $Bi(CH_3)_3$ at the inlet to a reactor where it was pulse heated by an infrared laser. Optical diagnostics that were both spatially and temporally resolved, as well as absolutely calibrated, were used to detect NF(a) and BiF(A) in emission and FN_3, $Bi(^2D)$ and $Bi(CH_3)_x$ species in absorption. Stimulated emission was also monitored in the output of an optically resonant cavity that surrounded the reactor. Both an external dye laser and the BiF(A-X) chemiluminescence were used to stimulate the potential gain medium. The following paragraphs describe the methods used to generate the FN_3, convert it to NF(a) and to pump the BiF(A) state. Attempts to develop an alternative Bi-donor (BiH_3) and to monitor self-amplification are also described in this section. The more definitive dye laser gain measurements are described in the following section of this report.

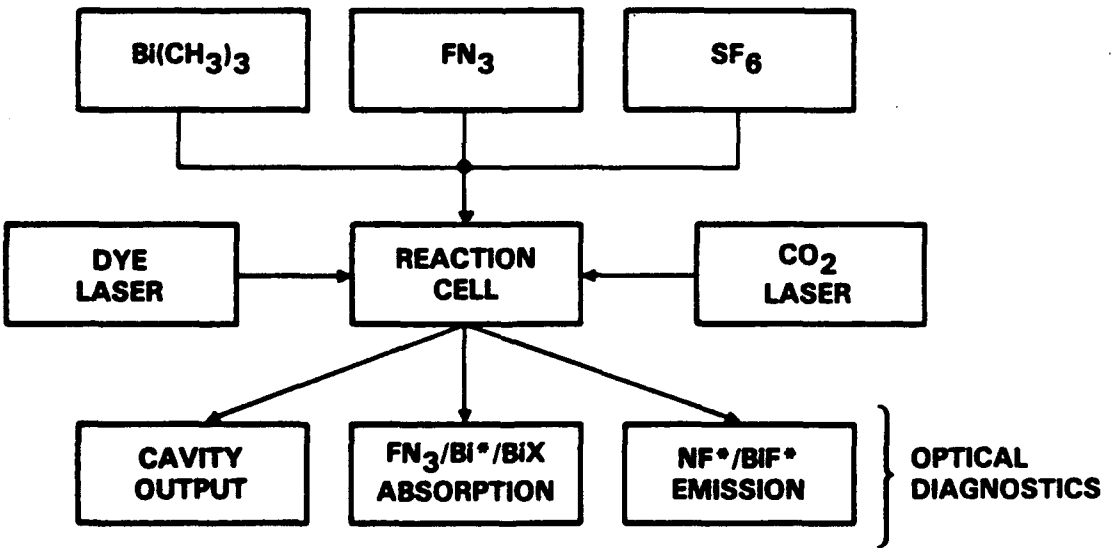

Fig. 1 Block diagram of experimental apparatus used to study excitation of NF(a) and BiF(A) by thermal dissociation of FN_3.

Generation of FN_3

Haller[4] first synthesized FN_3 in 1942 by reacting HN_3 with F_2. Fluorine azide is a highly volatile gas which condenses to an easily detonatable liquid at cryogenic temperature. As shown in Fig. 2, we produced and used FN_3 in the gas phase by use of Haller's method in which the HN_3 was obtained from a melt of NaN_3 and excess stearic acid at temperatures near 100°C. The HN_3 that was generated was entrained by a He diluent stream that carried it to a second reactor where it was titrated with a similarly diluted flow of F_2. The byproduct HF was subsequently eliminated from the gas stream by passage through a cold trap at -90°C. For safety reasons the cold trap was located inside a barricade and gas cooled by evaporated liquid nitrogen. Optical diagnostics were employed in the FN_3 generator to monitor the production of HN_3 (uv absorption), its titration with dilute F_2 (ir absorption) and the concentration of the final product (visible absorption). Under nominal conditions we produced 3 - 5 hours of FN_3 flow at 3 - 5% concentration in a 3 sccs flow of He at 350 torr pressure. Mass spectroscopy revealed the primary impurities to be CO_2 and N_2F_2, both of which were less than 5% of the FN_3 flow. We found it necessary to use a large (20/1) excess of stearic acid to NaN_3 and to carefully control the rate of mixing, temperature and stoichiometry of the titration to achieve good results. The FN_3/He gas stream was transported to the site of the experiment in stainless steel and teflon tubing without significant decomposition. Further details regarding the on-line synthesis of FN_3 have been published by the Air Force Astronautics Laboratory.[1]

Release of NF(a)

Experiments were performed using both HF/DF and CO_2 pulsed lasers to add energy to the gas mixtures in the reaction cell. In these experiments we attempted to learn the mechanism of reaction, the key kinetic rates and the reactions which limit scaling to high density, with the goal of demonstrating efficient production of $10^{16}/cm^3$ concentrations of NF(a) that would be suitable for use in a high energy laser system.

HF/DF Laser Experiments - The initial experiments were performed using either HF or DF as the sensitizer (in place of SF_6 in Fig. 1) and the corresponding HF or DF laser (in place of the CO_2 laser). By observing the decay of the HF($\Delta v = 3$) emission as a function of added FN_3, we concluded that vibrationally excited HF is quenched by FN_3 at an approximate rate of 2×10^{-12} cm^3/s. The corresponding decay of the FN_3 concentration

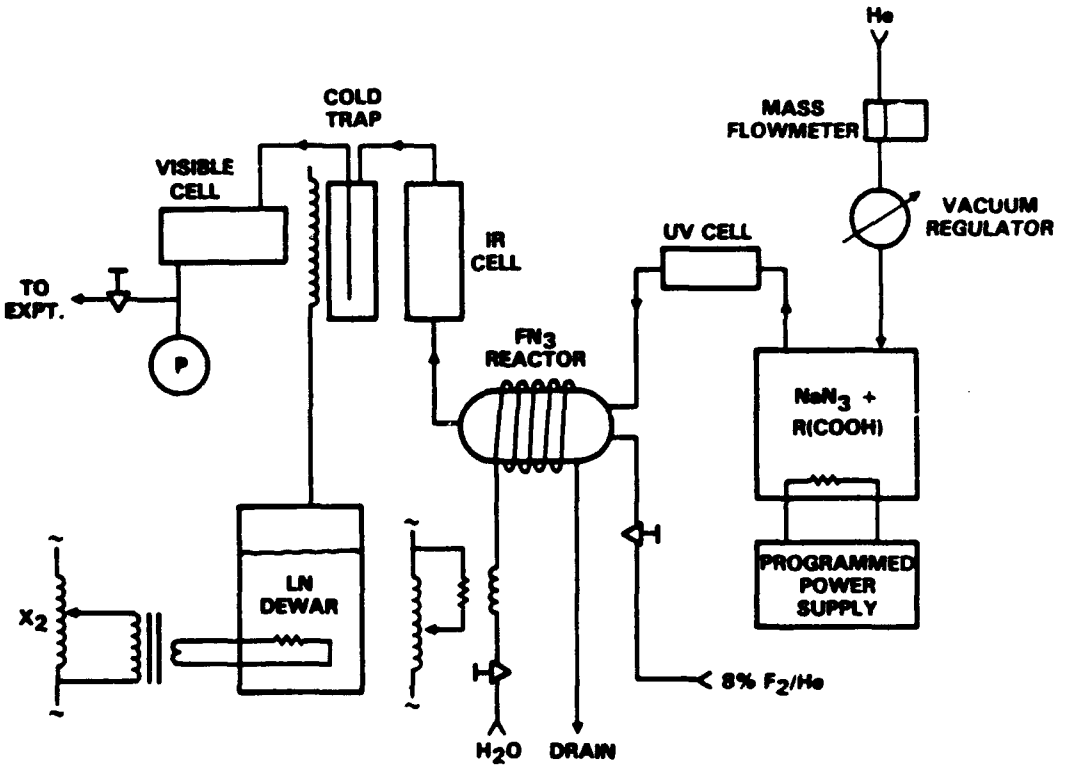

Fig. 2 Schematic diagram of on-line FN_3 generator.

was found to occur in two sequential stages. There was no measurable production of NF(a) associated with the first stage of FN_3 decay, which coincided with the decay of the vibrationally excited HF/DF molecules. Production of NF(a) did occur, however, in the second stage of decay, which was thought to be thermally induced. To test this hypothesis, SF_6 was added as a thermal diluent, which was found to delay and diminish the production of NF(a) without significantly increasing its decay rate. We therefore concluded that thermal, rather than vibrational, excitation of FN_3 was the most effective route to NF(a) production. This result also implied that use of a CO_2 laser and SF_6 as the sensitizer would be the preferred method to carry out future experiments.

CO_2 Experiments - Optimum production of NF(a) occurred in a gas mixture of 1.5 torr FN_3, 13.5 torr SF_6 and balance He to a total pressure of 150 torr. The incident CO_2 laser intensity (approximately 1 Joule/cm^2 in a 2 - 3 μs pulse) was too low to yield significant production of F-atoms by multiphoton dissociation of the SF_6 at this pressure, hence the major effect of the laser pumping was to heat the bath gas.[5]. The FN_3 was observed to dissociate promptly and the rise of the NF(a) was in temporal coincidence with the decay of the FN_3. The peak NF(a) concentration that was routinely achieved was 3×10^{16}/cm^3. We also observed that the NF(a) decayed at a rate which increased in pro-

portion to the peak NF(a) concentration. Analysis of this phenomena suggested that the NF(a) decay was dominated by self-annihilation at a rate of approximately 3×10^{-12} cm^3/s, in good agreement with the low density flowtube experiments performed by Setser.[6] The temperature at the peak of the NF(a) time profile was determined by using a temporally gated optical multichannel analyzer (OMA) to collect a spectrum of BiF(A-X) emission that was obtained upon trace addition of $Bi(CH_3)_3$ to the reaction cell.[7] The spectra were normalized for instrument response and compared to a temperature-dependent series of theoretically calculated BiF(A-X) spectra provided by Koffend,[8] With knowledge of the temperature, a barrier height of 0.5 eV for dissociation of FN_3 was estimated from a comparison of the high temperature FN_3 decay rate with the observed rate of decay at ambient temperature. This result was in good agreement with theoretical calculations by Michels[9] which reproduced the measured vibrational frequencies of the FN_3 molecule. Further details of the laser pumping experiments have been published in the Journal of Physical Chemistry.[2]

Kinetic Model - To test our understanding of the dissociation process, we assembled a kinetic model and compared it to the data. The model assumed 100% efficient production of NF(a) upon dissociation of FN_3 and loss of NF(a) solely due to self-annihilation, with no loss of species or thermal energy due to transport, mixing or diffusion. Temperature, however, was treated as a dynamic variable and the rate coefficients were explicitly temperature dependent, taking into account both the $T^{1/2}$ dependence of the cross sections and an Arrhenius term for the barrier in the dissociation channel of FN_3. The self-annihilation reaction was assumed to have no barrier and proceed to $N_2 + 2F$. Thermodynamic parameters were obtained from the JANAF tables[10] and prior work on ultraviolet photolysis[11] of FN_3. The model was defined by the coupled rate equations

$$\frac{d}{dt}[FN_3] = -k_d e^{-T_o/T}[M][FN_3] \quad (1)$$

$$\frac{d}{dt}[NF(a)] = -\frac{d}{dt}[FN_3] - k_q[NF(a)]^2 \quad (2)$$

$$\frac{d}{dt}T = \frac{1}{C}\{\sigma[SF_6]\, I(t) - H_d \frac{d}{dt}[FN_3] + H_q k_q [NF(a)]^2\} \quad (3)$$

where k_d and k_q are the dissociation and self-annihilation (quenching) rate constants, T_o is the barrier height in units of temperature, [M] is the concentration of collision partners, C is the heat capacity of the gas mixture, σ the absorption cross section of the CO_2 laser into SF_6, I(t) is the intensity time profile of the laser radiation and H_d and H_q are the heat releases in the dissociation and self-annihilation reactions, respectively. Both k_d and k_a increase as $T^{1/2}$ with respect to a reference state at 300 K. The model equations were integrated using a desktop computer to yield the results shown in Fig. 3 which correspond to the initial conditions that optimized the peak concentration of NF(a).

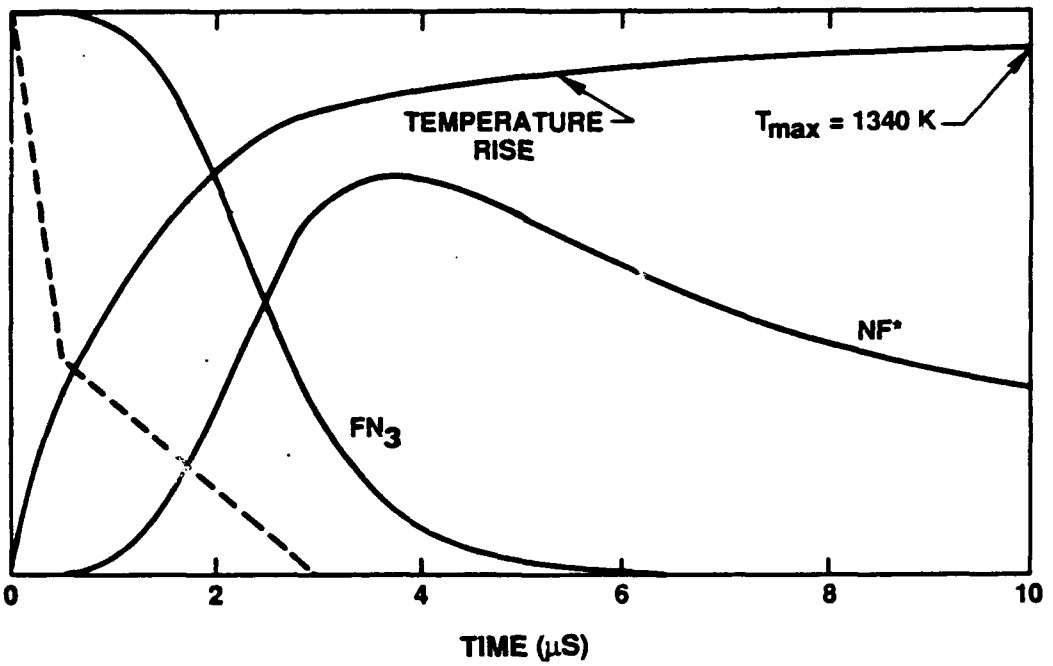

Fig. 3 Computed time profiles of the temperature rise (above 300 K) and concentrations of FN_3 and NF(a). The dashed line represents an approximation tc the time profile of the CO_2 laser.

Excellent agreement was obtained between the model and the data as shown in Table 1. The only parameters that were varied in the model equations were the cross section σ, the barrier height T_o and the rate coefficients k_d and k_a. The value of σ was set on the basis of the amount of CO_2 laser radiation that was actually absorbed into the reactor,

as measured (incident vs transmitted) on a joulemeter. Initial values of k_d and T_o were selected on the basis of Setser's and Michels work, respectively, and k_d was estimated by kinetic theory. The best fit to the data was achieved with only modest (± 25 %) variation of the rate parameters and ± 10 % variation of the barrier height. Therefore, we concluded that the model reproduces the essential features of the dissociation process accurately. The best fit parameters were $k_q = 2.5 \times 10^{-12}$ cm^3/s for the self-annihilation of NF(a) and $k_d = 1.0 \times 10^{-11}$ cm^3/s for the dissociation reaction with $T_o = 5500$ K for the barrier height.

Table 1

Comparison of Model to Data for CO_2 Laser Dissociation of FN_3

	Model	Data	Units
Peak NF(a)	4×10^{16}	3×10^{16}	cm^{-3}
Rise Time	2.6	2.4	μs
Decay Time	5.7	5.0	μs
Peak Temperature	1237	1150	°K

Based on the above results, it follows that high concentrations of NF(a) can only be generated efficiently if the temperature is increased rapidly, so that dissociation of FN_3 is complete before the NF(a) decays significantly. In a high energy laser, the dissociation reaction would be induced by mixing between a preheated gas stream and a stream at ambient temperature that carried the FN_3. Since mixing will require at least 10 μs to complete, we suggest that a peak NF(a) yield of $3 \times 10^{15}/cm^3$ is most appropriate for the laser application since the NF(a) lifetime will be on the order of 100 μs (which is long compared to the mixing time) but the power in the flow will still exceed 100 watts/cm^2, assuming heavy dilution in He at a stagnation temperature of 1200 K. Since we were able to achieve ten times this concentration in our premixed laboratory reactor, we concluded that there was little value in attempting to scale to higher NF(a) concentrations.

Recent work by Michels,[11] which has evaluated the heat of formation of FN_3, has suggested that the exothermicity of the dissociation reaction is much less than originally estimated. Since reactive heating does not significantly change the gas temperature in the above experiments, there is little potential for resultant error in the model calculations

done to date. If, however, the model were to be used for more concentrated gas mixtures, it would be necessary to correct the thermodynamics accordingly to obtain accurate results. Fortunately, the dilution ratios used in our present experiments approximate those of practical high energy laser systems with large heat release. A more subtle effect, potentially involving the NF(a) self-annihilation reaction, however, is also related to the heat of formation of FN_3. Michels calculation shows that the singlet (ground state) surface of FN_3, which correlates to NF(a) + N_2 is crossed by a triplet (excited state surface) that dissociates to NF(X) + N_2 on the product side of the barrier. While the barrier height on the FN_3 side remains near 0.5 eV, the change in the position of the FN_3 ground state relative to the separated NF + N_2 states, due to its reduced heat of formation, lowers the barrier height to about 1500 cm^{-1} on the product side. Consequently, the singlet-triplet crossing is thermally accessible in collisions between NF(a) and N_2 at high temperature, which may lead to quenching that is not evident at lower temperatures, as suggested by Setser.[13] This possibility is not supported by Setser's flowtube data,[6] however, since he measured essentially the same self-annihilation rate (at 300 K) that we obtained at 1200 K. Nonetheless, our experiments cannot distinguish between quenching of NF(a) by NF(a), NF(X) or N_2 since all three collision partners scale in proportion to the initial FN_3 concentration. The difference would be significant, however, in a supersonic laser (where the temperatures are reduced) if the majority of the quenching were due to N_2 and had a strong temperature dependence.

Reaction with $Bi(CH_3)_3$

Herbelin[7] first discovered that intense BiF(A-X) emission results when $Bi(CH_3)_3$ is added to a medium that contains NF(a). Figure 4 shows the energy levels and kinetic processes that are involved in this phenomena. The process is initiated by the dissociation of $Bi(CH_3)_3$ to yield Bi-atoms, which may in-turn form ground state BiF(X) molecules by subsequent reaction with FN_3 and NF(a). Higher fluorides such as BiF_2 and BiF_3 may also be formed but do not apparently participate in the production of BiF(A). The byproducts of the dissociation reactions are also likely quenchers of NF(a) and other electronically excited states.[14] Excitation of BiF(X) to the radiating BiF(A) state requires the energy of at least two interactions with NF(a).[15] While the details of the mechanism are not clear, it has been suggested[16] that the intermediate state between BiF(X) and BiF(A) is in fact $Bi(^2D)$. Therefore, the interactions of Bi species with NF(a) may involve chemical reaction as well

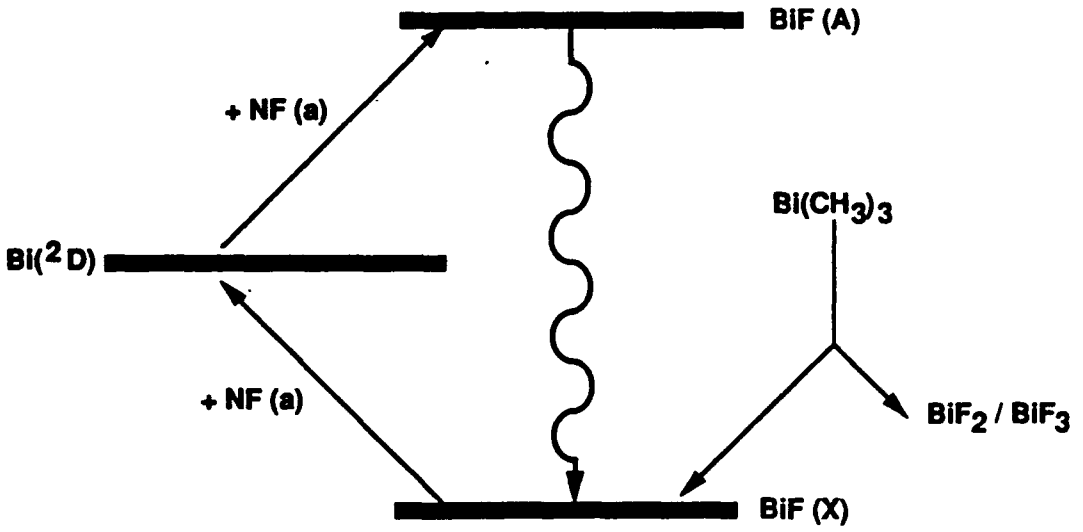

Fig. 4 Energy levels and kinetic processes relevant to the reaction of $Bi(CH_3)_3$ with NF(a).

as energy transfer. The rate coefficient for BiF(A) excitation by NF(a) is critical in relation to the radiative decay rate of the BiF(A) state, since this factor in combination with the NF(a) concentration determines the relative concentrations of the upper and lower levels of the laser transition. The radiative decay rate of the BiF(A) state[17] has been measured by Koffend, et al. to be 7×10^5/s.

In these experiments, optimum NF(a) was generated as described previously, but variable amounts of $Bi(CH_3)_3$ were added to the gas mixture in the reactor. The $Bi(CH_3)_3$ was stored as a liquid in a stainless steel cylinder that was immersed in a cold trap (0 to -60°C). A measured flow of He was bubbled through the liquid at a pressure that was set by a gas regulator, and at a flow rate that was set by a needle valve. The fraction of $Bi(CH_3)_3$ in the flow was calculated from the vapor pressure of $Bi(CH_3)_3$ at the temperature of the trap assuming complete saturation of the He flow. This method results in an overestimation of the mole fraction of $Bi(CH_3)_3$ that is entrained by the He carrier gas, however, prior experience has shown that the correction factor is typically less than a factor of two. The

$Bi(CH_3)_3$/He flow from the saturator was mixed with the FN_3/He flow at the inlet to the reactor as shown in Fig. 5. Therefore, the FN_3 and $Bi(CH_3)_3$ were in contact for approximately 0.5 seconds before excitation by the CO_2 laser. As will be described in the following section of this report, subsequent investigation showed that most (ca. 95 %) of the $Bi(CH_3)_3$ was prereacted with the FN_3 during this time. Since the FN_3 was typically present in an order of magnitude greater concentration than the initial supply of $Bi(CH_3)_3$, there was negligible effect on the FN_3 concentration due to the prereaction. Consequently some of our published conclusions[3] relevant to the yield of active Bi/BiF obtained from $Bi(CH_3)_3$ have been modified accordingly. The data and conclusions relevant to production of BiF(A) are summarized below and where prereaction is a significant factor the specific effects are identified and discussed in detail.

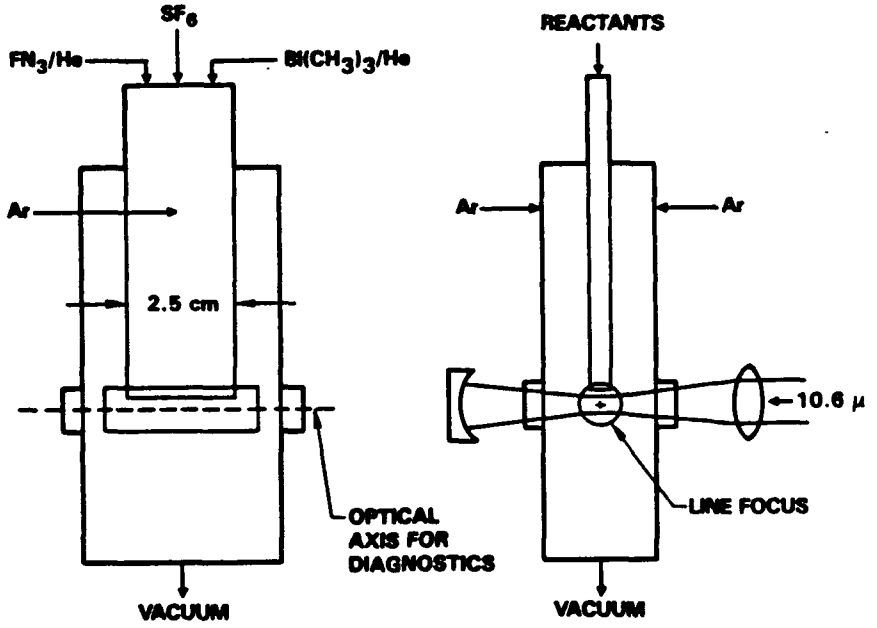

Fig. 5 Construction of reactor used to pulse heat mixtures of FN_3, $Bi(CH_3)_3$ and SF_6 by a CO_2 laser.

Bi(^{2}D) Time Profile - A pulsed hollow cathode lamp was used to follow the Bi(^{2}D) concentration by absorption of atomic resonance radiation.[18] Simultaneously the concentration of the BiF(A) state was followed in emission by a suitably filtered silicon photodiode. The Bi(^{2}D) was found to precede and track the BiF(A) time profile by approximately the radiative lifetime of the BiF(A) state. Our data therefore supports the notion that Bi(^{2}D) is the intermediate state in the production of BiF(A). By comparing the peak concentrations of Bi(^{2}D), BiF(A) and NF(a), the rate of the NF(a) + Bi(^{2}D) pumping reaction was shown to be approximately 4.7×10^{-11} cm^3/s in good agreement with an independent determination of the same rate coefficient by Herbelin.[19] The sum of the peak concentrations of Bi(^{2}D) and BiF(A), however, was only approximately 1% of the $Bi(CH_3)_3$ that was admitted to the reactor. Since 95% of the $Bi(CH_3)_3$ was prereacted we must account for the production of only one active Bi*/BiF* molecule for every five $Bi(CH_3)_3$ molecules that were not prereacted. This inefficiency may derive from significant concentrations of ground state Bi-atoms or BiF(X), from incomplete dissociation of the $Bi(CH_3)_3$ or from a low yield of active Bi/BiF due to production of BiF_2/BiF_3.

$Bi(CH_3)_3$ Time Profile - Monitoring of $Bi(CH_3)_x$ species for $x = 1,2,3$ was accomplished by ultraviolet absorption[20] using a D_2 lamp as the source of probing radiation. Since the intermediates (x = 1,2) absorbed more strongly than the $Bi(CH_3)_3$, the net absorption first increased and then decreased to zero. After modelling this phenomena, the time profile of Bi-atoms was computed and it was shown that dissociation requires approximately 10 μs to complete. Moreover the dissociation rate was unaffected by the presence or lack of FN_3. Therefore, we can conclude that the mechanism of dissociation was essentially thermal[20] under the conditions of our experiment. Since the BiF(A) signal peaked at about 2 μs, only 20% of the $Bi(CH_3)_3$ was dissociated in time to contribute to the peak generation of Bi(^{2}D) or BiF(A). Consequently, we can account for all the Bi-species without invoking significant concentrations of ground state Bi-atoms, BiF(X) or BiF_2/BiF_3.

Recycling BiF(X) - In order to allow all the $Bi(CH_3)_3$ that was not prereacted to contribute to BiF(A) formation, experiments were performed using reduced concentrations of FN_3 and only trace addition of $Bi(CH_3)_3$. Using this strategy, the self-annihilation of the NF(a) was slowed sufficiently that the $Bi(CH_3)_3$ could dissociate completely before the NF(a) decayed significantly. The resultant BiF(A) time profile showed a characteristic 10 μs rise that is consistent with the previously measured time scale for complete dissociation of the $Bi(CH_3)_3$. Under these conditions the integrated BiF(A) time profile corresponded to 0.7

photons emitted per $Bi(CH_3)_3$ molecule admitted to the reactor or roughly 14 photons per $Bi(CH_3)_3$ molecule that was not prereacted. This result demonstrates effective recycling of BiF(X) analogous to the recycling of I-atoms that occurs in the COIL laser system. The intensity of the BiF(A-X) emission was consistent with a limiting rate in the cycle (4×10^{-11} cm^3/s) that approximated the rate of the $Bi(^2D)$ + NF(a) reaction. Since these experiments were conducted at low NF(a) concentration, the majority of the dissociated $Bi(CH_3)_3$ is not in the $Bi(^2D)$ or BiF(A) states but rather in the ground states. Hence this measurement addresses the effective rate of pumping of BiF by NF(a) from the ground state to BiF(A) via the $Bi(^2D)$ intermediate energy level, whereas the previous measurement determined only the rate of the second step in the excitation process. We therefore conclude that the ground state of BiF(X) is removed by NF(a) at a rate that is no less than 5×10^{-11} cm^3/s. This result implies the possibility of an absolute population inversion of the BiF(A-X) transition for NF(a) concentrations greater than $10^{16}/cm^3$.

Scaling of BiF(A) - The experimental parameters were varied to establish optimal production of BiF(A-X) emission. The yield of BiF(A) increased with CO_2 laser energy and then saturated as expected, and increased with FN_3 or NF(a) concentration without any sign of saturation. From this result we can set an upper limit on the rate of any destructive interaction between BiF(A) and NF(a) by equating the quenching process to the radiative decay which yields $k < (7 \times 10^5/s)/(3 \times 10^{16}/cm^3)$ or approximately 2×10^{-11} cm^3/s. At low FN_3 concentration, the yield of BiF(A) initially increased with FN_3 concentration at a faster than linear rate which reflects effective quenching of $Bi(^2D)$ in competition with the $Bi(^2D)$ + NF(a) reaction that generates the BiF(A) state. As the FN_3 concentration was increased, however, the concentration of the BiF(A) state began to scale linearly with FN_3 addition, indicating that the rate of the $Bi(^2D)$ + NF(a) reaction was now competitive with any quenching of the $Bi(^2D)$ state. Upon varying the $Bi(CH_3)_3$ addition, peak BiF(A) occurred when the added concentration of $Bi(CH_3)_3$ admitted to the reactor reached $3 \times 10^{15}/cm^3$. Taking prereaction into account suggests that the actual optimal $Bi(CH_3)_3$ concentration was $1.5 \times 10^{14}/cm^3$. The peak yield of BiF(A) was measured as $1.0 \times 10^{13}/cm^3$ by absolute photometry. This result is consistent with a quadratic scaling relationship between the yield of BiF(A) and the concentration of NF(a) for (optimized $Bi(CH_3)_3$ addition) that was established at much lower NF(a) concentrations by Herbelin and coworkers, using an alternative source[22] of NF(a) to dissociation of FN_3. Under the

conditions which yielded the highest BiF(A) concentration, the peak (> 90%) yield of BiF(A) only lasted approximately 1 μs. The following section of this report will show, however, that the measured peak concentration of BiF(A) is large enough to yield gains on the order of 10^{-3}/cm if the BiF(X) ground state is evacuated.

Synthesis of BiH_3

Since addition of $Bi(CH_3)_3$ is limited by quenching and is an inefficient source of Bi-atoms due to the slow dissociation rate, we considered using BiH_3 as a potentially superior alternative donor, since it is much less stable[23] than $Bi(CH_3)_3$, has high vapor pressure[24] and the potential byproducts (HF) would be much less efficient as quenchers of electronically excited states.[25] Production of BiH_3 was attempted by reactions of $BiCl_3$ with $LiAlH_3$ in ether at -60°C and with $NaBH_4$ in aqueous solutions at ambient temperature.[24,26] We also studied production of BiH_3 by reaction of microwave discharged H_2 with a Bi metal film in a fast flow low pressure reactor and in pulsed discharges in H_2 between Bi electrodes at a variety of pressures and discharge energies.[27] The BiH_3 was separated from the H_2 byproducts by passage through a liquid nitrogen cold trap that was teflon coated and salinized by treatment with $Si(CH_3)_2Cl_2$ prior to use to prevent catalytic decomposition.[28] The BiH_3 product was measured by entrainment in a flow of H_2 that was burned in air, with detection of the resultant formation of Bi-atoms by atomic absorption, using a hollow cathode lamp as the source of resonance radiation.[18] Although considerable effort was invested, the results were fairly uniform and discouraging. While $10^{12-13}/cm^3$ yields of BiH_3 could be routinely produced by a number of methods the branching ratio between BiH_3 and H_2 byproducts was typically less than 10^{-5}. Therefore, it was impossible to collect an adequate charge of BiH_3 in a reasonable time to support optimal concentrations of the hydride to our FN_3 experiment, while allowing adequate time for measurements to be taken. We did, however, succeed in adding trace concentrations of BiH_3 to our reactor, which yielded BiF(A-X) emission that was identical to the chemiluminescence obtained from $Bi(CH_3)_3$. Consequently, we decided to continue the investigation using $Bi(CH_3)_3$ as the Bi-donor of choice and turn our attention to the issue of detecting the BiF(X) ground state to assess the feasibility of a population inversion.

Intracavity Spectroscopy

Preliminary experiments to asses the state of inversion of the BiF(A-X) transitions were conducted by using the BiF(A-X) chemiluminescence that was spontaneously emitted from the reactor as the source of probing radiation. The chemiluminescence was refocused into the reactor by a pair of dielectric mirrors and the radiation that leaked through the mirrors was analyzed spectroscopically. This approach facilitates easy spectroscopic alignment but yields data of lower signal-to-noise ratio that is obtained by use of an intense external source of probing radiation. Figure 6 compares three spectra of the $v' = 0$ to $v'' = 0$ band of the BiF(A-X) system that were collected under conditions which optimized the yield of BiF(A). The first spectrum (a) is a reference spectrum taken without an optical cavity about the reactor. Spectra (b) and (c) correspond to cavity outputs with mirrors of 95 and 99.9% reflectivity, respectively. The monochromator was placed sufficiently far away from the cavity and was apertured so that only on-axis radiation was detected. A KrF laser was employed in tandem with the CO_2 laser to collect the data in Fig. 6(c), since the 248 nm emission was strongly absorbed[20] by $Bi(CH_3)_3$ but was transparent[29] to the FN_3. The purpose of using the KrF laser was to assist the dissociation of $Bi(CH_3)_3$ and thereby achieve a higher level of gain. Since the response of the intracavity diagnostic is nonlinear, small improvements in gain can have a very large effect on the signal-to-noise ratio. All of the spectra were collected using an OMA that was temporally gated to the peak of the BiF(A) time profile. As reported in the following subsections, the data were analyzed for spectroscopic distortion either due to self-absorption or self-amplification. An analysis based on the bandshape was preferred over an analysis of band-to-band relative intensities, as the latter method probes the vibrational distribution and significant errors could result due to small deviations from a thermal distribution, which are not uncommon in pulsed experiments of μs duration. The bandshape, however, depends on the rotational distribution which is more rapidly thermalized and therefore less subject to error. The analysis is based on the principle that the spontaneous emission (chemiluminescence) and gain/absorption (cross section) spectra have a different wavelength dependence, the latter peaking to the red of the chemiluminescence band head, due to the rotational distribution.

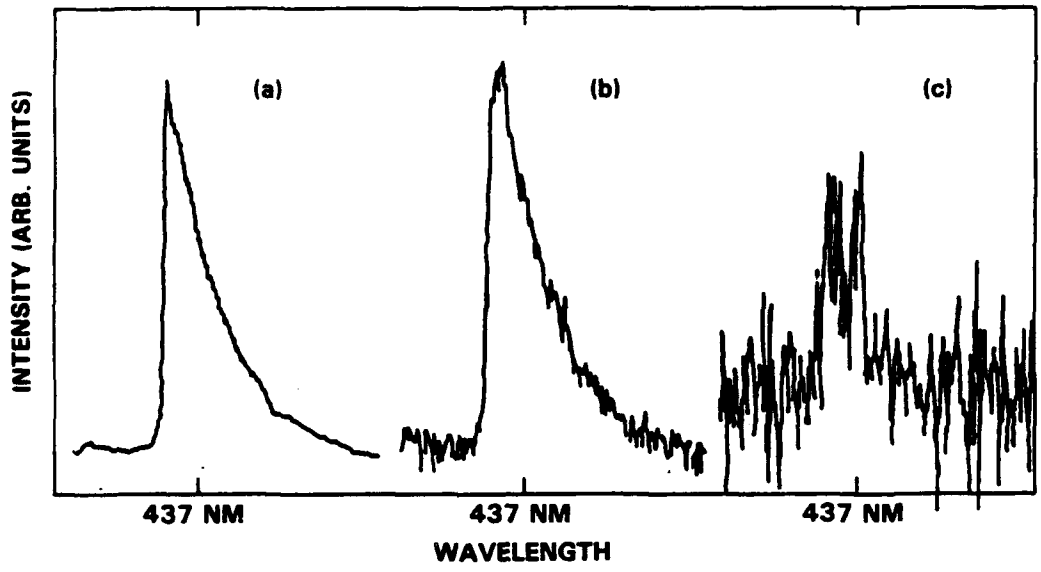

Fig. 6 Comparison of BiF(A-X, $v' = 0$ to $v'' = 0$) spectra (a) without an optical cavity, (b) with an optical cavity formed by 95% reflecting mirrors, and (c) with an optical cavity formed by 99.9% reflecting mirrors, and use of a KrF laser to aid the dissociation of $Bi(CH_3)_3$.

Self-Absorption - Comparison of Fig. 6(b) to Fig. 6(a) shows no measurable spectroscopic distortion above the noise level. An upper limit on the concentration of the BiF(X, $v'' = 0$) state can therefore be determined from the inequality

$$\left(\frac{2\,\ell}{1 - R^2}\right) \sigma \left([BiF(X, v' = 0)] - [BiF(A, v' = 0)]\right) S < 2\,N \qquad (4)$$

where ℓ is the gain length (2.5 cm), R is the mirror reflectivity and S/N is the signal-to-noise ratio (~ 20). The value of the cross section σ for the $0 \rightarrow 0$ transition at the peak of its rotational distribution (437 nm) is about 10^{-16} cm^2 based on the radiative rate and spectroscopic parameters measured by Jones,[30] assuming rotational equilibrium at 1200 K, Doppler broadening and no significant hyperfine splitting. The term $(2\ell/1-R^2)$ is the effective path length of a photon through the reacting medium before it escapes the cavity. Therefore, in the limit of weak absorption, Eq. (4) compares the distortion of the signal due to self-absorption to the noise that is present in the measurement. Taking [BiF(A, $v' = 0$)] as $3 \times 10^{12}/cm^3$ (corresponding to [BiF(A, total)] = $10^{13}/cm^3$ at 1200 K) yields an upper bound on [BiF(X, $v'' = 0$)] of $2.3 \times 10^{13}/cm^3$ or $5 \times 10^{13}/cm^3$ for the entire BiF(X) ground state. Since the peak NF(a) concentration was measured as $3 \times 10^{16}/cm^3$ prior to addition of $Bi(CH_3)_3$, and the $Bi(CH_3)_3$ mole fraction was increased until the associated byproduct

quenching of NF(a) was significant to optimize the yield of BiF(A), an effective yield of NF(a) of ~ $1.5 \times 10^{16}/cm^3$ is estimated. Since the BiF(A) radiates into the BiF(X) ground state at $7 \times 10^5/s$ and is removed by reaction with NF(a) at a rate of $(5 \times 10^{-11}\ cm^3/s)$ $(1.5 \times 10^{15}/cm^3) \sim 7.5 \times 10^5/s$, we should expect the concentrations of BiF(A) and BiF(X) to be comparable. The self-absorption analysis, which is limited in sensitivity by S/N considerations, shows that our expectations cannot be in error by more than a factor of five.

Incipient Lasing - Since the noise in the self-absorption experiment is due to the detector, while the amplitude of the signal which is transmitted decreases for mirrors of higher reflectivity, the increased sensitivity of the experiment caused by a larger effective path length (with mirrors of higher reflectivity) is cancelled by the reduced signal-to-noise ratio. Consequently, when using the 99.9% mirrors, we analyzed instead for incipient lasing (or self-amplification) to take advantage of the nonlinear (exponential) amplification that occurs near laser threshold. Since the sensitivity of the experiment increases in proportion to the achievable gain we decided to enhance the yield of BiF(A) by using a KrF laser to aid the dissociation of the $Bi(CH_3)_3$, since this bottleneck prevents efficient utilization of the Bi-donor. It was necessary first, however, to ensure that the KrF laser did not contribute to pumping the BiF(A) state directly and thereby invalidate the experiment. Pumping with the KrF laser, while blocking the CO_2 laser, however, was found to produce no significant yield of BiF(A). Consequently, apart from dissociation of the $Bi(CH_3)_3$, the only other potential effect of the KrF laser was to yield $Bi(^2D)$ as a photolysis product.[20] To investigate this possibility, we collected time profiles of $Bi(^2D)$ both with and without the KrF laser, as shown in Fig. 7. These data demonstrate that the principal effect of the KrF laser was not to increase the yield of $Bi(^2D)$ but rather the rate at which it was produced. This latter effect is significant, because (with the KrF laser) the $Bi(^2D)$ peaks before the NF(a) has decayed significantly, which accounts for the observed 50% increase in the yield of BiF(A) which also peaked earlier in time than without the KrF laser. Since the excimer laser improves the effective NF(a) concentration, a higher ratio of BiF(A) to BiF(X) is expected in this case. Because this ratio is thought to approach unity without the KrF laser, it seemed feasible that an absolute inversion could be achieved when the KrF laser was used to aid the dissociation of $Bi(CH_3)_3$. We continued to focus on the $v' = 0$ to $v'' = 0$ transition because the BiF(A-X) cross sections are largest for the 0 - 0 and 0 - 1 bands.

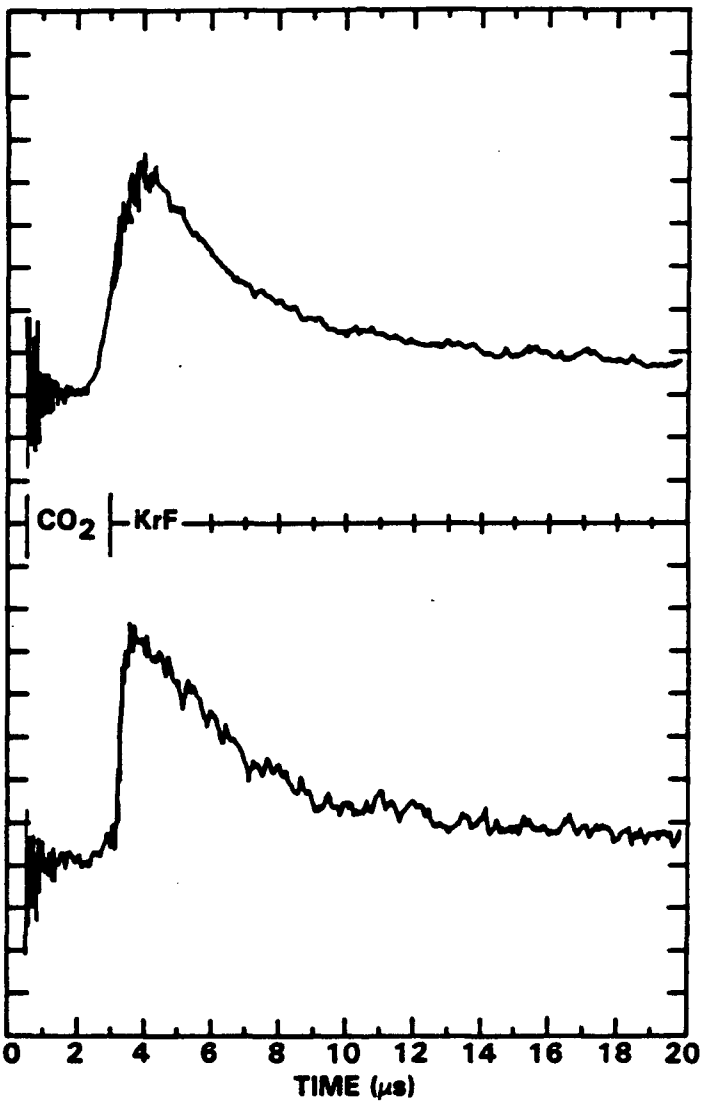

Fig. 7 Comparison of Bi(^{2}D) time profiles with (bottom) and without (top) use of a KrF laser to assist the dissociation of $Bi(CH_3)_3$.

The potential gain in the incipient lasing experiment is limited to 10^{-3}/cm (by the peak yield of BiF(A)) and the peak gain time is less than 2 μs (FWHM). A spontaneous photon can therefore experience at most 700 round trips through the 2.5 cm gain medium since the mirror spacing corresponds to a round trip time of 3 ns. The mirror spacing is set by the requirement that the mode spacing be smaller than the Doppler width to ensure a coherent interaction with the cavity. Consequently, the maximum amplification factor for any spontaneous photon is exp (3.5) or 33. Therefore, since the amount of light leaking through the maximum-reflectance dielectric mirrors is very small, we do not expect a significant output beam or efficient power extraction in this experiment. Moreover, the above estimate is an upper limit since it does not take into account the actual temporal variations of the spontaneous emission or the gain which occur on a time scale that is comparable to the photon lifetime in the cavity. To more accurately model the cavity buildup in this regime we assembled a computer program which calculates the cavity output (I) as a function of time (t) according to the relation

$$I(t) = K \int_0^t dt' \; E(t') \exp\left(\frac{c}{2L} \int_{t'}^t dt'' \; (2\gamma(t'')\ell - 2(1 - R))\right) \qquad (5)$$

where K is an overall constant, L is the cavity length and ℓ is the gain length. This expression takes into account spontaneous emission at all times $t' \leq t$ and amplification at all times t" in the interval between t' and t. To calculate the output intensity we need a model for the time dependence of the spontaneous emission (E) and the time dependence of the gain (γ). The function E(t) was generated by fitting the BiF(A) time profile to a function of the form A sin ($\pi t/2t_0$) which yields a good match over the time scale of interest, with t_0 = 2.5 μs. The constant A is absorbed into the overall constant K in Eq. (5). To generate a time dependent model of the gain we used three cases. The first case assumed a gain of zero as a reference. The second case, referred to as the "fast recycling limit" assumes that the BiF(X) ground state is totally depopulated, in which case, the time profile of the gain is the same as for the spontaneous emission, except in this case the constant A is replaced by a peak gain constant (γ_0) which is used as a fitting parameter. In the third case, referred to as the "bottleneck limit" we assume that the BiF(X) state is initially depopulated, but is filled by radiative decay from the BiF(A) state but is not depopulated by any means. Solu-

tion to the corresponding rate equation for BiF(X), given the initial conditions and time profile of BiF(A) yields a gain model that is similar to the fast cycling model except that t_o is replaced by $t_o/2$ and γ_o by 0.3 γ_o for the specific case where t_o = 2.5 μs and the radiative rate is 7×10^5/s. In the fast recycling case the maximum value of γ_o is 1.5×10^{-3}/cm based on a peak BiF(A) yield of 1.5×10^{13}/cm^3 and a gain cross section of 10^{-16} cm^2. In the bottleneck case, peak gain is limited to 30% of this value or approximately 5×10^{-4}/cm.

Using a desktop computer, we calculated the relative time profiles from Eq. (5) in the zero gain, fast recycling and bottleneck limits, as shown in Fig. 8 for the case where $\gamma_o = 5 \times 10^{-4}$/cm. As can be seen, significantly higher output is obtained when the BiF(X) state is rapidly removed as expected. Results such as presented in Fig. 8 were then generated for a variety of γ_o estimates and integrated to simulate the action of the OMA gate. The fractional increase (relative to $\gamma_o = 0$) was then plotted vs γ_o as shown in Fig. 9 for both the fast recycling and bottlenecked limits. As can be seen the actual amplification resulting from intracavity gain is only a factor of five, in the case of fast recycling with $\gamma_o = 10^{-3}$/cm, and is much less in the bottlenecked limit. Comparison of Fig. 6(c) to Fig. 6 (a) does show a positive distortion of the bandshape (albeit at a low signal-to-noise ratio) of approximately two. The distortion at 437 nm, however, was reproduced on three separate runs and does appear at the wavelength which matches the peak gain cross section. Using the results presented in Fig. 9 we can immediately conclude that the ground state is not bottlenecked. Therefore, the observed distortion is less than expected because either the BiF(X) ground state is not totally removed or because there are intracavity losses that are not accounted for in the calculation.

The following section of this report will demonstrate, however, that these measurements were conducted under conditions leading to prereaction of the $Bi(CH_3)_3$ with the FN_3. This condition served to diminish the $Bi(CH_3)_3$ concentration and resulted in the formation of solid particulates that induced scattering losses of approximately 10^{-3}/pass inside the optical cavity. The calculations that were used to produce Figs. 8 and 9 were therefore repeated for the case defined by the fast recycling limit with $\gamma_o = 10^{-3}$/cm by using an effective mirror reflectivity of 99.8% instead of 99.9% to account for the loss due to particulate scattering. In this case the fractional enhancement was reduced by a factor of approximately two in good agreement with the data. We can therefore conclude that the ground state was significantly depopulated and the peak gain approached 10^{-3}/cm. These results would not be obtained, however, without use of the KrF laser which resulted in a

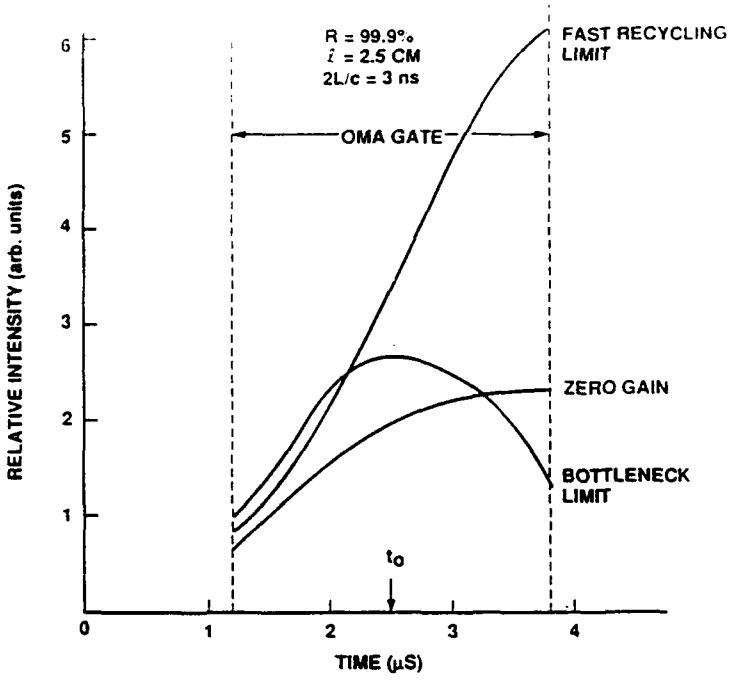

Fig. 8 Computed time profiles of cavity output based on the measured BiF(A) time profile and assuming either zero gain or loss or a peak gain of 0.05%/cm in the limits of fast recycling or bottlenecked removal of BiF(X).

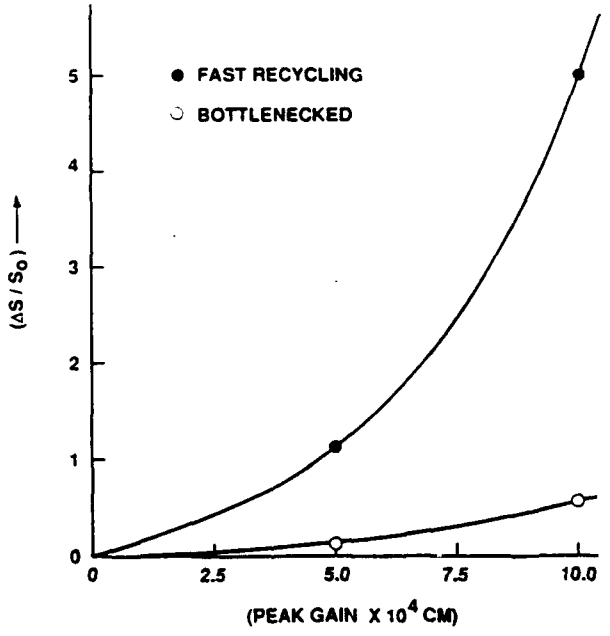

Fig. 9 Fractional enhancement of cavity output due to intracavity gain as a function of peak gain.

higher effective concentration of NF(a) by providing an adequate supply of Bi(^{2}D) atoms before the NF(a) decayed significantly, since the higher NF(a) concentration enhanced the yield of BiF(A) relative to BiF(X). Nonetheless, the results were sufficiently encouraging that we decided to go ahead and probe the gain region of our reactor (without the aid of a KrF laser) by means of a dye laser to obtain more quantitative results and data with a higher signal-to-noise ratio. The methods used and the results obtained are described in the following section of this report.

MEASUREMENT OF BiF(X)

In order to probe the ground state with a high signal-to-noise ratio, it was necessary to increase the intensity of the probing radiation to eliminate statistical noise. Fortunately, the stimulated emission signal increases in proportion to the probe intensity and the saturation level of the BiF(A-X) transition is large enough that the detector noise associated with the OMA can be eliminated as well by use of an appropriate laser source. Therefore, a pulsed dye laser was constructed, using a XeCl excimer laser as the pump, following the design of Hansch,[31] which included intracavity tuning elements to narrow the bandwidth of the emitted radiation. The tuning elements in our laser were a prism telescope, a weak dispersing prism and a temperature stabilized solid etalon with a finesse of 30 and a free spectral range of 3.4 cm^{-1}. The strength of the dispersing prism was selected to allow several modes of the etalon to run simultaneously. Course and fine tuning were accomplished by tilting the rear mirror and the etalon, respectively. The function of the prism telescope was to expand the intracavity beam (in one dimension only) in order to minimize the walk-off loss that occurs when the etalon is tuned off of normal incidence. The pump beam from the XeCl laser was suitably attenuated so that the dye laser output was approximately 50 μJ in pulses of less than 10 ns duration. The following subsections of this report describe how the dye laser was employed to monitor intracavity losses and measure the concentration of BiF(X). Based on the results that were obtained, and known scaling relations, a measurable gain is predicted under conditions that are achievable in the present apparatus with only minor modifications.

Intracavity Scattering

The initial experiments were conducted using the gated OMA and dye laser (without an intracavity etalon) to probe the reactor through a pair of 99.9% mirrors that were arranged in a stable cavity configuration. We immediately observed that the transmission of the dye laser through the cavity dropped approximately 50% upon admitting the reagents to the reactor, indicating an intracavity loss of approximately 10^{-3}/pass. Further testing revealed that the loss required the presence of both $Bi(CH_3)_3$ and FN_3 in the reactor and was independent of CO_2 laser intensity or dye laser wavelength. We therefore concluded that a slow reaction between FN_3 and $Bi(CH_3)_3$ was occurring in the common inlet duct of the reactor that resulted in formation of entrained solid particulates which acted as optical

scattering centers to induce the measured loss. The reactor was therefore redesigned as shown in Fig. 10 to delay the mixing of the FN_3 with the $Bi(CH_3)_3$ until just upstream of the optical axis in the reactor. The cross sectional dimensions of the original duct were left unchanged but the duct itself was shortened slightly and was surrounded by an annular duct which carried the $Bi(CH_3)_3$/He flow. The FN_3/He and SF_6 flows were admitted to the central duct as before. One dimensional diffusion calculations were employed to ensure that the FN_3/SF_6 and $Bi(CH_3)_3$ flows were thoroughly mixed at the optical axis. Once these modifications were in place, testing with the dye laser revealed that particulate formation and the attendant intracavity loss were effectively suppressed.

The yield of NF(a) that was obtainable with the new reactor was suppressed, however, because the cross sectional area of the reaction zone (shaded area in Fig. 10) was enlarged and hence the FN_3 concentration was decreased since its molar flow rate is fixed

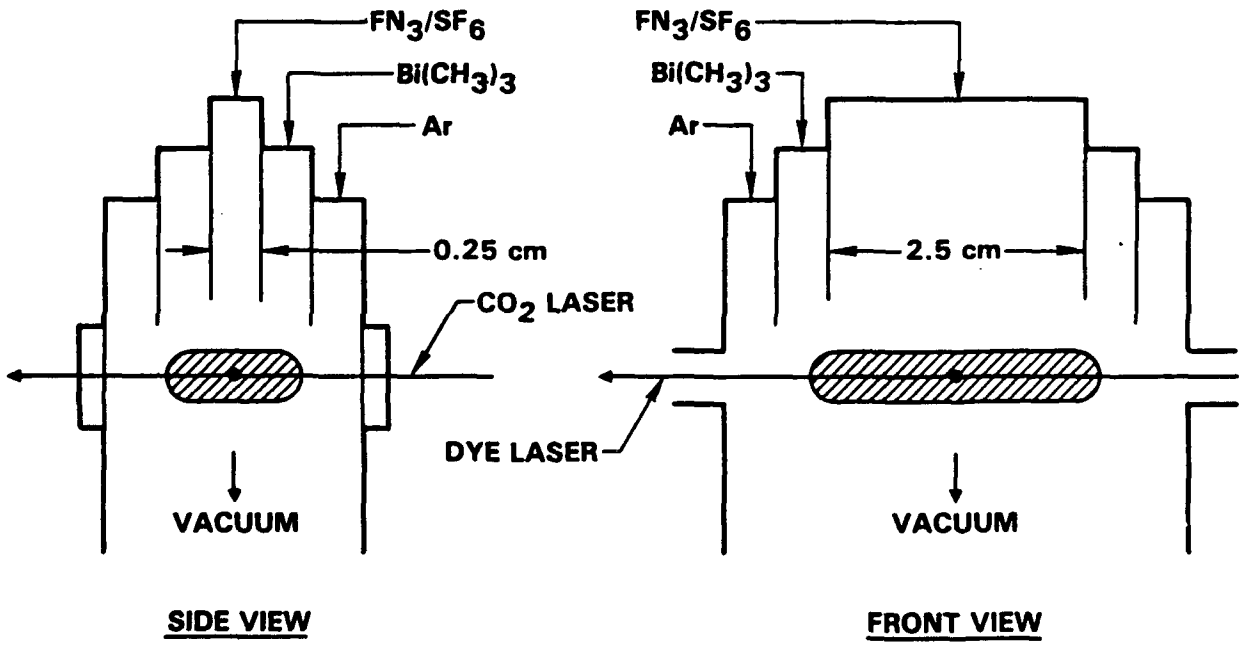

Fig. 10 Schematic diagram of reactor modification used to eliminate intracavity scattering.

by the generator. Also, the larger reaction zone increased the heat capacity of the gas sample that was coupled to the CO_2 laser, which resulted in lower peak temperatures. Since the FN_3 dissociated more slowly at the reduced temperature, the loss due to self-annihilation was increased and the FN_3 was converted to NF(a) with lower efficiency. The best NF(a) concentration that could be obtained after re-optimizing all flows was $6 \times 10^{15}/cm^3$. Based on the quadratic scaling relationship[21] between NF(a) and BiF(A) concentrations a peak BiF(A) yield of $4 \times 10^{11}/cm^3$ was expected upon optimal addition of $Bi(CH_3)_3$. The peak yield of BiF(A), however, was measured as $1.4 \times 10^{13}/cm^3$. We therefore concluded that prereaction with FN_3 was responsible for consuming approximately 95% of the $Bi(CH_3)_3$ that was admitted to the reactor prior to arrival at the optical axis and that the improved yield of BiF(A) at the lower NF(a) concentration resulted from the effective elimination of this condition.

The $Bi(CH_3)_3$ flow in the subsequent experiments was backed off until the peak BiF(A) concentration was reduced to $7 \times 10^{12}/cm^3$ or approximately half of the peak value that was obtained with optimal addition of the Bi-donor. This procedure was adopted to achieve a higher ratio of BiF(A) to $Bi(CH_3)_3$ and hence suppress the concentration of the BiF(X) ground state in relation to the BiF(A) excited state, since the BiF(A) yield is saturated with optimal addition of $Bi(CH_3)_3$. Nonetheless, the NF(a) concentration in these experiments was too low to invert the $v' = 0$ to $v'' = 0$ transitions of the BiF(A-X) system, since the excitation rate (5×10^{-11} cm^3/s) ($3 \times 10^{15}/cm^3 \sim 1.5 \times 10^5/s$ is about one-fifth of the ($7 \times 10^5/s$) radiative decay rate. Therefore, BiF(X) was measured in absorption rather than gain. This result does not preclude gain at higher NF(a) concentrations or in the present experiment on transitions from $v' = 0$ to energy levels with $v'' > 0$, depending on the temperature.

Cavity Ringdown Method

The concentration of the BiF(X) ground state was determined with knowledge of the excited state BiF(A) concentration and the optical cross sections for the A-X transitions by noting the change in transmission of the dye laser through the cavity-reactor due to the presence of the intracavity reactions. This method has high sensitivity because the photons that are injected into the optical cavity oscillate back and forth between the mirrors many times (through the reacting medium) before escaping to the detector. Since our goal was to measure the ground state, the laser was tuned to the $v' = 0$ to $v'' = 0$ transition at 437 nm

which was expected to yield the largest signal, since higher v'' levels of the ground state are less populated and the Franck-Condon factors favor transitions with small Δv between the excited and ground states in BiF. We used 99.5% reflecting mirrors for this measurement as a compromise between sensitivity (which favors higher reflectivity) and temporal resolution. If the mirror reflectivity is too high, then the lifetime of the photon in the cavity becomes comparable to the chemical kinetics.

Figure 11 is a schematic diagram of the cavity ringdown experiment. Initially an electrical synchronization signal is obtained from the CO_2 laser that is used to initiate the reaction inside the optical cavity. After a variable time delay, which is adjusted to allow the yield of BiF(A) to peak in the reactor, the XeCl excimer laser is fired which energizes the dye laser and injects a pulse of photons into the cavity. A second time delay, synchronized to the XeCl laser is then used to allow time for the photons to oscillate back and forth through the reacting medium before detection by a gated OMA. These temporal relationships are shown in Fig. 12. Intracavity gain or absorption is detected because it changes the time constant of the cavity decay by either offsetting or increasing the round trip loss factor, which in turn affects the intensity of photons which are leaked from the cavity and detected by the OMA. In our experiments, the OMA gate was adjusted to detect photons arriving between 200 and 400 ns after the dye laser was fired.

An optical (path length) isolator and an attenuator were inserted between the output of the dye laser and the input mirror of the reactor cavity to ensure that the wavelengths emitted by the dye laser were not influenced by cavity feedback and to prevent optical bleaching (saturation) of the medium inside the cavity by the intense dye laser beam. The OMA was also modified by placing a lens between the output plane of the monochromator and the diode array to affect a 5X demagnification of the individual detector elements, so that by using a narrow entrance slit, sufficient resolution was obtained to separate the etalon modes of the dye laser. Figure 13 shows the typical output of the dye laser as recorded by the OMA, after the digitization noise has been smoothed out of a 128 shot overage. Repeated measurements showed that the dye laser signature was reproducible within ± 2%.

In practice the measurement was performed by aligning one of the etalon modes of the dye laser with a selected rotational line of the BiF(A-X) band system. Since the free spectral range of the etalon is comparable to but different than the rotational spacing, the

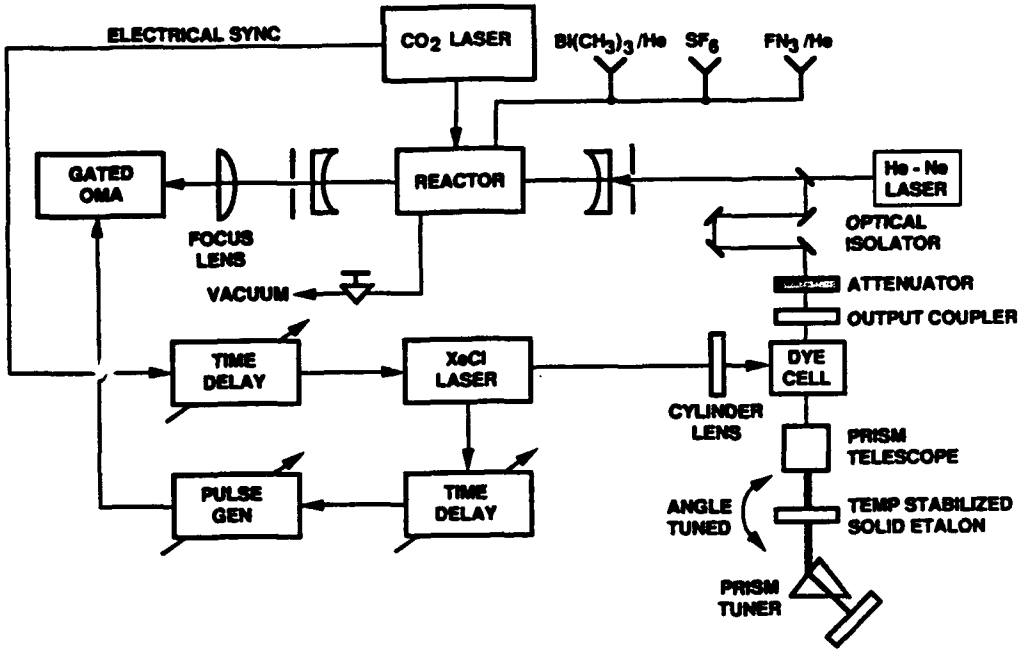

Fig. 11 Schematic diagram of cavity ringdown experiment.

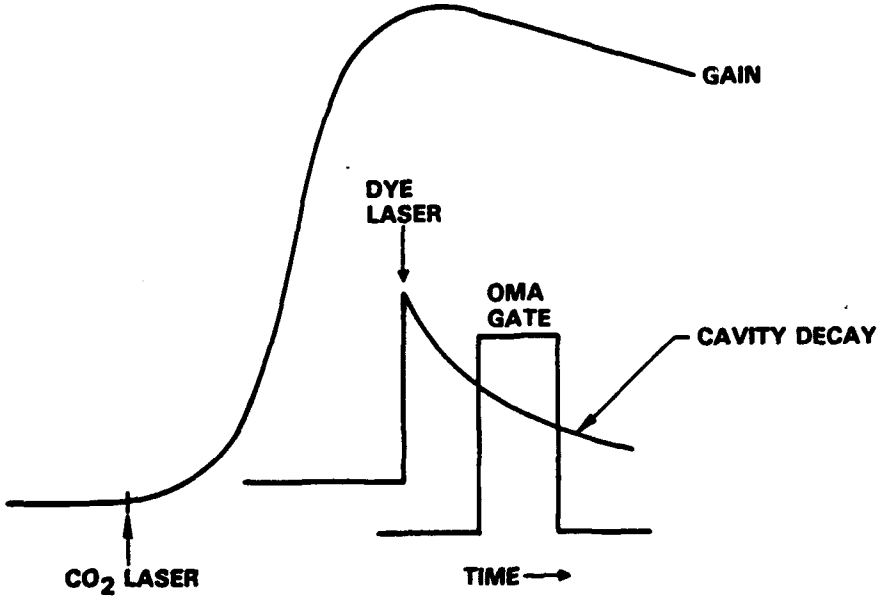

Fig. 12 Timing diagram of cavity ringdown experiment.

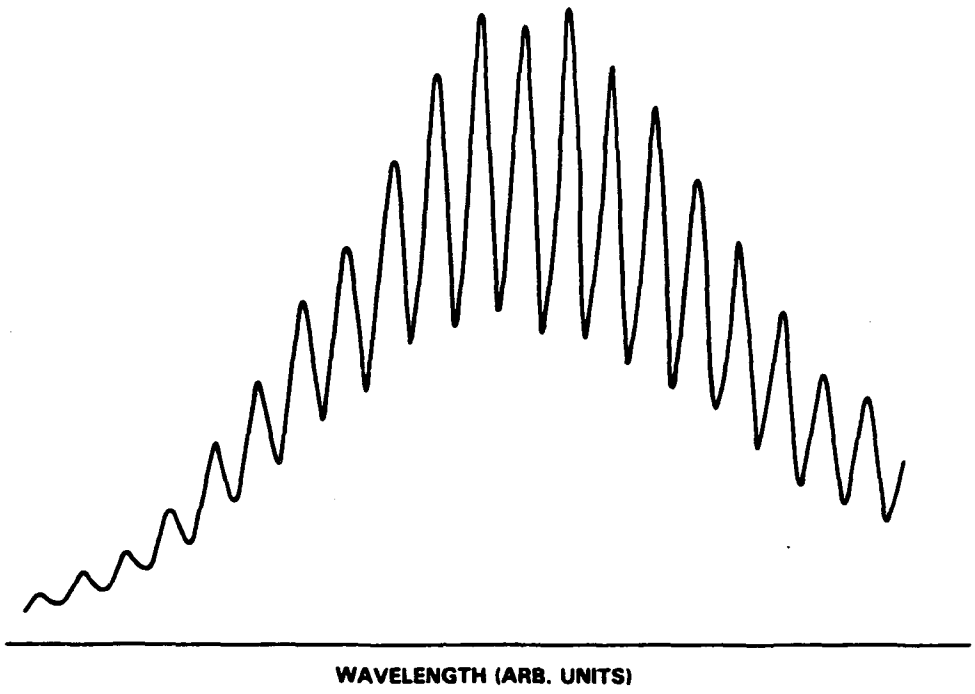

Fig. 13 Spectrum of dye laser as measured by the OMA.

adjacent etalon modes will fall between the rotational lines and therefore serve as a zero gain/loss reference. Spectroscopic alignment was accomplished by using a Thulium hollow cathode lamp to wavelength calibrate the OMA, which was accurate enough to place an etalon mode within fine tuning range of the intended transition. During the alignment procedure the time delay between the CO_2 and XeCl lasers and the addition of $Bi(CH_3)_3$ were both increased as needed to produce a strong absorption signal that was easily detected. Once the dye laser was tuned, the $Bi(CH_3)_3$ flow was reduced and the time delay was set to fire the XeCl laser at the peak of the BiF(A) time profile.

Calibration of Sensitivity

The cross sections (σ) used to relate the BiF(A) and BiF(X) concentrations to intracavity gain or loss are given by the relation

$$\sigma = (4 \ln 2/\pi)^{0.5} \; A \, f_v \, f_J \, (\lambda^2/8\pi\Delta\nu) \, n(J) \qquad (6)$$

where A is the radiative rate, f_v is the Frank Condon factor, f_J is the Honl-London factor, λ is the wavelength, $\Delta\nu$ is the linewidth and n(J) is the rotational distribution factor. We used Koffend's values for the radiative rate[17] and Jone's results for the Franck-Condon factors

and wavelengths.[30] The Honl-London factor was assumed to be zero except for the P and R branches, for which $f_J = 0.5$ in the limit of high J values. As will be shown, the linewidth cancels out of the sensitivity equation and the rotational distribution is given by

$$n(J) = (2J + 1)\ (B/RT)\ \exp\left[-\ J\ (J + 1)\ (B/RT)\right] \tag{7}$$

where $B = 0.22\ cm^{-1}$ is the mean rotational parameter for the BiF(A) and BiF(X) states and $1/R \sim 1.5\ °K/cm^{-1}$ is the gas constant.

The time constant (τ_o) for the decay of the empty cavity is given by the relation

$$\tau_o = \ell/cL \tag{8}$$

where ℓ is the loss per mirror and L is the cavity length. The intensity (I_o) leaking from the cavity is therefore

$$I_o = D \int_{t_1}^{t_2} e^{-t/\tau_o}\, dt \tag{9}$$

where D is an overall detection constant and (t_1, t_2) define the OMA gate in relation to the firing of the dye laser at t = 0. If the intracavity gain per pass is G, then the effective loss per pass of the loaded cavity is L-G. Therefore, the time constant of the loaded cavity (τ) can be obtained by replacing L in Eq. (8) by L-G and then using Eq. (8) to eliminate L from the result to yield

$$\tau = \tau_o/(1 - G_c\ \tau_o/\ell) \quad . \tag{10}$$

The corresponding loaded intensity (I) is therefore given as

$$I = D \int_{t_1}^{t_2} e^{-t/\tau}\, dt \quad . \tag{11}$$

The quantity that is actually measured ($\Delta S/S$) is the fractional increase or decrease of transmitted intensity due to the presence of intracavity gain or loss. If the linewidth of the laser where narrow in comparison to the linewidth of the BiF transition then $\Delta S/S$ would be given by $(I - I_0)/I_0$. In the current experiment, however, the linewidth of the laser is larger than the linewidth of the transition and the measurements were performed at a wavelength that corresponds to a near resonance between the P(45) and R(65) transitions that allows both lines to be probed simultaneously. Therefore, the fractional effect that is observed is actually given by

$$\Delta S/S = (2\Delta\nu/\Delta\nu_L)\ \{I - I_0\}/I_0 \tag{12}$$

where $\Delta\nu_L$ is the linewidth of the laser. If the gain or loss is approximately constant over the interval $t_1 < t < t_2$ then the integrals can be performed simply in Eqs. (9) and (11) to yield

$$\Delta S/S = (2\Delta\nu/\Delta\nu_L)\ \{(\tau/\tau_0)\ \frac{e^{-t_1/\tau} - e^{-t_2/\tau}}{e^{-t_1/\tau_0} - e^{-t_2/\tau_0}}\} \tag{13}$$

from Eq. (12). Since ℓ, t_1 and t_2 are known and τ can be related to τ_0 by Eq. (10) we only have to determine τ_0 and $\Delta\nu_L$ to evaluate (13) for the quantity $(\Delta S/S\Delta\nu)$ as a function of the gain parameter (G). In general, this relation will be nonlinear, however, for sufficiently small valeus of G or $\Delta S/S$ a linear approximation can be used instead, as expressed by the equation

$$(\Delta S/S\Delta\nu) = K\ G \tag{14}$$

where K is calibration constant. Comparison of Eqs. (13) and (14) shows that K is independent of the linewidth ($\Delta\nu$). Using Eq. (14) the gain equation

$$G = \sigma\ \{[B1F(A,\ v' = 0)] - [B1F(x,\ v'' = 0)]\}\ x \tag{15}$$

can be rewritten as

$$[B1F\ (X,\ v'' = 0)] = [B1F\ (A,\ v' = 0)] - \frac{\Delta S/S}{K\ (\Delta\nu\sigma)\ x} \tag{16}$$

where x is the gain length. Since Eq. (6) shows that σ is inversely proportional to $\Delta\nu$, the product ($\Delta\nu\sigma$) in Eq. (16) is independent of the linewidth ($\Delta\nu$). It is necessary, however, when using Eq. (6) for this application, to replace the n(J) term by the average value of n(45) and n(65) calculated from Eq. (7) since both lines are detected simultaneously in the present experiment. Fortunately, as the temperature is increased n(45) decreases while n(65) increases so that the average is nearly constant over the range from 700 to 1700 °K. Therefore, it is not necessary to know the temperature with precision to calculate the BiF(X, $v'' = 0$) concentration from a relative measurement of $\Delta S/S$ and in a determination of [BiF(A, $v' = 0$)] by absolute photometry.

The value of τ_o was determined, as shown in Fig. 14, by using the dye laser to pulse excite the cavity (with the reactor evacuated) and using a fast photodiode and signal averager to collect the time profile of the intensity of radiation that leaks through the mirrors. The dashed line in Fig. 14 is a fit to an exponential decay with $\tau_o = 409$ ns which yields a loss per mirror of 0.37% in good agreement with the manufacturer's data which shows 0.41% loss at 438 nm. The linewidth of the laser was determined by scanning the dye laser over a single line of the BiF band system near R(30) and plotting $-\Delta S/S$ as a function of etalon tilt angle as shown in Fig. 15. The angular data was obtained from the micrometer screw on the etalon mount and normal incidence was defined by tuning the etalon to act as a retroreflector in the dye laser with the prism and near mirror blocked. Using Snell's law for small angles shows that the angle of the radiation inside the etalon is the tilt angle (θ) divided by the index of refraction (n) which is 1.466 for fused silica at 438 nm. Since the frequency of each etalon pass band tunes as the cosine of the internal angle, the linewidth of the laser can be determined using the relation

$$\Delta\nu_L/\nu = \theta\,\Delta\theta\,/\,n^2 \qquad (17)$$

from the data in Fig. 15, which yields $\Delta\nu_L = 0.24\ cm^{-1}$.

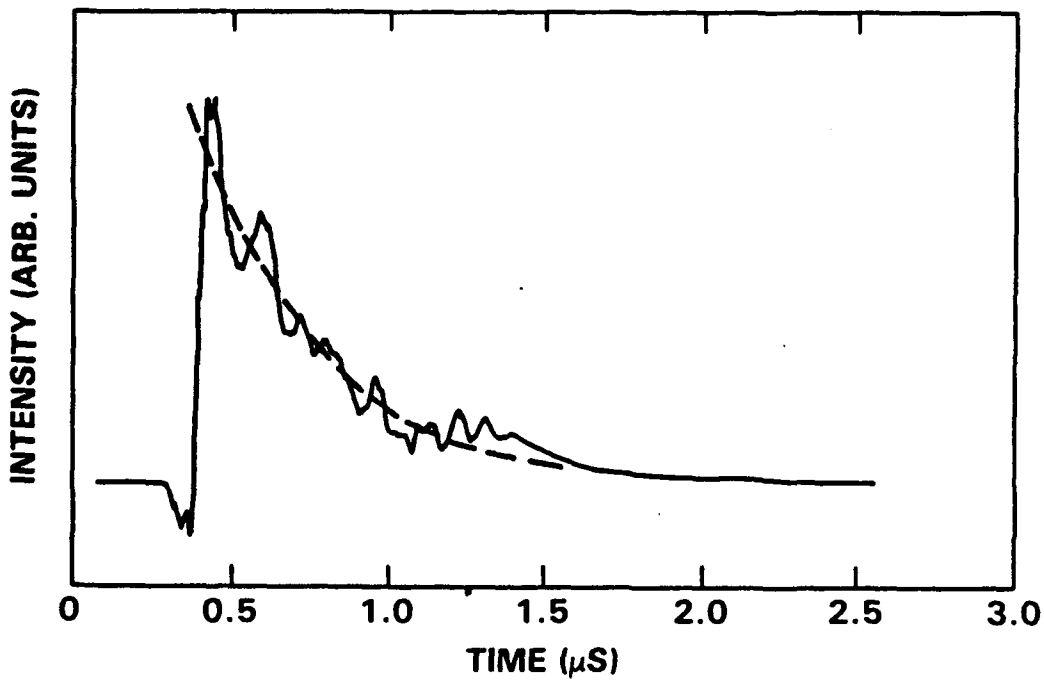

Fig. 14 Determination of empty cavity decay time.

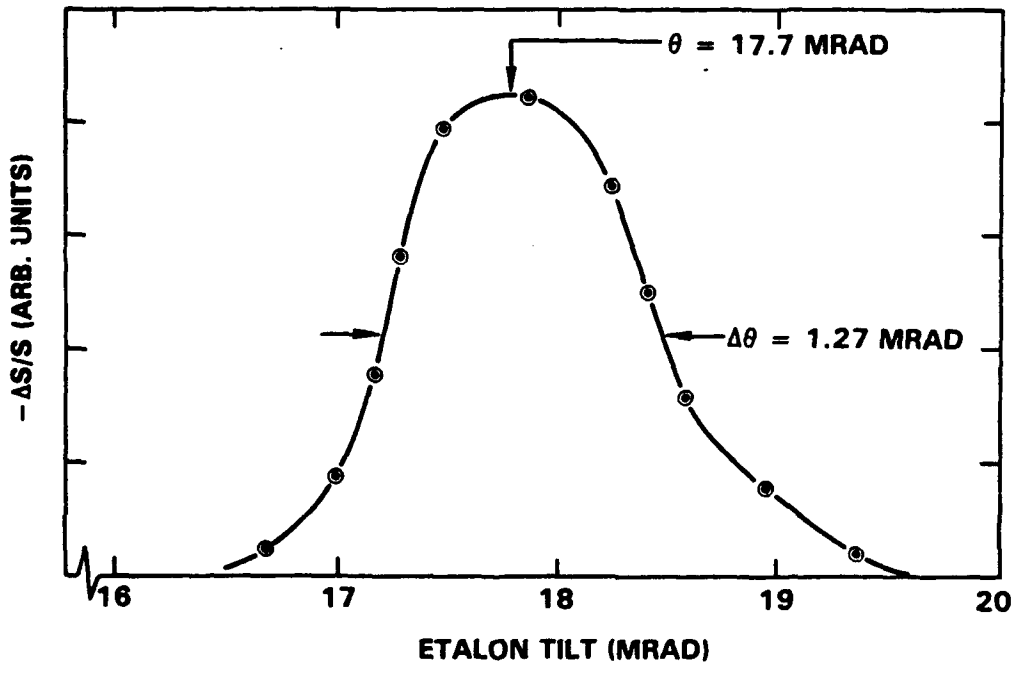

Fig. 15 Determination of linewidth of dye laser.

Figure 16 shows the value of $-\Delta S/S$ calculated from Eq. (13) vs negative values of the gain parameter (G) which corespond to absorption assuming a linewidth that corresponds to the Doppler broadening at 1200 K for the sake of presentation. The dashed line which corresponds to K = 40.4 ns in Eq. (14) is accurate below $|\Delta S/S| \sim 0.2$ to approximately ± 10%. Using Eqs. (6) and (7) to calculate the cros section yields $\sigma\Delta\nu = 1.1 \times 10^{-7}$ cm^2/s for the J = 45/65 combination of lines at T = 1200 K. Combining this result with Eq. (16) and x = 2.5 cm (for the gain length of our reactor) yields

$$[BiF(X, v'' = 0)] = [BiF(A, v' = 0)] - (9.1 \times 10^{13}/cm^3)\ \Delta S/S \qquad (18)$$

as the final result that calibrates the experiment.

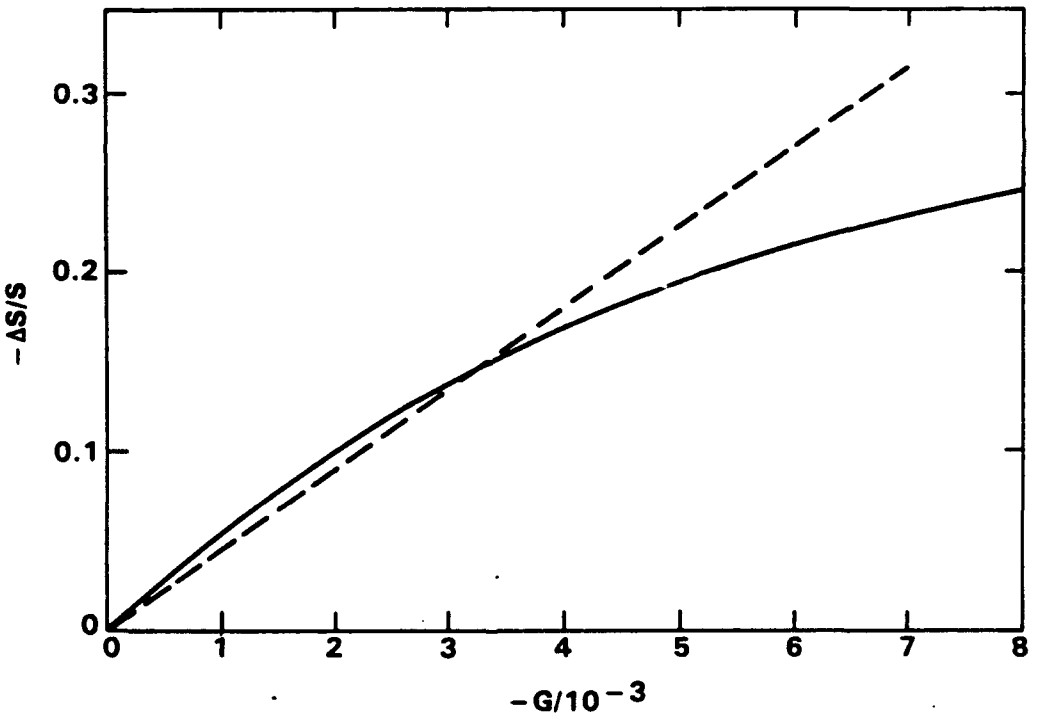

Fig. 16 Plot of response function $\Delta S/S$ assuming ($\Delta\nu$ = 1.13 GHz) vs intracavity single pass absorption.

Extent of Inversion

In this subsection we review the experimental checks that were performed to verify the measurement, the results obtained for BiF (X, $v'' = 0$) concentration and vibrational temperature and the calculations which determine which transitions are inverted in the present experiment. The associated gain/loss coefficients are also calculated. In the following subsection, we use these results to calculate the gain factors that can be achieved at higher NF(a) concentrations or reduced temperatures. These conditions favor substantially larger gain coefficients.

Verification - The sensitivity of the reactor cavity to absorption was tested by blocking the CO_2 laser to prevent dissociation of the FN_3, which has a weak continuum absorption in the 400 - 450 nm range.[11,29] The absorption due to the FN_3 was measured, en route to the reactor, in a commercial spectrophotometer at elevated pressure and the partial pressure of FN_3 admitted to the reactor was adjusted to produce a single pass loss equal to the measured mirror loss. This procedure had the expected effect of reducing the observed ringing time by a factor of two. Also, upon allowing the CO_2 laser to pump the reactor (ahead of the dye laser in time), the ringing time was restored, confirming complete dissociation of the FN_3 and the formation of no absorbing byproducts. These tests were conducted without addition of $Bi(CH_3)_3$ to the reactor gas flow. The following additional tests were also made, when $Bi(CH_3)_3$ was admitted to the reactor and absorption signals were obtained.

We observed that the absorptions induced by addition of $Bi(CH_3)_3$ only affected selected etalon modes of the dye laser and thus were caused by a discrete rather than continuum absorber. Replacing the $Bi(CH_3)_3$ flow by He eliminated these signals. With $Bi(CH_3)_3$ in the reactor, the absorptions vanished when the excimer laser was fired ahead of the rise of the BiF(A) time profile or with the excimer laser positioned on the peak of the BiF(A) time profile when the dye laser was tuned just beyond the short wavelength side of the red degraded $v' = 0$ to $v'' = 0$ bandhead where the cross section vanishes. The absorption signal on the combined $J = 45/65$ lines was approximately twice as strong as measured on lines in the vicinity of the R(30) transition, where only single transitions can be probed. Finally, at the higher J values, we confirmed the correct values of the interline rotational spacing (by etalon tuning) and we detected the absorptions, within an etalon bandwidth at the values measured by Jones using our hollow cathode lamp calibration for the absolute

wavelengths. These data were repeatable and were collected with all aspects of the measurement properly functioning under nominal conditions. Therefore, we are very confident that the measured signals are due to absorption by BiF molecules on the P(45) and R(65) transitions of the $v' = 0$ to $v'' = 0$ band of the A-X system, near 438 nm.

Data - The key result is shown in Fig. 17 which illustrates an absorption signal of $\Delta S/S = -0.2$ under the condition described above. According to Eq. (18) this result corresponds to a BiF(X, $v'' = 0$) concentration of $2.1 \times 10^{13}/cm^3$. The vibrational distribution of the BiF(A) state was measured under corresponding conditions, using the OMA and knowledge of the Frank-Condon factors to normalize the data. The instrument response was assumed to be a linear function of wavelength over the range between the $0 \rightarrow 2$ and $0 \rightarrow 3$ transitions, whose slope was adjusted to bring the corresponding peak heights into agreement with the relative transition rates. The $0 \rightarrow 2$, $1 \rightarrow 3$, $2 \rightarrow 4$ and $3 - 5$ transitions were used after correction for both instrument response and transition rate to determine the vibrational distribution that is shown in Fig. 18. A straight line fit to the data that is forced

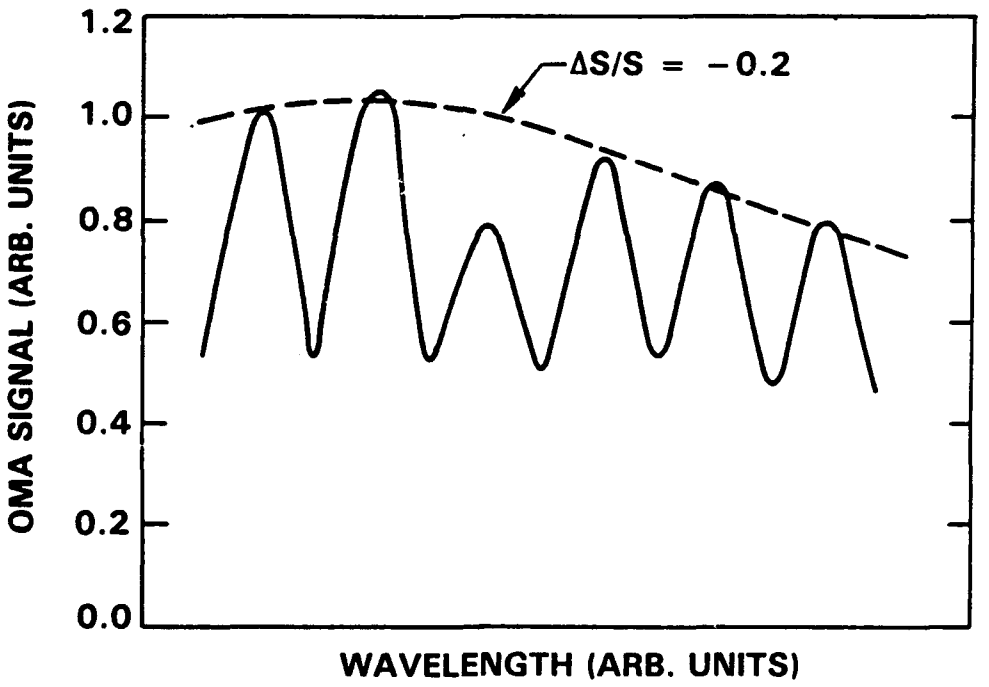

Fig. 17 Expanded section of OMA data showing the absorption of one etalon mode by BiF.

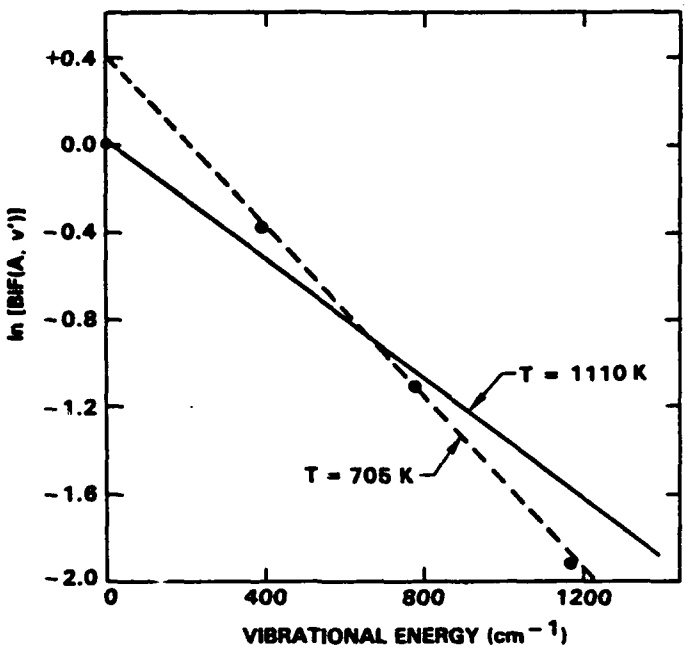

Fig. 18 Determination of temperature from emission data.

to pass through the $v' = 0$ data point, yields a temperature of 1110 K if the slope is adjusted to yield the same total $v' = 0 - 3$ concentration as the data. Deviations from linearity of less than ± 50% magnitude occur at $v' = 1$ and $v' = 3$. On the other hand, a much better straight line fit to the data can be achieved for $v' = 1 - 3$, if a 50% deviation is accepted for the $v' = 0$ state, which yields a somewhat lower temperature of 705 K. Clearly, the vibrational distribution is only approximately Boltzmann and the nature of the deviations from linearity in Fig. 18 suggest that the BiF(A) state is populated at levels higher than the $v' = 0$ state. A third temperature of 950 K was derived from the rate of rise of the NF(a) signal, in the absence of $Bi(CH_3)_3$, using the model that is described in Section 2.2 of this report.

Analysis - In order to calculate the potential for partial inversions on transitions from $v' = 0$ to v'' energy levels greater than zero, it is necessary to assume that the BiF(X) state is characterized by a Boltzmann vibrational distribution with the same temperature as the excited state. The potential for errors in this assumption and in the determination of the temperature are evident in Fig. 18, however, the deviations from linearity are less than the population ratios for adjacent vibrational energy levels. Therefore, the calculation of the v'' energy level at which partial inversion begins is in error by at most one vibrational

quantum. The distribution equations for the vibrational energy levels of the BiF(A) and BiF(X) states are

$$[BiF(A, v')] = [BiF(A, total)]\,(1 - e^{-w_A/RT})\,(e^{-w_A/RT})^{v'} \tag{19}$$

$$[BiF(X, v'')] = [BiF(X, total)]\,(1 - e^{-w_X/RT})\,(e^{-w_X/RT})^{v''} \tag{20}$$

where Jones[30] gives $w_A = 384\ cm^{-1}$ and $w_X = 513\ cm^{-1}$. Using these equations and the measured concentrations of BiF(A, $v' = 0$ and BiF (X, $v'' = 0$), as well as the measured value of the temperature, it is possible to calculate the total concentrations of BiF(A) and BiF(X) as well as the concentrations of BiF(A, v') and BiF(X, v'') for any choice of v' and v''. The total state concentrations are significant to the calibration of scaling relationships to be discussed in the following section and the BiF(X, v'') distribution is important to calculating the gain and loss coefficients that correspond to the present data. We shall calculate results for both T = 700 and 1100 K to illustrate the effects of the uncertainty in regard to temperature.

Table 2 was calculated using Eqs. (19) and (20) and the data that is presented in Figs. 17 and 18. The gain or loss coefficients were calculated from the BiF(A, v') and BiF(X,v'') concentrations and Eq. (15) using x = 2.5 cm. The cross sections, however, were calculated from Eq. (6) using the peak value of n(J) which occurs when

$$(2J + 1)^2 = RT/B \tag{21}$$

in the limit of large values of J. The linewidth (Δv) was taken at the Doppler limit, which is 1.13 GHz for the BiF(A-X) transitions at 1200°K, and scales as the square root of the temperature. The entries in the table correspond to temperatures of 1100 (700) K. The ratio (n_u/n_ℓ) indicates the concentration of the upper state in relation to the lower state for the selected vibrational transition. As can be seen from the table, partial inversions may occur from $v' = 0$ to states as low as $v'' = 2$ depending on temperature, but all transitions from $v' = 0$ to $v'' \geq 4$ are clearly inverted in any case. The associated gain coefficients, even in the best case, however, are too small to be useful. This result occurs because, the Franck-Condon factors in BiF are small for the transitions (with $v' = 0$ and large v'') that are inverted in the present experiment. As the following section will show, this result is a

consequence of the conditions (temperature, NF(a) concentration) under which the experiment was performed rather than any failure of the NF/BiF kinetics.

Table 2

Calculated Gain/Loss Coefficients for Selected BiF(A-X) Transitions

Transition	n_u/n_ℓ	Gain/Pass*
0 → 0	0.12 (0.12)	-0.56 (-0.88) %
0 → 1	0.25 (0.36)	-0.26 (-0.23) %
0 → 2	0.48 (1.06)	-0.05 (+0.00) %
0 → 3	0.96 (3.17)	-0.00 (+0.02) %
0 → 4	1.92 (9.45)	+0.00 (+0.01) %

*Divide by 2.5 for gain/cm.

Scaling Predictions

In this section we develop relations that are anchored to the data reported in Section 3.3, which allow calculation of the expected gain coefficients as a function of NF(a) concentration and temperature. To do this we need a kinetic model that predicts total BiF(A) and BiF(X) concentrations from the NF(a) concentration. Then the gain (G) on any $v' \rightarrow v''$ transition can be calculated from

$$G = \sigma \{[BiF(A,v')] - [BiF(X,v'')]\} x \qquad (22)$$

where x is the gain length and the cross section (σ) is calculated from Eqs. (6), (7), and (20) (assuming Doppler linewidth) while the concentrations of the vibrational energy levels are obtained from Eqs. (19) and (20). The needed kinetic model is developed in the following subsection and is then employed to scale our current results to higher NF(a) or lower temperature conditions where sizeable gain coefficients are predicted.

Kinetic Model - For the purpose of these calculations a simple global model with effective rate constants will be used. In this model, the yield of BiF(X) is taken as proportional to the concentration of $Bi(CH_3)_3$, and it is assumed that BiF(X) is pumped to the BiF(A) state at an effective rate k_e by the initial peak concentration of NF(a), as measured

prior to the addition of the donor species, and the BiF(A) state is lost by spontaneous radiative decay back to the ground state at rate (A).

$$[BiF(A)] \; / \; [BiF(X)] = k_e \; [NF(a)] \; / \; A \qquad (23)$$

is therefore valid at the peak of the BiF(A) time profile. The optimal addition of $Bi(CH_3)_3$ and hence the BiF(X) concentration is itself a function of the NF(a) concentration. Addition of the donor increases the yield of BiF(A) until the quenching induced by the donor, which occurs at a rate proportional to $[Bi(CH_3)_3][NF(a)]$ becomes competitive with the self-annihilation rate, which is proportional to $[NF(a)]^2$. For higher additions of $Bi(CH_3)_3$, the effect of donor quenching begins to outweigh the greater availability of Bi-atoms. Therefore, optimum $[Bi(CH_3)_3]$ and [BiF(X)] both scale in proportion to [NF(a)]. Equation (23), therefore, shows that [BiF(A)] scales as $[NF(a)]^2$ which is the trend that is in fact observed over several decades of NF(a) and BiF(A) concentration,[21] provided that the $Bi(CH_3)_3$ addition is optimized as a function of the NF(a) concentration. Therefore, since we know the functional relationship and have absolutely calibrated results at one point, we can write the equation

$$[BiF(A)] = (2 \times 10^{-19} \; cm^3) \; [NF(a)]^2 \qquad (24)$$

which can be used to quantify the scaling of BiF(A) vs NF(a). Upon calculating the values for BiF(A) and BiF(X), from Eqs. (19) and (20) and the data in Section 3.3, one finds that the left hand side of Eq. (23) has a value of 0.145 ± 0.005 over the temperature range from 700 to 1100 K. This result, together with the NF(a) concentration of $6 \times 10^{15}/cm,^3$ and the value of the A coefficient (7×10^5/s) implies a value for k_e of 1.7×10^{-11} cm^3/s. This result, which corresponds to about one-third of the pump rate derived in Section 2.3, is reasonable since it must take into account the loss of NF(a) due to self-annihilation and byproduct quenching resulting from the addition of $Bi(CH_3)_3$. Combining Eqs. (23) and (24), and inserting the numerical values for k_e and A then yields

$$[BiF(X)] = (8 \times 10^{-3}) \; [NF(a)] \qquad (25)$$

which in combination with Eq. (24) provides the necessary information to support calculation of the expected gain coefficients as outlined above.

Temperature Scaling - Figure 19 shows the calculated gain on the 0 → 2 and 0 → 3 transitions, assuming that total BiF(X) and BiF(A) are maintained at the values that have actually been demonstrated in the present experiment. Therefore, these results do not depend on use of Eqs. (24) or (25). The increase in gain in this case comes solely from the improved vibrational distributions and cross sections that correspond to the lower temperatures. As expected, one finds that the 0 → 3 transition is more tolerant of high temperature, but has less potential gain than the 0 → 2 transition, which has the larger Frank-Condon factor and receives less help from the Boltzmann distribution of the ground state vibrational energy levels. The initial concentration of NF(a) and the temperature regime of interest in this calculation are conducive to the generation of a supersonic mixing laser because the low initial NF(a) concentration prevents the self-annihilation process from competing with the mixing rate and because the gas expansions that are required to lower the temperature are not severe. The reduction of total BiF(A) concentration due to the adiabatic expansion can

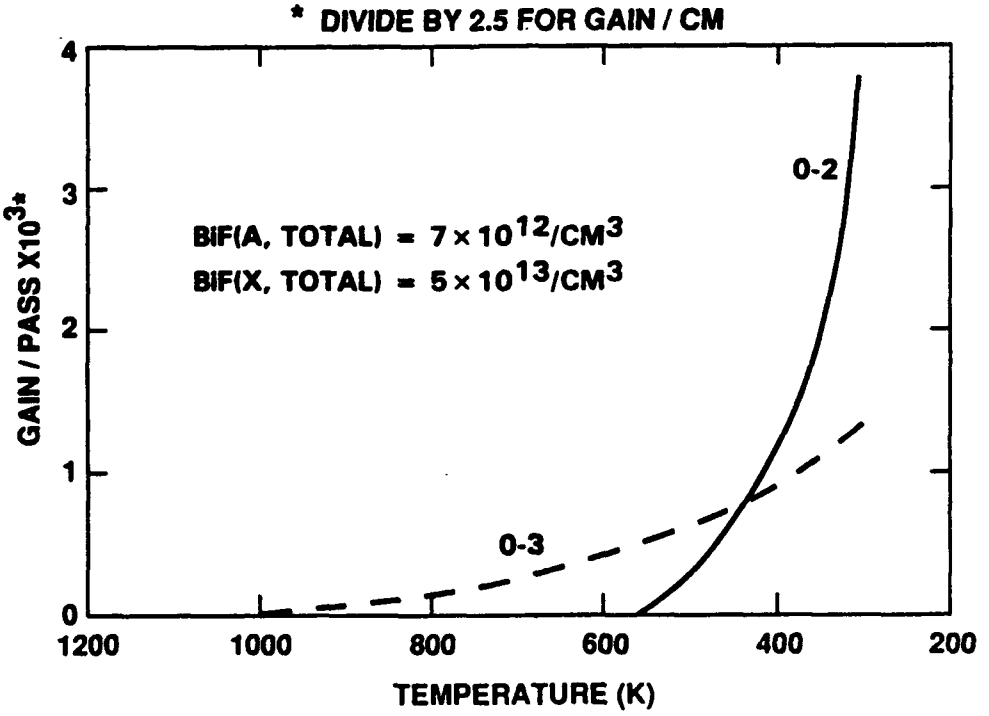

Fig. 19 Calculated gain vs temperature at [NF(a)] = $6 \times 10^{15}/cm^3$.

be compensated by replacing $Bi(CH_3)_3$ with Bi-atoms. Work by Herbelin[21] has shown that such a substitution increases the BiF(A) yield (at fixed NF(a) concentration) by typically an order of magnitude. This result occurs because substitution of Bi for $Bi(CH_3)_3$ eliminates both the dissociation bottleneck and the methyl-related byproduct quenching.

Concentration Scaling - Since lowering the gas temperature is not a practical way to proceed with the present benchtop apparatus and there is room for improving the NF(a) yield in the present benchtop experiment significantly, we used the kinetic model to estimate the gain that could be achieved at high temperature (1200 K) upon increasing the NF(a) concentration from $6 \times 10^{15}/cm^3$ to the previously achieved value of $3 \times 10^{16}/cm^3$. In this case, we found that the highest gain transitions were not always out of the $v' = 0$ state, but rather in some cases out of $v' = 1$. This anomaly occurs because at high temperatures the $v' = 0$ and $v' = 1$ states are nearly equally populated and the $v' = 1$ state has more favorable Franck-Condon factors to higher v'' energy levels which carry less thermal population. Also, the vibrational spacing of the BiF(A) state is smaller than for the BiF(X) state, hence the $1 \rightarrow 4$ transition has a better Boltzmann factor than the $0 \rightarrow 3$ transition, in addition to a superior cross section. In general there was a tradeoff between the n_u/n_ℓ ratios and the potential gains such that the highest gain transition ($0 \rightarrow 2$) had an n_u/n_ℓ ratio less than 2, while transitions such 0 - 4 or 1 - 5 had n_u/n_ℓ ratios greater than ten but significantly lower gain. The $1 \rightarrow 4$ transition was selected as the best compromise with two-thirds the gain of the $0 \rightarrow 2$ transition and an n_u/n_ℓ ratio of approximately five. Maintaining an adequate n_u/n_ℓ ratio is important since it is this factor which creates a margin of safety for errors in the calculation or less than optimal experimental conditions. Figure 20 shows the calculated gain on the $1 \rightarrow 4$ transition at 1200 K as a function of NF(a) concentration. The dashed line shows the sensitivity limit of our current gain diagnostic. Hence, upon improving the NF(a) concentration to previously achieved levels and modifying the experiment to detect gain in the vicinity of 470 nm, a positive gain signal is expected. Higher NF(a) concentrations can be achieved in the present experiment by using a row of hypodermic needles (inside the FN_3/SF_6 duct) to add the $Bi(CH_3)_3$ flow (in place of the annular duct) so that prereaction is still eliminated but the reaction zone is returned to its original dimensions.

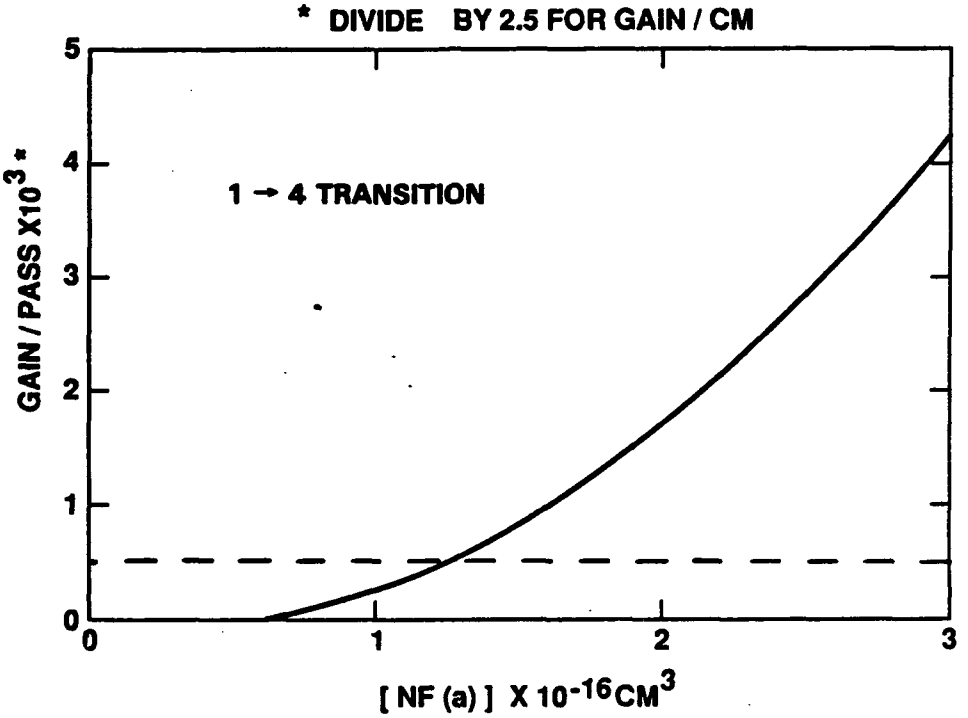

Fig. 20 Calculated gain vs [NF(a)] at a temperature of 1200 K.

CONCLUSIONS AND RECOMMENDATIONS

The results obtained in the course of this contract have shown that thermal dissociation of FN_3 can be used to generate adequately high concentrations of NF(a) metastable species to power a high energy laser. Moreover, the coupling of this new metastable generator to an extraction scheme involving formation of BiF(A) is shown to be a feasible method of generating adequate gain at visible wavelength. Clearly, the laser will operate better if the $Bi(CH_3)_3$ donor is replaced by Bi-atoms, however, the feasibility of a laboratory scale demonstration of lasing or gain using the organometallic donor is also established.

In order to reduce risk and advance this laser concept we recommend continued work using a sensitive gain diagnostic to probe the BiF(X) ground state in greater detail. An immediate goal should be to establish a positive gain signal by measuring the $1 \rightarrow 4$ transition at high NF(a) concentration. Subsequent work should concentrate on establishing the vibrational distribution of the BiF(X) ground state and determining the vibrational relaxation rates, since these unknown parameters directly influence the ability of the laser to maintain an inversion under the load of stimulated emission at a rate that is competitive with the spontaneous decay of the BiF(A) state. In any case, the government will have to devote substantial effort to the design of fast mixing nozzles, since the kinetic lifetime of NF(a) is limited at high concentration due to the self-annihilation reaction. For this reason, additional work should also be done to determine the mechanism and temperature dependence of this dominant loss mechanism for NF(a).

If the remaining issues are resolved satisfactorily, then it will be appropriate to begin considering demonstration projects that will establish the high energy capabilities of the NF/BiF laser system. Since all of the risk issues have not yet been fully resolved, however, we also recommend that the government invest some of its resources in the development of alternatives to BiF which do not have highly vertical potential energy curves which optimize the gain cross sections on the transitions that are the most difficult to invert. In the IF(B-X) system for example, the potential curves are displaced and the gain is optimized on transitions to the $v'' \sim 6$ energy levels that are not thermally populated.[32] Therefore, efforts to couple the FN_3 source of NF(a), which requires high temperatures, to the IF(B-X) laser transitions may be highly profitable.

REFERENCES

1. T.A. Seder, D.J. Benard and R.H. Cohn, "Model Studies of CBES Decomposition," Air Force Astronautics Laboratory (Edwards AFB, CA) Final Report AL-TR-89-076 (February, 1990); and D.J. Benard and R.H. Cohn, "Model Studies of CBES Decomposition," Air Force Astronautics Laboratory (Edwards AFB, CA) Interim Report AFAL-TR-87-071 (February, 1988).

2. D.J. Benard, B.K. Winker, T.A. Seder and R.H. Cohn, "Production of $NF(a^1\Delta)$ by Dissociation of Fluorine Azide," J. Phys. Chem. 93 (1989) 4790.

3. B.K. Winker, D.J. Benard and T.A. Seder, "Chemical Pumping of Potential Visible Laser Transitions in Bismuth Monofluoride by Thermal Dissociation of Fluorine Azide," Proceedings of the SPIE Symposium on High Power Gas Lasers (Los Angeles) 1225 (1990) 543.

4. J.F. Haller, "A Study of the Preparation, Structure, Properties and Decomposition of Azine Fluoride and of Difluorodiazene," Ph.D. Dissertation, Cornell University (Ithaca, NY) 1942.

5. C.R. Quick and C. Wittig, "Time-Resolved HF Vibrational Fluorescence from the IR Photodissociation of SF_6/H_2 Mixtures," Chem. Phys. Letters, 48 (1977) 420; and M. Lenzi, E. Molinari, G. Piciacchia, V. Sessa and M.L. Terranova, "A Kinetic Study of Infrared Multiple Photon Absorption in SF_6-Noble Gas Mixtures During a TEA CO_2 Laser Pulse," Chem. Phys. 142 (1990) 473.

6. E. Quinones, J. Habdas and D.W. Setser, "Gas-Phase Chemistry of $NF(a^1\Delta)$: Quenching Rate Constants," J. Phys. Chem. 91 (1987) 5155.

7. J.M. Herbelin and R.A. Klingberg, "Efficient Production of Electronically Excited $BiF(AO^+)$ via Collisions with $NF(a^1\Delta)$," Int. J. Chem. Kinetics, 16 (1984) 849.

8. J.B. Koffend, Aerospace Corporation (El Segundo, CA) private communication.

9. H.H. Michels and J.A. Montgomery, United Technologies Research Laboratory (E. Hartford, CT) results reported under Contract F04611-86-C-0071 to the Air Force Astronautics Laboratory (Edwards AFB, CA).

10. M.W. Chase, et al. "JANAF Thermochemical Tables" (Third Edition) J. Phys. Chem. Ref. Data 14 (1985) Supplement No. 1, Parts 1 and 2.

11. D. Patel, A.T. Pritt and D.J. Benard, "Photolysis of FN_3 at 193 nm," J. Phys. Chem. 90 (1986) 1931.

12. H.H. Michels, United Technologies Research Center (E. Hartford, CT) private communication.

13. D.W. Setser, Kansas State University (Manhattan, KA) private communication.

14. D.W. Trainor, "Collisional Relaxation of Electronically Excited Bismuth: $6p^3(^2D_{3/2})$ and $6p^2(^2D_{5/2})$," J. Chem. Phys. 66 (1977) 3094.

15. B. Rosen, "Selected Constants Relative to Diatomic Molecules" (Pergammon Press, 1970).

16. J.M. Herbelin, Aerospace Corporation (El Segundo, CA) private communication; and G.A. Capelle, D.G. Sutton and J.I. Steinfeld," Near Resonant Electronic Energy Transfer from $NF(a^1\Delta)$ to Bi," J. Chem. Phys. 69 (1978) 5140.

17. R.F. Heidner, H. Helvajean, J.S. Holloway and J.B. Koffend, "$BiF(AO^+,v')$ Radiative Lifetimes and Rate Coefficients for V-T Transfer and Electronic Quenching," Aerospace Corporation (El Segundo, CA) Technical Report SD-TR-87-19 (April, 1987).

18. M. Stanek, K. Musiol and S. Labuz, "Experimental Determination of Transition Probabilities in Bi I and Bi II," Acta Physica Polonika, A59 (1981) 239.

19. J.B. Koffend and R.F. Heidner, "Time-Resolved Kinetics of the NF*-BiF* Candidate Chemical Laser System," Aerospace Corp. (El Segundo, CA) Technical Report No. TOR-0086(6604)-1 (September, 1986).

20. J. Connor, P.J. Young and O.P. Strauz, "Flash Photolysis of Trimethylantimony and Trimethylbismuth and the Quenching of Excited Antimony and Bismuth Atoms," J. Am. Chem. Soc. 93 (1971) 822; and S.J.W. Price and A.F. Trotman-Dickenson, "Metal Carbon Bonds: Part 3 - The Pyrolysis of Trimethyl Bismuth, Trimethyl Antimony and Dimethyl Tin-Dichloride," Trans. Faraday Soc. 54 (1958) 1630.

21. J.M. Herbelin, Aerospace Corp. (El Segundo, CA) White Paper "Scaling of the NF(a)/BiF Reaction System to a CW Supersonic Laser" (July, 1988).

22. J.M. Herbelin, D.J. Spencer and M.A. Kwok, "Scale-Up of $NF(a^1\Delta)$ Produced by the $H + NF_2$ System in a Subsonic CW Laser Device," J. Appl. Phys. 48 (1977) 3050.

23. I.A. Brovko et al., "Kinetics of Thermal Decomposition of Bismuthine on a Graphite Tube," Uzh. Khim. Zh. 1 (1985) 25.

24. E. Amberger, "Hydride des Wismuts," Chem. Ber. 94 (1961) 1447.

25. D.J. Benard, M.A. Chowdhury and A.T. Pritt, "Quenching of NF Singlet States in a Hybrid Chemical Laser System," J. Appl. Phys. 60 (1986) 4051.

26. T. Nakahara, "Different Procedures of Bismuthine Evaluation for Hydride Generation-Nondispersive Atomic Fluorescence Spectroscopy of Bismuth," Bunko Kekyu 32 (1983) 334; and E.J. Weeks and J.G.F. Druce, "Bismuth Dihydride," J. Chem. Soc. 127 (1925) 1799.

27. B.F. Foresti and M. Moscavitti, "Use of Oscillating Discharges in the Formation of Some Gaseous Hydrides," Gazz. Chem. Ital. 60 (1930) 745.

28. D.C. Reamer, C. Veillon and P.J. Tokosbalides, "Radiotracer Techniques for Evaluation of Selenium Hydride Generation Systems," Anal. Chem. 53 (1981) 245.

29. K. Gholivand, G. Schatte and H. Willner, "Properties of Triazadienyl Fluoride: N_3F," Inorg. Chem. 26 (1987) 2137.

30. W.E. Jones and T.D. McLean, "The Electronic Spectrum of Bismuth Monofluoride: A Reinvestigation of the $AO^+ - X_1O^+$ System," J. Mol. Spectr. 80 (1981) 481.

31. T.W. Hansch, "Repetitively Pulsed Tunable Dye Laser for High Resolution Spectroscopy," Appl. Optics, 11 (1972) 895.

32. S.J. Davis and L. Hanko, "Optically Pumped Iodine Monofluoride $B^3\pi(O^+) - X^1\Sigma^+$ Laser," Appl. Phys. Letters, 37 (1980) 692.

APPENDIX

This section contains reprints of three publications which relate to safe lab scale generation[1] of FN_3 gas, thermally-induced dissociation[2] of FN_3 to yield NF(a) and pumping of the BiF(A-X) lasing transition[3] by NF(a) obtained from thermal dissociation of FN_3. The key results from these papers are summarized in the second section of this report. The papers were published by AFAL, the Journal of Physical Chemistry and SPIE, respectively. Only the relevant pages from the AFAL publication (on FN_3 generation) have been reproduced. The remainder of the paper deals with the preparation and detonation spectroscopy of thin cryogenic films of FN_3 (condensed from the gas phase) as a means to investigate its propellant applications. This related work is covered in detail in a parallel final report.[1]

EXPERIMENTAL DETAILS

The following subsections contain information relative to the safe generation of FN_3 gas, the reproducible formation and detonation of FN_3 films and the detection system employed to gather the resulting emission spectra. In developing the apparatus, some specialized electronic circuits were required to accomplish certain control and timing functions. The operation of these circuits can be appreciated only with a suitable background in electrical engineering. Therefore, the principles relating to their design will not be discussed. Schematics of the circuits are given, however, in sufficient detail to allow easy replication. The designs are noncritical with respect to layout, tolerance of components and supply voltage.

Safety Considerations

Before proceeding, we feel it important to warn potential experimenters that FN_3 is a chemical which deserves much respect. Its energy storage per unit mass is twice that of TNT and it is highly sensitive in its liquid state. Haller reports that the explosions of FN_3 were very brissant, that it was harder to keep liquid FN_3 from detonating than not, and that detonation of as little as one drop of FN_3 pulverized glassware up to 25 cm away and at closer distances drove small pieces of glass through 24 gauge steel. Haller also noted that slight mechanical vibration or simple evaporation of the liquid were sufficient to cause detonation of FN_3.[1] From our own experiments, we can say that Haller did not exaggerate. In our laboratory, detonations of microscopically thin films of FN_3 have cracked 0.25 in. thick substrates of both CaF_2 and SiO_2.

To handle FN_3 safely, particular care must be exercised to prevent condensation of any significant quantity of the liquid or reaction of the FN_3 gas with other materials. Haller reports that FN_3 gas is adsorbed irreversibly on KF at room temperature to form a compound that explodes upon heating[1] and we have found that passage of FN_3 gas over copper generates an explosive film, most likely copper azide. By keeping the FN_3 concentrations below 10 torr, using only glass, teflon or stainless steel for construction, and avoiding condensation except of microscopically thin films, we were able to prevent accidental explosions, although flashbacks were occassionally

observed in teflon lines carrying the FN_3 gas. Nonetheless, we recommend the use of blast shields, sand fills, barracades and other safety features, as discussed in the following subsection.

The HN_3 that is produced as an intermediate to the generation of FN_3 has similar explosive tendencies and requires equal attention to safety.[8] Procedures for handling NaN_3, used as a starting material, are available from the manufacturer.[9] While less energetic that FN_3 or HN_3, NaN_3 is still an exothermic material that is capable of spontaneous decomposition if activated by excess heat or friction. Also, NaN_3 can react with acids to form HN_3 and with metals to form explosive metal azides. All azides are highly toxic, thus care must be taken to prevent exposure. Finally, the use of even dilute F_2 can be hazardous if handled improperly. Instructions for the safe use of F_2 are typically available from the manufacturer.[10]

Synthesis of Fluorine Azide

Fluorine azide was synthesized in a continuous manner using the method of Haller,[1] by reacting HN_3 with F_2, with some variations, as shown in Fig. 2. The HN_3 was generated by the thermally activated reaction of NaN_3 with stearic acid[11] rather than dilute H_2SO_4. This approach had the advantage of producing a bone-dry flow of HN_3 in contrast to the sulfuric acid reaction which requires a downstream trap to remove water vapor. From previous experiments using the sulfuric acid technique, we found that explosive compounds built up around metal fittings between the HN_3 generator and a trap that was filled with $CaSO_4$. We also noticed that the $CaSO_4$ significantly attenuated the HN_3 flow which raised the possibility of explosive compound formation in the trap. Finally, we found that the NaN_3-stearic acid reaction was smoother, more predictable and easier to clean up safely than the sulfuric acid technique.

<u>HN_3 Generator</u> - Figure 3 is a cross sectional view of the HN_3 generator assembly. A 2-liter Kimax reaction kettle containing the NaN_3 and stearic acid was supported inside a 400 W electric deep fat fryer by a stainless steel support structure. The pot was filled with cooking oil whose temperature (T_1) was measured by a metal band thermometer. Stainless steel cooling coils in the annulus between the reaction kettle and the pot were

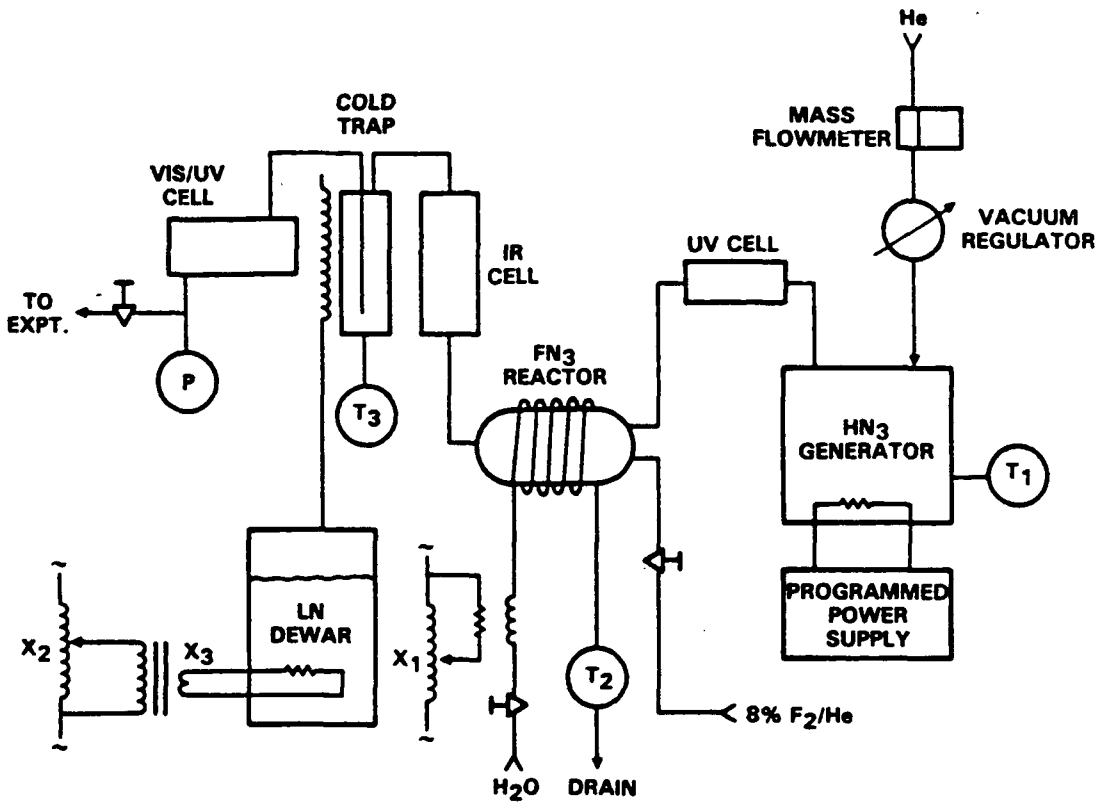

Fig. 2 Schematic of apparatus for synthesis of FN_3 gas.

also attached to a source of tap water. Water was admitted to this structure only for the purpose of cooling the oil to stop the NaN_3-stearic acid reaction in an emergency or at the end of a day's run. A heavy stainless steel lid, atop the reaction kettle, was sealed to the ground glass mating surface of the kettle by an O-ring. The He carrier gas entered the reaction kettle via an electronic mass flowmeter, a vacuum regulator and the steel lid, mixed with the evolving HN_3 inside the kettle and exited via a second line through the lid. The regulator was set to maintain 350 torr absolute pressure inside the kettle and the He flow was approximately 3.5 sccs. Also, atop the lid, a 1 RPM gear motor with 600 in. oz. torque rating was mated to a teflon lined paddle inside the kettle via an O-ring seal on the shaft. Operation of the HN_3 generator without stirring caused the HN_3 yield to fall off quickly, which raised concerns about potential buildup of high HN_3 concentrations in the stearic acid melt and the possibility of explosion. The entire HN_3 generator assembly was operated inside an 0.25 in. thick lexan blast shield located inside a conventional fume hood.

<u>FN_3 Generator</u> - Contrary to Haller's thesis,[1] we found copper to be incompatible with FN_3 in that mixing of HN_3 and F_2 over copper shot produced very little FN_3, but the shot became coated with a greenish layer which exploded when struck forcefully with a hammer. Therefore, the FN_3 was formed inside an 0.6 liter stainless steel cylinder packed with 0.25 in. dia. stainless steel balls. The HN_3/He flow was admitted to this reactor along with an adjustable flow of 8 - 10% F_2 in He through a nozzle which prevented rapid mixing of the reagents. A copper tube carrying resistively-heated tap water was soldered onto the exterior of the steel cylinder to maintain the reactor at constant temperature. The water was heated by passage over a brass block in which two 1000 W cartridge heaters were inserted and connected in parallel to a Variac (X_1) The temperature of the water (T_2) was measured by a metal band thermometer as it exited from the reactor to a drain. Consistent with Haller's work, we found that the highest FN_3 yields were obtained at 35°C with substantial reduction below 20°C or above 50°C.

<u>Cold Trap</u> - Downstream of the secondary reactor, the gas stream was passed through a cold trap to remove the HF by-product of the FN_3 and any residual HN_3. Early experiments which utilized a NaF trap were discontinued because the FN_3 was severely attenuated which raised the possibility of eventual detonation. The cold trap was

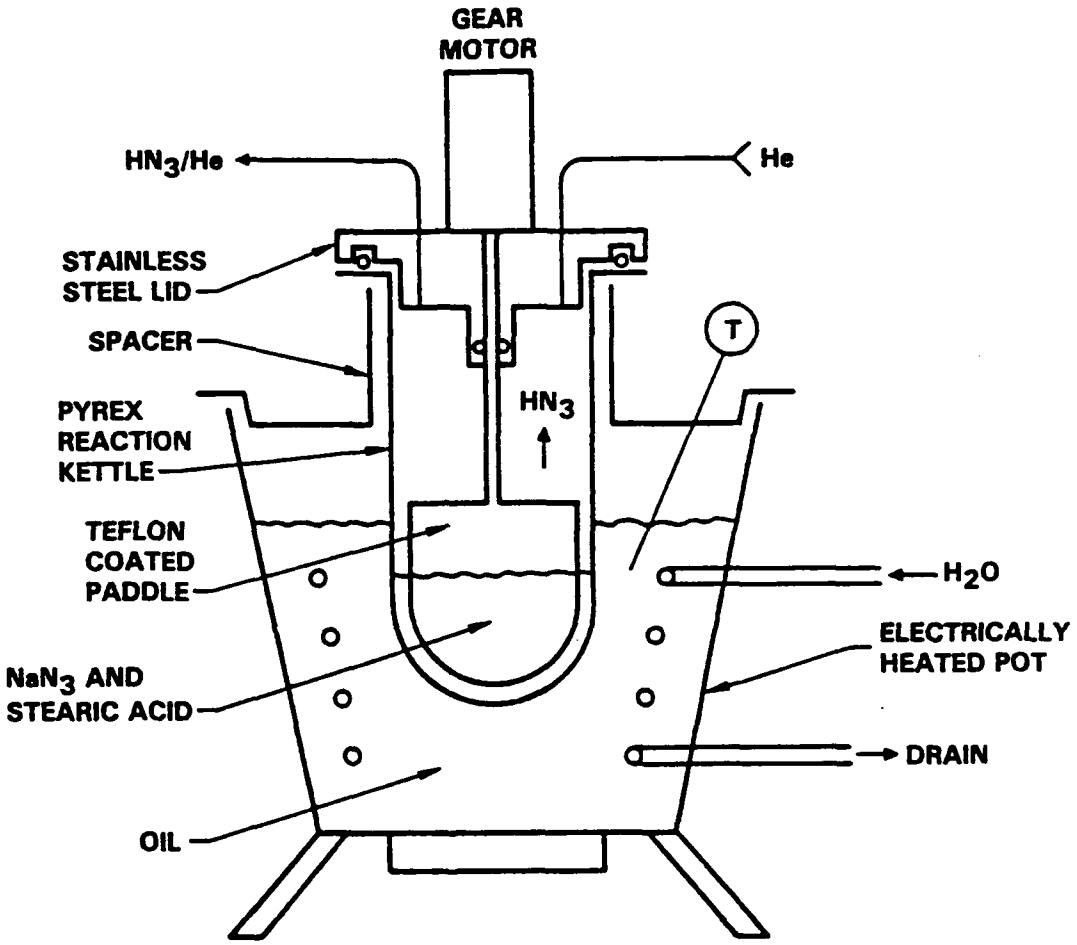

Fig. 3 Detailed view of HN_3 generator.

constructed of a 0.3 liter stainless steel cylinder with a dip tube and 1/4 in. stainless steel balls in the bottom third. A copper cooling coil soldered to the exterior of the trap was connected via insulted lines to a sealed 5 liter liquid nitrogen dewar. Two 50 W, 10 Ω power resistors in the bottom of the dewar were used to boil off gaseous nitrogen at 77 K to cool the trap remotely. The lid of the dewar was spring loaded so that it would lift off and relieve pressures in excess of 6 psig. The temperature at the base of the trap (T_3) was monitored via a thermocouple gauge and meter. The resistive heater for the liquid nitrgen dewar was powered by a Variac (X_2) and a 120 to 24 V stepdown transformer (X_3) rated at 100 W. Since unintentional condensation of either HN_3 or FN_3 in the trap could lead to detonation, the trap was buried in sand inside an aluminum cylinder with 1 in. thick walls, inside a 1/4 in. thick lexan blast shield. The sand was kept dry by a continuous purge of N_2 through the base of the aluminum cylinder. With this arrangement, trap temperatures of -100°C could be maintained for approximately 1 h with a single fill of liquid nitrogen in the dewar.

UV Cell - Absorption cells were inserted in the lines following the HN_3 and FN_3 reactors and the cold trap as diagnostics. The first cell, located after the HN_3 generator was operated at 253.7 nm using a Hg lamp as the source. The intensity of the lamp was attenuated by passage through a pinhole and the lamp supply was driven from a 60 W constant voltage harmonic neutralized transformer to prevent variations in lamp intensity with changes in the line voltage. The probing radiation was directed through a 1/2 in. dia. by 25 cm stainless steel cell (containing the HN_3/He flow) with quartz windows at either end. Opposite the end with the lamp, the probing radiation was detected through a Hg resonance line interference filter by a 1P28 photomultiplier tube. With no HN_3 in the cell, a bias of approximately 750 V generated a steady photocurrent of 100 μa. Under normal operating conditions, the HN_3 in the cell attenuated the probing ultraviolet radiation so that the photocurrent was typically reduced to 25 - 50 μa, depending on the temperature of the HN_3 generator. Based on the known extinction coefficient[12] of HN_3 at 253.7 nm, this result corresponds to an HN_3 yield of 2-4% relative to the flow. This diagnostic provided continuous monitoring of the HN_3 generator that was independent of the other reactions occurring further downstream.

Preliminary experiments tested the operation of the HN_3 generator using a similar absorption cell of commercial design with a D_2 lamp source. Initially, the generator was charged with 2.0 moles of stearic acid (approximately half the volume of the reaction kettle) and 0.5 moles of NaN_3. As shown in Fig. 4, application of constant heater power (by a Variac) produced an exponential approach to a constant temperature over several hours. At the same time, the yield of HN_3 (as measured by absorption) was found to initially increase with the rising temperature and then fall off as the NaN_3 was reacted to completion. The flow rate of gas through the reactor was controlled by a downstream metering valve which exhausted to a vacuum. Therefore, since the generator pressure was regulated, the total gas flow through the metering valve was constant. Consequently, as HN_3 gas was evolved, less He flow was required to maintain the pressure in the reactor. The generation rate of the HN_3 could therefore be monitored by the change of He flow through the mass flowmeter as well. Unfortunately, as the absorption signal began to drop at long times, the change in He flow continued to increase demonstrating that a gas other than HN_3 was also being produced in the reaction kettle. It was theorized that the gas was CO_2 resulting from second order reactions of the sodium stearate produced in the melt as a by-product of HN_3. To test this hypothesis, the experiment was repeated with the NaN_3 charge reduced to 0.1 mole, to reduce the concentration of sodium stearate that was built up. The flow rates of the He carrier gas were adjusted in th two experiments to give approximately the same HN_3/He ratio in either case so that the HN_3 yield could be measured by the same absorption diagnostic. As shown in Fig. 5, reducing the NaN_3 mole fraction had the intended effect. Therefore, the reduced NaN_3 charge was used in all subsequent experiments.

IR Cell - Following the FN_3 generator, the gas was passed through an infrared absorption cell. The function of this cell was to detect residual HN_3 without being affected by FN_3 or HF that might also be present. Haller[1] found that excess F_2 reacted slowly with FN_3 to yield NF_3 and N_2. Consequently, the FN_3 yield peaks when the HN_3 and F_2 flows are titrated. Also, it was undesirable to condense residual HN_3 in the cold trap. Therefore, a residual HN_3 diagnostic was required. The 3.0 μm infrared wavelength was selected for this diagnostic on the basis of the known infrared spectra of FN_3, HF and HN_3, since none of these gases absorb at visible wavelengths, except FN_3, and at ultraviolet wavelengths HN_3 and FN_3 are indistinguishable.[3,6,13]

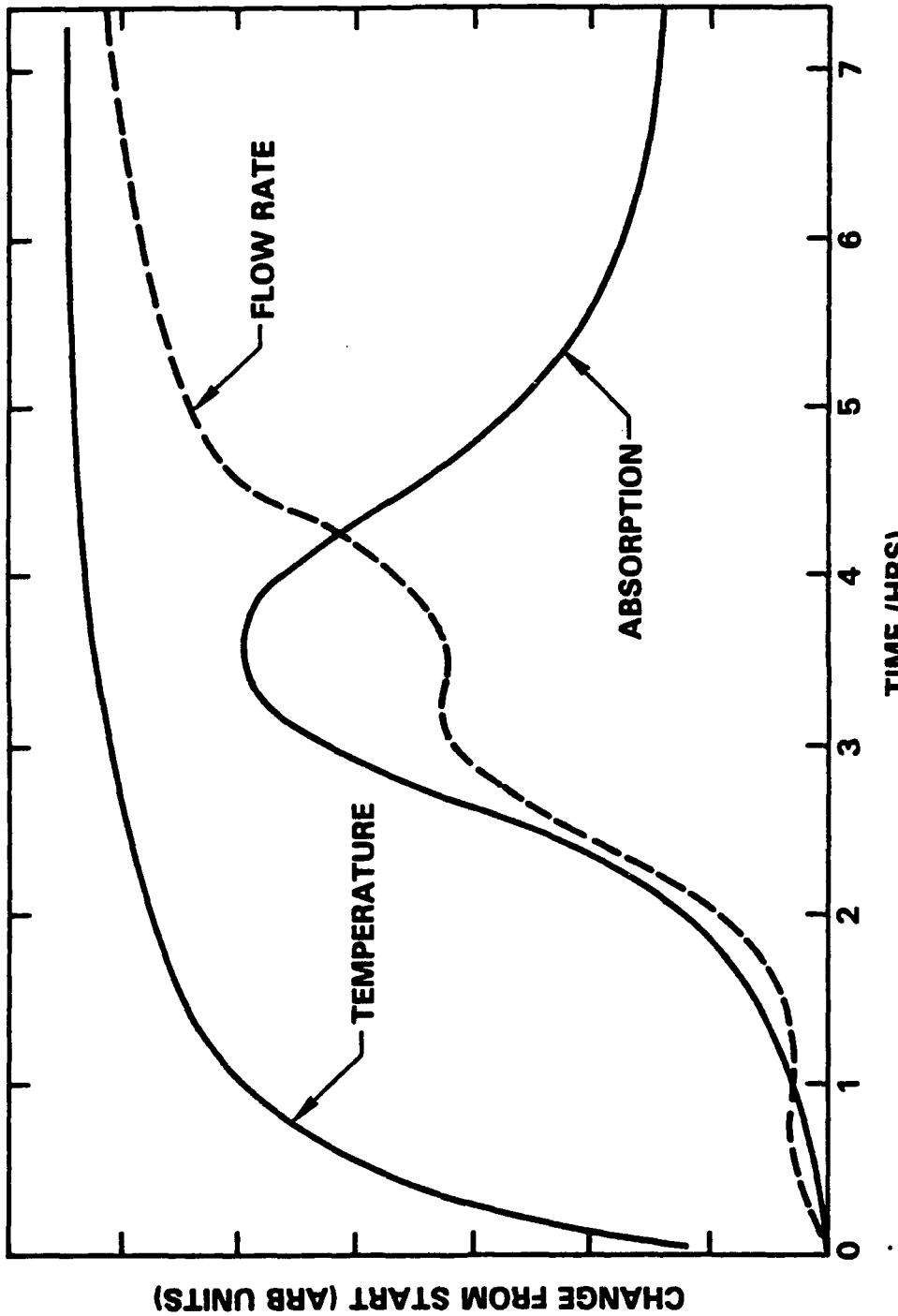

Fig. 4 Temporal behavior of HN_3 generator with constant heater power and 0.5 moles NaN_3 with 2.0 moles stearic acid.

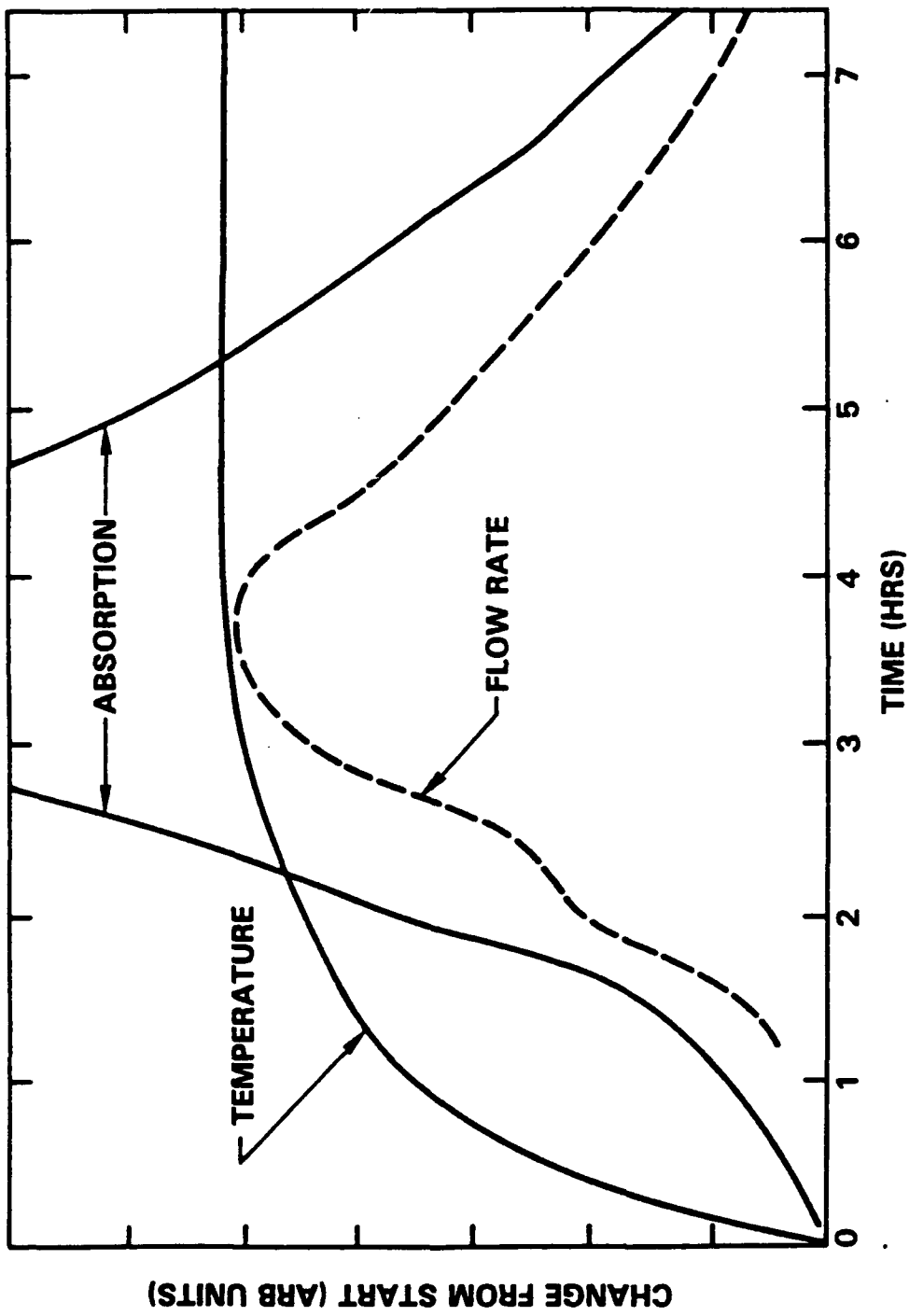

Fig. 5 Temporal behavior of HN_3 generator with constant heater power and 0.1 moles NaN_3 with 2.0 moles stearic acid.

The infrared diagnostic, shown in Fig. 6, was constructed of a 19 mm O.D. × 100 cm long Suprasil quartz tube with sapphire windows at either end. The radiation source was a 900°C (temperature regulated) blackbody with a 3 mm dia. aperture. A 1 KHz mechanical chopper was interposed between the blackbody and the entrance to the absorption cell. At the opposite end of the cell, the radiation was analyzed by an interference filter (60 nm FWHM) and detected by a room temperature 0.4 × 0.4 cm^2 PbSe chip located inside an aluminum box. The detector was biased at 75 V and the photocurrents were passed to a lock-in amplifier via a 2 pole R-C bandpass filter to limit out of band noise. The lock-in amplifier was referenced to the chopper and typically 100 μV signals were recovered to S/N ≥ 10 with 10 s of integration.

The amplitudes of the detected signals, however, were found to be sensitive to variations in the temperature of the detector chip. It was therefore necessary to stabilize the temperature of the detector. A copper plate carrying a resistive heater, a temperature sensing element and a small expansion nozzle was fit to the back of the aluminum box which surrounded the detector and the entire detector box was encased by fiberglass insulation. Application of 60 psig CO_2 to the nozzle produced a steady cooling action which was counteracted by the heating of the resistor. The feedback circuit shown in Fig. 7 was then employed to adjust the resistor current so that the temperature sensor was held at a constant level. The circuit was adjusted to balance at close to room temperature and the test point was monitored with a voltmeter to check the feedback stability. From the amplitude and the frequency of the stable oscillation of the test point about its mean value, it was possible to calculate that the temperature variation at the sensor was less than ± 0.1°C. Application of the temperature stabilizing circuit cured the drifts in the measurement that were caused by the variations of the room temperature.

The infrared diagnostic was tested by operating it in series with a commercial ultraviolet absorption cell (D_2 lamp) and the HN_3 generator; the results are shown in Fig. 8. Clearly, the infrared and ultraviolet diagnostics track the same species, but while the infrared diagnostic is noisier, it shows less baseline drift than does the measurement at the ultraviolet wavelength. The baseline drift of the ultraviolet measurement was traced to adsorption of HN_3 on the cell widnows which typically would recover under vacuum overnight.

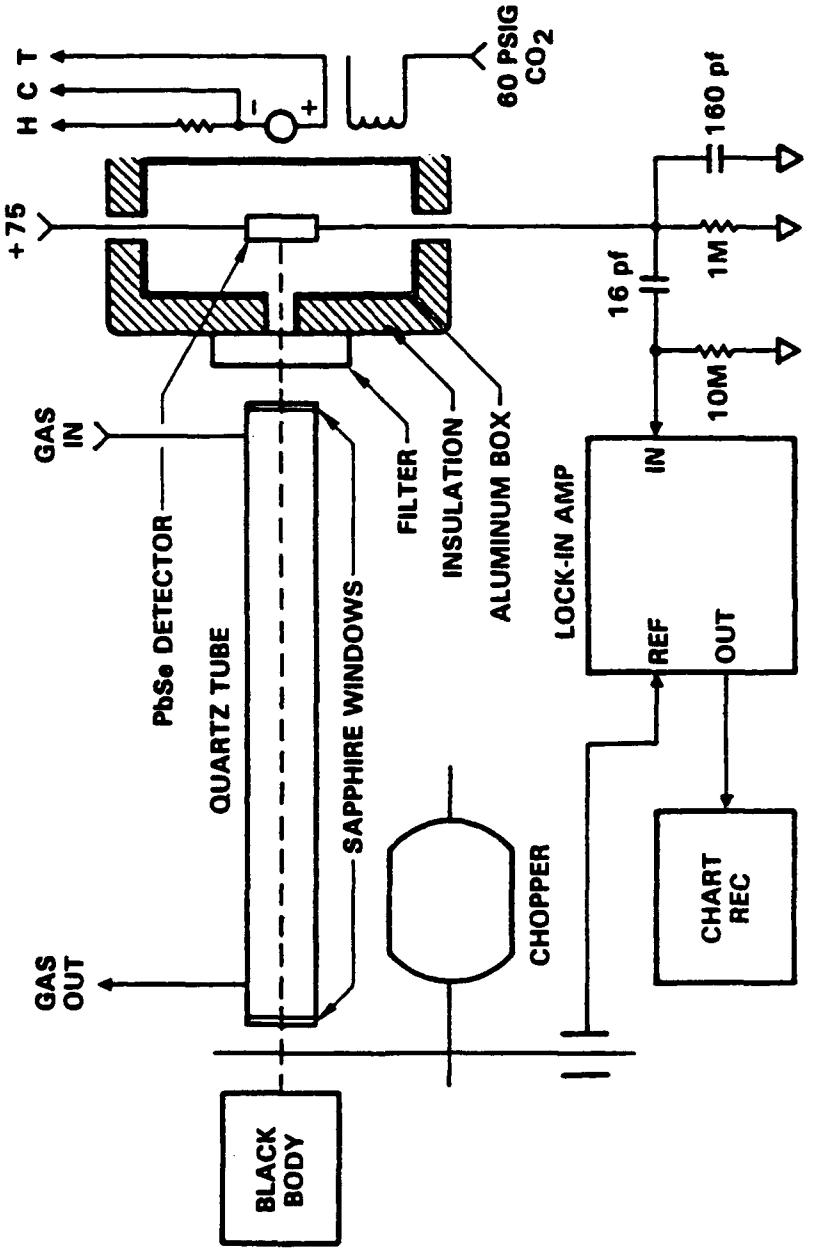

Fig. 6 Schematic of infrared absorption diagnostic.

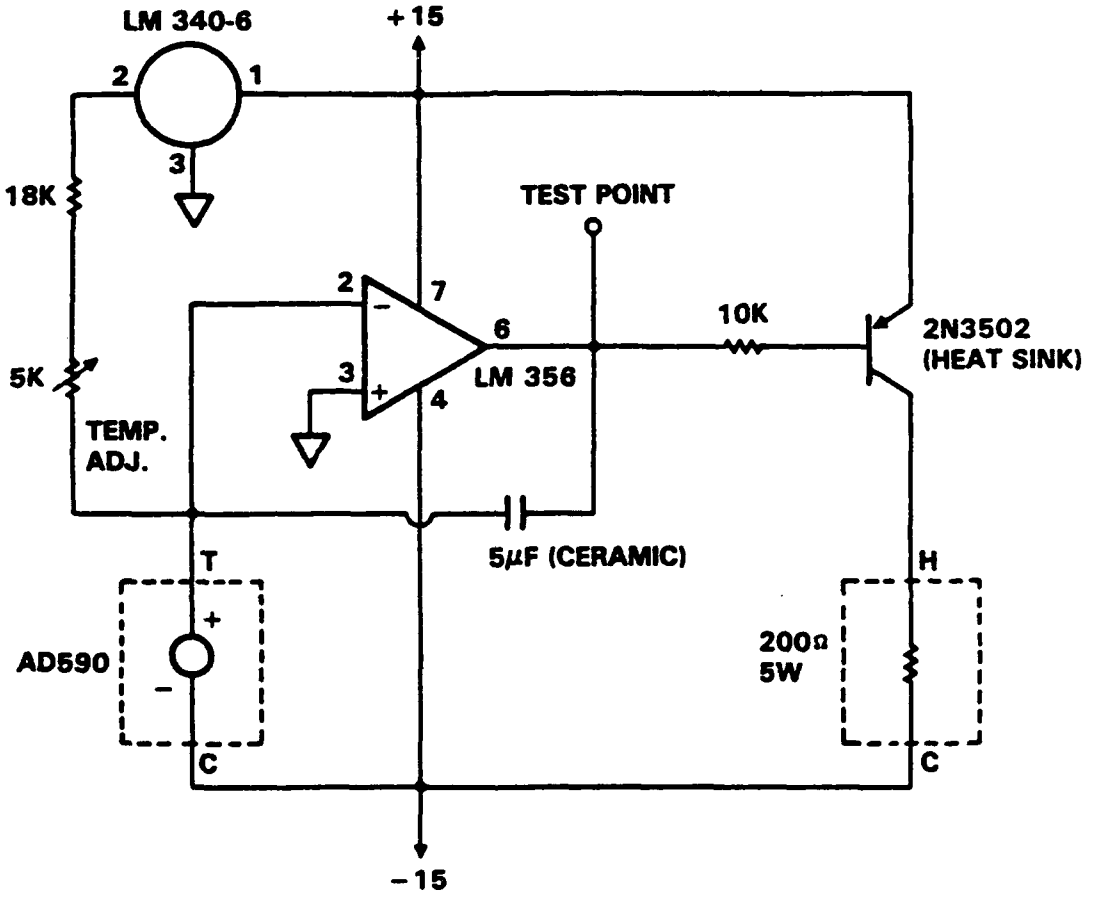

Fig. 7 Feedback circuit for temperature stabilization of PbSe detector.

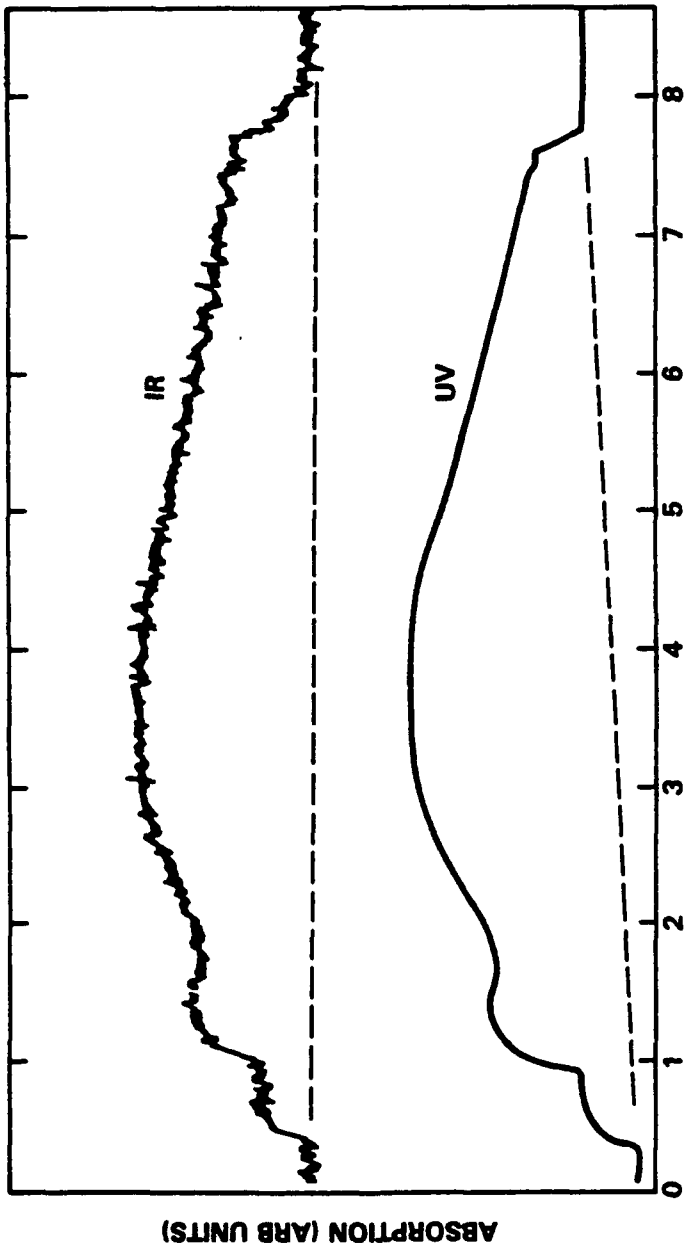

Fig. 8 Comparison of infrared and ultraviolet absorption diagnostics with constant heater power.

Programmed Power Supply - The time profiles of the HN_3 yield shown in Figs. 4, 5 and 8 were still problematical with respect to variation of the yield during the course of the experiments, since continuous adjustment of the F_2 flow was required to maintain an optimal titration with the HN_3 flow. Therefore, the circuit shown in Fig. 9 was employed to program the power to the oil bath of the HN_3 generator in such a way as to counteract the variation of the HN_3 yield. The circuit operates by switching the heater on and off and by slowly varying the duty cycle. The circuit is designed to operate at full power, a constant reduced power and at a power level that linearly increases with time according to the selector switch. Initially, the power is set to full until the oil bath reaches a specified temperature (~ 160°C) and then the circuit is switched to reduced power for typically 3 h. During this time, the temperature falls to a constant level near 100°C and the HN_3 generation rate builds up in a rather complicated, but nonetheless reproducible manner, due to the melting of the stearic acid. Following this, the HN_3 yield would begin a slow linear decline if the power was held constant. Instead, the supply circuit is switched to ramp the power linearly with time over the next 4 h. The increasing temperature accelerates the generation of HN_3 with time, resulting in the near constant HN_3 yield that is evident in Fig. 10 from 4 - 7 h into the run.

The internal controls of the power supply must, of course, be adjusted to produce the temperature vs time curve that is shown in Fig. 10 to achieve the desired result. The adjustments are as follows: (1) controls the cycle rate and should be set for a 60 s cycle period; (2) controls the continuity of the transition from low power to ramped power; (3) controls the low power setting; and (4) controls the amplitude of the ramp. These controls can be set relatively quickly by trial and error using a voltmeter to measure the control voltages and linear extraoplation to predict the desired result from two or more runs. Once set, the stabilized production of HN_3 is quite reproducible if sufficient care is given to precise loading of the generator, the initial heating peak and the time of switchover to ramped power. The use of high heat at early times accelerates the melting of the stearic acid and has a profound effect on the HN_3 time profile thereafter.

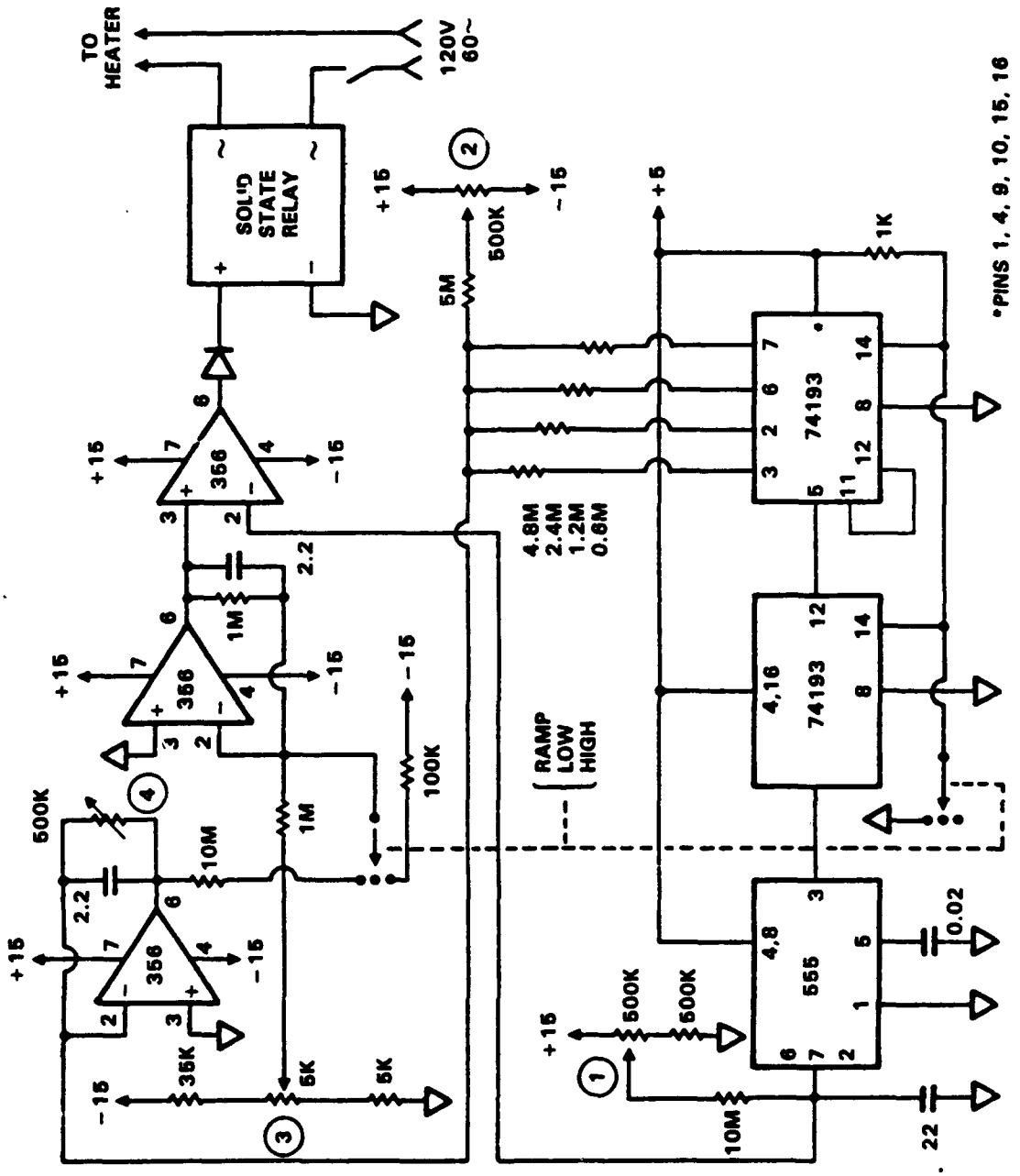

Fig. 9 Schematic of programmed power supply used to stabilize HN_3 generation rate.

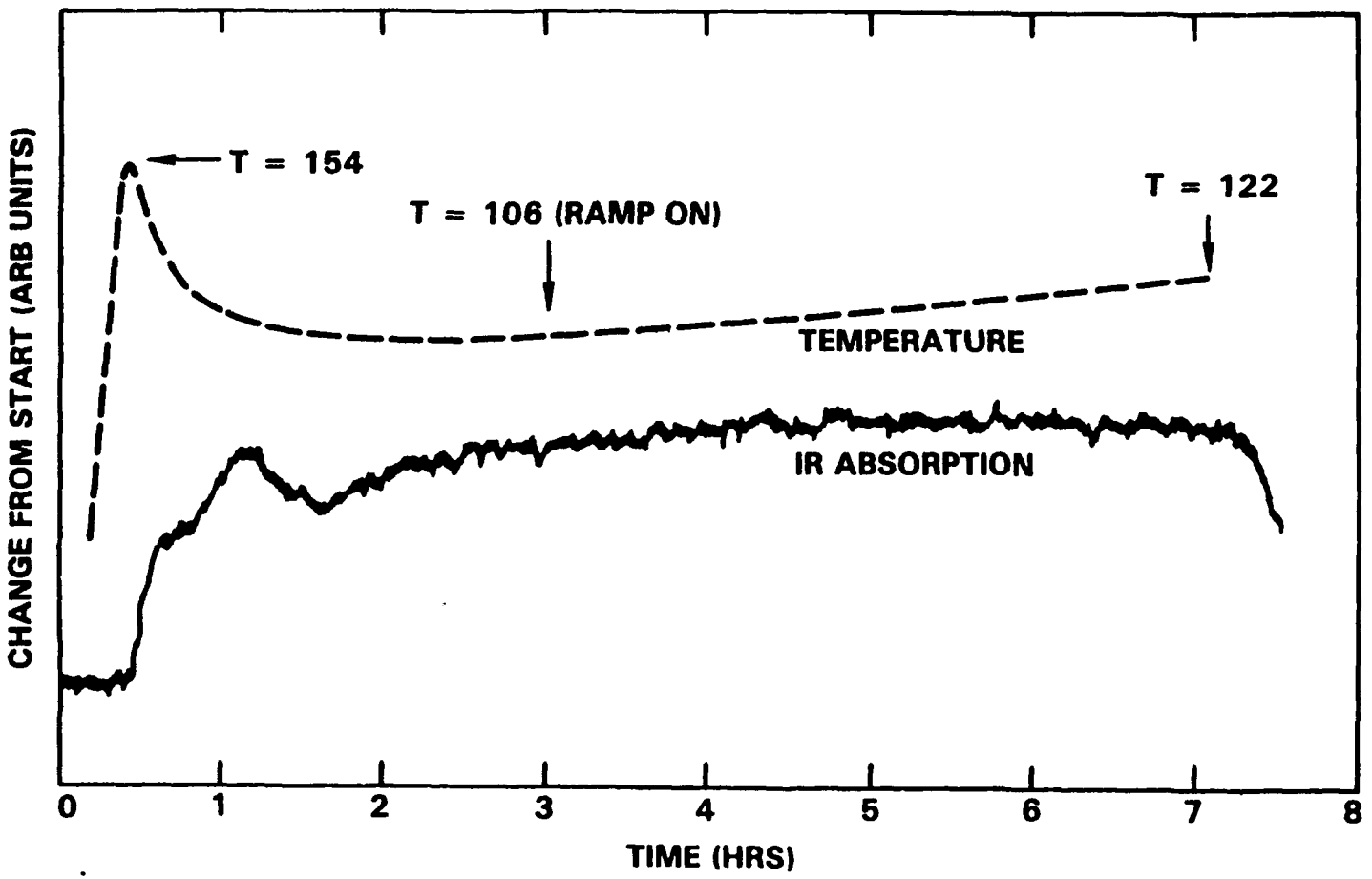

Fig. 10 Temporal behavior of HN_3 generator using programmed power supply.

As a safety measure to prevent prolonged heating at high power, the automatic temperature control on the electric pot is set at 200°C. Normally, since the pot will always be cooler, this control will be inactive (always on). If, on the other hand, the temperature reaches 200°C, the control unit will begin to cycle on and off, thereby preventing any further rise in temperature. The control unit therefore provides an added degree of protection against thermally-induced NaN_3 decomposition[14] which starts at about 250°C.

Once the HN_3 yield was stabilized, it was then possible to test the infrared absorption diagnostic during FN_3 generation. In Fig. 11, the HN_3 yield is first stabilized, then F_2 is added in sufficient quantity to react all of the HN_3. The complete disappearance of absorption shows that the infrared diagnostic is insensitive to F_2, FN_3 and HF, and that there is no baseline drift associated with production of FN_3 since full recovery of the HN_3 absorption occurs once the F_2 flow is shut off. Therefore, the infrared diagnostic can be reliably used as an on-line monitor of residual HN_3.

VIS/UV Cell - Finally, after the trap, the gas stream is passed to a 6 cm stainless steel cell with quartz windows inside a commercial spectrophotometer[15] operated at 420 nm with a tungsten lamp source. At this wavelength, FN_3 can be detected without interference from HF or HN_3.[3,6,12] By systematically varying the F_2 flow, it was found that the FN_3 yield peaked at a slightly lower F_2 flow than was required to eliminate the residual HN_3 entirely (as measured by the infrared absorption diagnostic). During a typical stabilized run, the 420 nm cell transmission decreased from 100 to 92 - 94%, when the FN_3 was generated. Using Gholivand's data for the extinction coefficient[3] of FN_3 indicates that the HN_3 was converted to FN_3 with 50 - 100% efficiency, yielding typically 7 torr of FN_3 in 350 torr of He buffer gas. The metering valve which controlled the system flow rate was located just downstream of the 420 nm absorption cell. From here, the FN_3/He gas stream was conducted to the experiment and exhausted to vacuum by 1/4 in. dia. stainless steel and teflon lines. A pressure gauge just upstream of the metering valve showed little pressure difference between the visible wavelength absorption cell and the vacuum regulator just upstream of the HN_3 generator.

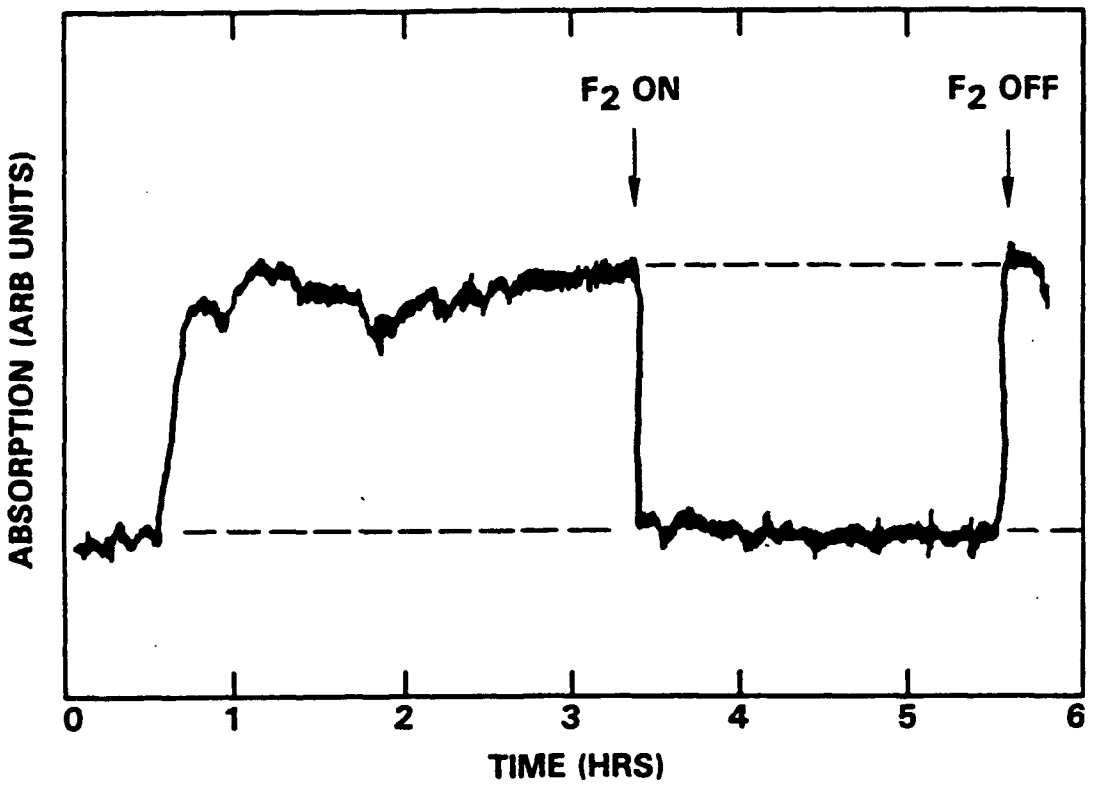

Fig. 11 Response of infrared absorption diagnostic to generation of FN_3.

Miscellaneous - Several additional features of the FN_3 source, not shown in Fig. 2 for reasons of clarity, are discussed below. Some of these have significant safety consequences. Large area course glass frits were placed in the gas lines at the exit of the HN_3 and FN_3 generators. The funtion of these filters is to stop entrainment of particulates from the two reactors by the gas stream. A frit is required downstream of the FN_3 reactor because solid NH_4F can be formed under some conditions as noted by Haller.[1] We strongly recommend that the meter which monitors the output voltage of the mass flowmeter be alarmed to provided an audible warning if the He flow either stops or falls below a preset level, typically half of the nominal flow rate. This is necessary because a vacuum pump failure or clogged valve downstream can stop the He flow resulting in a buildup of high pressures of HN_3 or FN_3 at the generator, intermediate reactor, or trap, resulting in potential for explosion. The stainless steel balls in the intermediate reactor should be checked for signs of corrosion or reaction at regular intervals to prevent buildup of metal azides. Periodic checks at 3-month intervals in our apparatus (with daily runs) showed only trace contamination by NH_4F. Three-way valves and bypass lines were installed to pass the gas stream around the secondary reactor and trap, to divert the gas stream from the trap exit directly to vacuum and to substitute pure He for F_2/He mixture at the inlet of the secondary reactor. These additional lines provide options that may be of value if the trap or metering valve clogs, while substituting He for F_2/He during warm up minimizes the perturbation of the HN_3 yield that occurs when F_2 addition displaces the He flow through the HN_3 generator. An air line tied in with the effluent of the liquid nitrogen boiler is also recommended as a method to remotely return the cold trap to room temperature to assure that all of the contents are expelled. Finally, while a small floor pump could provide the needed vacuum, we exhausted all of our azide experiments to a 300 cfm mechanical pump which had its oil changed on a monthly basis. This practice prevents any significant accumulation of organic azides in the pump oil.

REFERENCES

1. J.F. Haller, Ph.D. Dissertation, Cornell Univerzsity, 1942.

2. D. Patel, A.T. Pritt and D.J. Benard, J. Phys. Chem. 90 (1986) 1931.

3. K. Gholivand, G. Schatte and H. Willner, J. Inorg. Chem., to be published.

4. H.H. Michels, United Technology Research Center, private communication.

5. D.J. Benard, Science Center proposal SC4339T (1987), to be published.

6. B. Rosen, Spectroscopic Data Relative to Diatomic Molecules, Pergammon Press (New York).

7. H.H. Michels, United Technology Research Center Report No. 77-05-236-8.

8. N.I. Sax, Dangerous Properties of Industrial Materials, Sixth Edition, Van Nostrand (New York).

9. J.T. Baker Chemical Co., Material Safety Data Sheet No. S2906-01.

10. Matheson Gas Products, Technical Brief No. TB-115.

11. B. Krakow, R.C. Lord and G.O. Neely, J. Mol. Spectroscopy 27 (1968) 148.

12. J.R. McDonald, J.W. Rabalais and S.P. McGlynn, J. Chem. Phys. 52 (1970) 1332.

13. D.A. Dows and G.C. Pimentel, J. Chem. Phys. 23 (1955) 1258.

14. L.G. Piper, R.H. Krech and R.L. Taylor, J. Chem. Phys. 71 (1979) 2099.

15. Pye-Unicam Model 6-550 UV/VIS Spectrophotometer.

Reprinted from The Journal of Physical Chemistry, 1989, 93, 4790.

Production of NF($a^1\Delta$) by Dissociation of Fluorine Azide

D. J. Benard,* B. K. Winker, T. A. Seder, and R. H. Cohn

Rockwell International Science Center, Thousand Oaks, California 91360 *(Received: November 8, 1988; In Final Form: February 14, 1989)*

The reactions of vibrationally excited HF or DF molecules with FN_3 were found to dissociate the azide, but not to yield metastable NF fragments. Thermal dissociation of FN_3, on the other hand, yielded metastable NF($a^1\Delta$) with near-unit efficiency. Concentrations of NF($a^1\Delta$) approaching $3 \times 10^{16}/cm^3$ were obtained at temperatures near 1000 K, and the decay of NF($a^1\Delta$) was found to be dominated by self-annihilation. The activation energy for production of NF($a^1\Delta$) by thermal dissociation of FN_3 was found to agree with ab initio calculations by Michels.

Introduction

Fluorine azide (FN_3) was first synthesized in 1942 by Haller, upon gas-phase reaction of HN_3 with F_2. In preliminary studies, Haller found that FN_3 reacted by fracture of the azide group which he attributed to a weak central bond. Haller also found that FN_3 was highly explosive when condensed and the gaseous material was slowly but efficiently converted to N_2F_2 and N_2 upon mild heating.[1] Later, Gipstein and Haller[2] obtained an ultraviolet absorption spectrum of FN_3, while Pankratov et al.[3] demonstrated that FN_3 could be obtained by the reaction of F_2 with NaN_3. Also, Milligan and Jacox[4] obtained the infrared absorption spectrum of FN_3 in an Ar matrix. More recently, we studied the ArF laser photolysis of FN_3 and determined the heat of formation as 125–135 kcal/mol, sufficient to allow the molecule to dissociate to electronically excited NF radicals by an exothermic reaction.[5] Moreover, analysis of the direct products in this experiment suggested that FN_3 had a singlet ground state; therefore, upon dissociation, only metastable NF($a^1\Delta$,$b^1\Sigma$) should be formed if spin is conserved. Similar results were obtained for ClN_3 and BrN_3 by Coombe et al.[6] and Coombe and Lam,[7] respectively. On the basis of these findings, we began an investigation of FN_3 dissociation in hopes of developing an efficient and chemically clean (scalable) source of singlet NF. Since Hartford[8] had demonstrated analogous production of ND($a^1\Delta$) upon CO_2 laser multiphoton dissociation of DN_3, we decided to concentrate on methods to add thermal or vibrational energy to the FN_3 ground state. In parallel with our study, Michels[9] performed ab initio calculations of the FN_3 potential energy surfaces which yielded vibrational frequencies in good agreement with infrared absorption data[4,10] and which demonstrated a 0.5–0.7-eV barrier to dissociation of the electronic ground state by central bond rupture. A substantially larger

(1) Haller, J. F. Ph.D. Thesis, Cornell University, Ithaca, NY, 1942.
(2) Gipstein, E.; Haller, J. F. *Appl. Spectrosc.* **1976**, *20*, 417.
(3) Pankratov, A. V.; Sokolov, O. M.; Savenkova, N. I. *Zh. Neorg. Khim.* **1964**, *9*, 2030.
(4) Milligam, D. E.; Jacox, M. R. *J. Chem. Phys.* **1964**, *40*, 2461.
(5) Patel, D.; Pritt, A. T.; Benard, D. J. *J. Phys. Chem.* **1986**, *90*, 1981.
(6) Coombe, R. D.; Patel, D.; Pritt, A. T.; Wodarczyk, F. *J. Chem. Phys.* **1981**, *75*, 2177.
(7) Coombe, R. D.; Lam, C. H. T. *J. Chem. Phys.* **1983**, *79*, 3746.
(8) Hartford, A. *Chem. Phys. Lett.* **1978**, *57*, 352.
(9) Michels, H. H. United Technologies Research Center, Hartford, CT, private communication.
(10) Gholivand, K.; Schatte, G.; Willner, H. *Inorg. Chem.* **1987**, *26*, 2137.

0022-3654/89/2093-4790$01.50/0

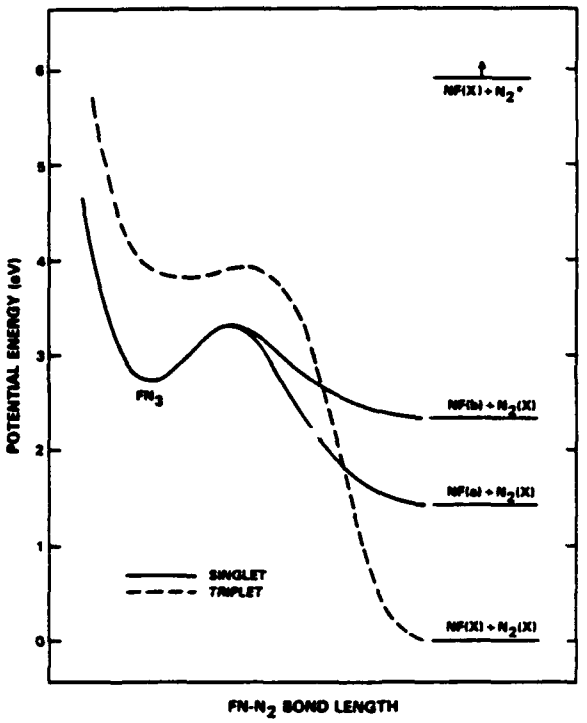

Figure 1. Illustrative potential energy curves of FN_3. The excited states of N_2 lie at and above the energy level indicated by $NF(X) + N_2^*$.

barrier to dissociation of FN_3 was found for rupture of the $F-N_3$ bond. These results implied that FN_3 could possibly be dissociated to yield $NF(a^1\Delta,b^1\Sigma)$ by vibrational energy transfer from molecules such as HF/DF or even by rapid pyrolysis at modest temperatures. Also, in parallel with our work, Gholivand et al.[10] developed a batch method for the preparation of distilled samples of FN_3. These authors investigated the vapor pressure curve, the infrared and visible/ultraviolet absorption spectrum, and the mass spectrum/NMR signatures of the molecule.

The dissociation physics of FN_3 can be understood by examination of the potential energy surfaces that correlate to the various electronic states of N_2 and NF at infinite separation, as shown in Figure 1. The triplet surface derived from $NF(X^3\Sigma)$ and $N_2(X^1\Sigma)$ is strongly repulsive, because as the N_2 and NF molecules are brought together, some of the triplet character originally associated with NF becomes associated with N_2 in which the triplet states are highly excited.[11] The singlet states derived from $NF(a^1\Delta,b^1\Sigma)$ and $N_2(X^1\Sigma)$ are less repulsive but are nonetheless still influenced by other higher lying states. The interaction of the excited triplet states of N_2 with $NF(X^3\Sigma)$ yields higher lying singlet states that are strongly bound due to spin cancellation. These states repel the lower singlet states derived from $NF(a^1\Delta,b^1\Sigma)$ and $N_2(X^1\Sigma)$, resulting in a potential well that forms the singlet ground state of the FN_3 molecule. The repulsive triplet state, arising from $NF(X^3\Sigma)$ and $N_2(X^1\Sigma)$, must pass above the minimum of this well for FN_3 to be a stable molecule, since otherwise the bound FN_3 molecules would spontaneously dissociate following radiative decay. Michels[9] has calculated that the triplet state actually crosses the lowest singlet state of FN_3 on the outside of the dissociation barrier and that the singlet–triplet splittings inside the barrier lie in the range 1–2 eV. Addition of energy to the FN_3 molecule can therefore result in dissociation to NF and N_2 by either of two mechanisms. Transfer of thermal or vibrational energy to the FN_3 ground state, sufficient to surmount the barrier, should lead to dissociation on the singlet surface, yielding $NF(a^1\Delta,b^1\Sigma)$ and $N_2(X^1\Sigma)$ as products. On the other hand, transfer of larger amounts of vibrational or even electronic energy to the ground state of FN_3 could access the triplet state of FN_3, which dissociates to $NF(X^3\Sigma)$ and $N_2(X^1\Sigma)$ instead. To investigate these phenomena, we have studied the production of $NF(a^1\Delta,b^1\Sigma)$ from FN_3 molecules that were suddenly exposed to either a high-temperature inert buffer gas environment or vibrationally excited molecules such as HF/DF, which have harmonic spacings that approximate the barrier to dissociation.

(11) Rosen, B. *Spectroscopic Data Relative to Diatomic Molecules*; Pergamon Press: New York, 1970.

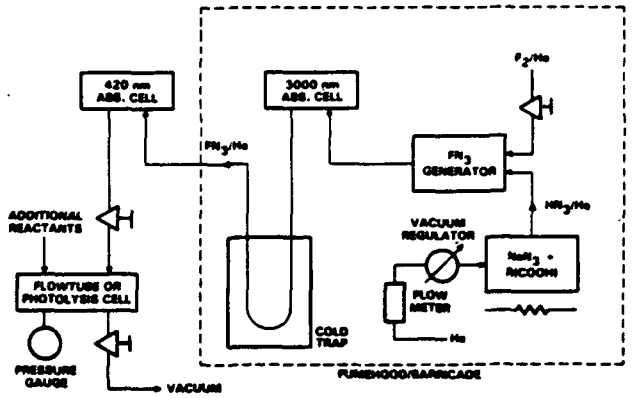

Figure 2. Schematic of gas flow system used to generate and study dissociation of FN_3.

Experimental Section

A gas flow system, shown schematically in Figure 2, was developed as a continous or "on-line" source of FN_3 molecules. The lasers and optical diagnostics used to induce and monitor the FN_3 dissociation have been omitted from this figure for the sake of clarity. FN_3 was produced following the method of Haller,[1] with some refinements, by titrating HN_3 diluted in He with a similarly diluted flow of F_2 at 35 °C. HN_3 was obtained by electrically heating a mixture of NaN_3 and a large (20/1) excess of stearic acid to approximately 100–110 °C.[12] The end point of the titration was determined by monitoring the residual HN_3 concentration in absorption at 3000 nm.[13] To maintain an optimum yield of FN_3, the temperature of the NaN_3/stearic acid mix was programmed so that the HN_3 evolution was constant, since excess F_2 slowly reacts[1] with FN_3 to yield NF_3 and N_2. The FN_3/He stream was purified of residual HN_3 and byproduct HF by passage through a cold trap[10,14] at −100 °C, and the FN_3 concentration was monitored in absorption at 420 nm, using the extinction coefficient data of Gholivand et al.[10] The entire apparatus, except the 420-nm absorption cell, was barricaded inside a fume hood for the protection of the experimenter. Typical concentrations of FN_3 were 7 Torr in 350 Torr of He at a net flow rate of 3 cm^3 (STP)/s, which (within the accuracy of our measurements) corresponds to converting approximately 50–100% of HN_3 into FN_3. Mass spectrometric analysis revealed that initial N_2F_2 formation was less than 10% of FN_3, and roughly 50% of FN_3 decayed to N_2F_2 over a period of about 1 h when stored at a temperature of 14 °C and at a net pressure of 150 Torr in a Teflon-lined cylinder. The mass spectrometer was calibrated by monitoring the mass 61 (FN_3) and mass 66 (N_2F_2) peaks before and after passing the FN_3 flow through a heated section of tubing which induced complete conversion to N_2F_2. The FN_3/He stream was reduced in pressure and carried to the various experiments by stainless steel and Teflon tubing, which typically delivered FN_3 to the reactor in less than 60 s from generation. Further details regarding the production and measurement of FN_3 are contained in a previous publication.[15]

Three experiments were performed in which FN_3 was reacted to form NF(a,b). In the first experiment, the FN_3/He flow was

(12) Krakow, B.; Lord, R. C.; Neeley, G. O. *J. Mol. Spectrosc.* **1968**, *27*, 148.
(13) Dows, D. A.; Pimentel, G. C. *J. Chem. Phys.* **1955**, *23*, 1258.
(14) Weast, R. C. *Handbook of Chemistry and Physics*, 60th ed.; CRC Press: Boca Raton, FL, 1980.
(15) Benard, D. J.; Cohn, R. H. "Model Studies of CBES Decomposition"; Technical Report 87-071; Air Force Astronautics Laboratory: Edwards AFB, CA, Feb 1988.

admitted to a chemiluminescence flow tube reactor along with a variable flow of D_2 and a fixed flow of dilute F_2 in He that was passed through a microwave discharge[16] to generate approximately 50 mTorr of F atoms.[17] The flow tube was operated at a plug flow velocity of 10^3 cm/s and at a net pressure of 1–2 Torr. The concentration of FN_3 in the flow tube was approximately 5–10 mTorr, and the D_2 flow was adjusted in the range 0–50 mTorr, with the balance of the gases as He. The D_2 and FN_3 flows were admitted to the reactor through coaxial injectors whose position was variable with respect to a fixed (1-in. diameter) sapphire window on the side of the flow tube. The F atoms were admitted to the outer annulus of the flow tube well upstream of the mixing region, and the interior of the flow tube was Teflon coated to minimize wall recombination. Additional details[17] regarding the flow tube reactor are contained in a prior publication. Previous studies using this reactor and the Cl_2 titration method[17,18] have demonstrated negligible loss of F atoms enroute to the mixing region. The injectors were staged so that the D_2 was admitted to the reacting flow approximately 2 cm upstream of the FN_3 inlet. The resulting chemiluminescence was monitored by an optical multichannel analyzer (OMA) through the observation port.

In the second experiment, the FN_3/He gas mixture was admitted to a slowy flowing stainless steel photolysis cell, along with a variable concentration of HF or DF and a variable concentration of SF_6. The cell was then optically pumped through a sapphire window by a pulsed HF or DF electrical discharge laser, and the resulting chemiluminescence was monitored at right angles to the laser beam through a sapphire window by a temporally gated OMA and a filtered Si photodiode that was interfaced to a digital signal averager. The concentration of FN_3 in these experiments was also followed on a time-resolved basis by absorption of 210-nm radiation,[5,10] from a D_2 lamp that was propagated through the cell coaxial with and internal to the HF/DF laser beam. Overtone emission[11] from vibrationally excited HF or DF was also monitored with 1-μs temporal resolution by a liquid nitrogen cooled intrinsic Ge detector filtered to a narrow band around 1300 nm. Typical cell conditions were 100–150-Torr total pressure, of which 1–2 Torr was FN_3, 1–10 Torr of either HF or DF, and 0–50 Torr of SF_6, with the balance as He. The HF/DF laser was constructed following references in the literature[19] by suitable modification of an excimer laser. The maximum obtainable pulse energy was 350 mJ with a submicrosecond pulse width. The reactants in the laser (H_2 or D_2 and SF_6) were typically adjusted, however, to yield 10–20-μs-long pulses of 20–40-mJ energy that were focused to a uniform 0.3 × 0.5 cm^2 spot inside the photolysis cell as measured by exposure of thermal image paper. Based on measurements of the laser energy that was transmitted through the cell (2-cm active length), only a small fraction (<5%) of the incident radiation was absorbed. Spectral and temporal analysis of the HF laser revealed simultaneous operation on the 2 → 1 and 1 → 0 transitions over most of the laser pulse, with the majority of the pulse energy concentrated in the P(6) and P(7) rotational lines.[20] The DF laser was used in preference to the HF laser when $NF(a^1\Delta)$ measurements were critical, because $HF(\Delta v=3)$ overtone emission, typically present at early times, spectrally overlapped the NF(a–X) band.[11]

In the third experiment, approximately 5 J of multimode untuned 10.6-μm radiation from a carbon dioxide TEA laser (300-ns pulse width) was focused to a 1-cm-diameter spot inside a second photolysis cell that was equipped with NaCl windows at Brewster's angle for passage of the laser beam and orthogonal quartz windows for viewing of the chemiluminescence. The cell contained approximately 0.1 Torr of FN_3, 5 Torr of SF_6, 0–1 Torr of H_2, and 5 Torr of Ar used to purge the NaCl windows, with the balance He to a total pressure of 25 Torr. Apertures were placed in the side arms of the reactor for passage of the laser beam and Ar purge flows, which were set to limit the absorption of the laser radiation to the center of the photolysis cell. The resulting chemiluminescence emissions were analyzed by the gated OMA and filtered Si photodiode/signal averager. The same experiment was repeated in a redesigned cell using a line-focused 500-mJ CO_2 laser to optically side-pump a 0.25-cm length of a 0.25 × 2.5 cm^2 jet of reactive gas contained inside a velocity-matched Ar shield flow. In the active portion of this reactor, the partial pressures were approximately 1.5 Torr of FN_3, 15 Torr of SF_6, and balance He to a total pressure of 150 Torr.

In both laser experiments, trace quantities (<2% of initial FN_3) of $Bi(CH_3)_3$ were admitted to the reactors by injecting a small flow of He that was bubbled through the liquid, which was stored in a trap that was cooled to −63.5 °C by a chloroform slush bath. The gas pressures in all of the reactors were monitored by electronic manometers, and the concentrations of $Bi(CH_3)_3$ in the reactors were inferred from the vapor pressure curve provided by the manufacturer. Absolute concentrations of NF(a) and NF(b) were calculated from the Si photodiode signals by using the known A coefficients for the a → X and b → X emission bands at 874 and 528 nm, respectively.[21,22] Calibration factors were determined for the photodiode/filter combinations using a standard lamp whose spectral output is traceable to the National Bureau of Standards. The major uncertainty in these measurements was estimation of the emitting volume which was defined by the exciting laser beam and other apertures in the optical detection system. The accumulated error in the absolute NF(a,b) concentrations is estimated to be in the range 25–50%.

Results

Flow Tube Chemiluminescence. Flow tube experiments were conducted with the cold trap (used to purify the FN_3/He flow) at ambient temperature, since the presence of HF byproduct impurities was not critical to the results or their interpretation. In the absence of D_2 addition, no visible emission resulted from the reaction of F atoms with FN_3. Upon addition of D_2, however, a bright diffuse rose-colored flame appeared and extended 10–20 cm downstream of the mixing region. Spectral scans with the OMA revealed that the major emitters were $N_2(B)$ and NF(a,b).[11] The N_2 emissions were expected following production of NF(a), since D atoms (obtained from the F + D_2 reaction) are known to initiate a chain with NF(a) that leads to formation of $N_2(B)$.[23] To quantify the yield of NF(a), the D_2 flow was stopped and the F_2 flow that was titrated with HN_3 (for generation of FN_3) was also turned off, so that HN_3 was admitted to the flow tube in place of FN_3. The reaction of HN_3 with excess F atoms is known to produce NF(a) with near-unit efficiency[24] as well as a much smaller yield of NF(b) due to energy pooling between NF(a) and vibrationlly excited HF from the F + HN_3 reaction.[25] The green NF(b–X) emission was readily visible, while the near-infrared NF(a–X) emission was monitored by the OMA. The HN_3 is completely reacted, the NF(a) reaches its peak concentration, and the NF(b–X) emission is totally contained within the field of view in this experiment. Turning on the F_2 flow to the FN_3 generator progressively diminished the NF(b–X) emission, which was extinguished entirely when the F_2 was adjusted to either maximize the yield of FN_3 (measured at 420 nm) or just eliminate the residual HN_3 (measured at 3000 nm), as expected. With the F_2 flow turned off again, D_2 was then added to the flow tube until the NF(a–X) emission was attenuated significantly (~4×) due to competition between the F + D_2 and F + HN_3 reactions. The F_2 flow to the FN_3 generator was then reestablished to optimally

(16) Fehsenfeld, F. C.; Evenson, K. M.; Broida, H. P. *Rev. Sci. Instrum.* **1965**, *36*, 294.
(17) Chowdhury, M. A.; Pritt, A. T.; Patel, D.; Benard, D. J. *J. Chem. Phys.* **1986**, *84*, 6687.
(18) Ganguli, P. S.; Kaufmann, M. *Chem. Phys. Lett.* **1974**, *25*, 221.
(19) Pummer, H.; Kompa, K. L. *Appl. Phys. Lett.* **1972**, *20*, 356.
(20) Deutsch, T. F. *Appl. Phys. Lett.* **1967**, *10*, 234.
(21) Malins, R. J.; Setser, D. W. *J. Phys. Chem.* **1981**, *85*, 1342.
(22) Tennyson, P. H.; Fontijn, A.; Clyne, M. A. A. *Chem. Phys.* **1981**, *62*, 171.
(23) Cheah, C. T.; Clyne, M. A. A.; Whitefield, P. D. *J. Photochem.* **1981**, *15*, 21.
(24) Hadbas, J.; Wategaonkar, S.; Setser, D. W. *J. Phys. Chem.* **1987**, *91*, 451.
(25) Pritt, A. T.; Patel, D.; Coombe, R. D. *Int. J. Chem. Kinet.* **1984**, *16*, 977.

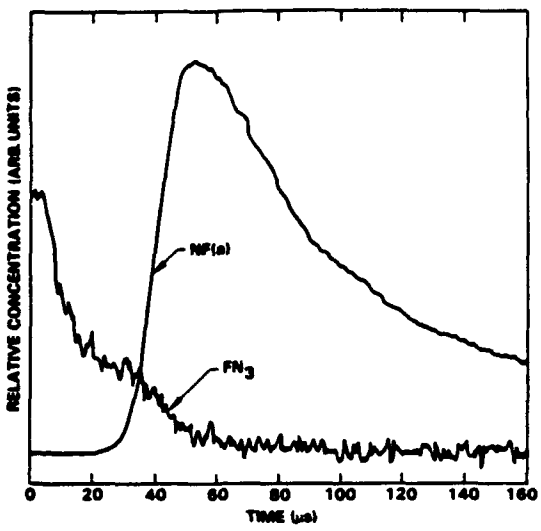

Figure 3. Comparison of typical NF(a) and FN_3 time profiles following pulsed DF laser excitation of FN_3/DF gas mixture.

convert HN_3 to FN_3. This procedure restored the NF(a–X) emission to near its original intensity (F + HN_3 reaction). Since at most one FN_3 molecule is formed from each HN_3 molecule (upon titration with F_2) and since HN_3 is an efficient precursor of NF(a), these results show that FN_3 is also an efficient precursor of NF(a). The mechanism of reaction, however, cannot be determined from the flow tube experiment, since there is no temporal resolution and D_2 addition both heats the bath gas and generates vibrationally excited DF molecules. These data, nonetheless, provided the initial motivation for the more definitive experiments that followed.

HF/DF Laser Photolysis. Since the infrared absorption bands[4,10] of FN_3 do not match the HF/DF laser wavelengths,[20] HF/DF was added to FN_3 in the photolysis cell to act as a sensitizer. Laser excitation of the FN_3/sensitizer gas mixture also resulted in rose-colored chemiluminescence. The principal emitters, as in the flow tube, were NF(a,b) and N_2(b). Overtone emission from the HF/DF was also present. Careful titration of HN_3 with F_2 (to generate FN_3), use of the cold trap to remove residual HN_3 (and byproduct HF), and freeze–thaw–pumping of the HF/DF sensitizer before use (to remove H_2/D_2 generated by passivation of the cylinder walls) were almost completely effective in eliminating the N_2 emissions. When these procedures were not followed, the laser pulse occasionally initiated a deflagration of all gas inside the photolysis cell. By avoiding this condition and using apertures to limit the field of view of the detector, we were able to confirm that the HF/DF overtone and the NF emissions were confined to the volume of gas that was optically pumped by the laser.

The time profile of the HF/DF emissions closely followed the laser pulse in most experiments, while the appearance of NF(a) due to DF laser excitation was delayed, as shown in Figure 3. (The laser was fired at $t = 0$.) The peak concentration of NF(a) increased with increasing HF/DF concentration and moved forward in time. With lower HF/DF concentrations, a significant gap in time opened up between the decay of the HF/DF emissions and the appearance of NF(a) during which there was no significant emission. Figure 4a shows a similar time profile of the 874-nm emission collected with HF in place of DF as the sensitizer and by use of the HF laser for excitation. In this experiment, the detector responded to both the HF(Δv=3) and the NF(a–X) emissions; however, an emission spectrum collected with the OMA temporally gated to the early portion of the time profile demonstrated that the initial (0–25 μs) decay is due solely to HF emission. This result is expected in view of the absence of any NF(a) emission during the similar time period in Figure 3. Figure 3 also demonstrates that the corresponding decay of the FN_3 concentration occurred in two stages. The first stage of FN_3 decay was coincident with the decay of the HF/DF emission, while the second

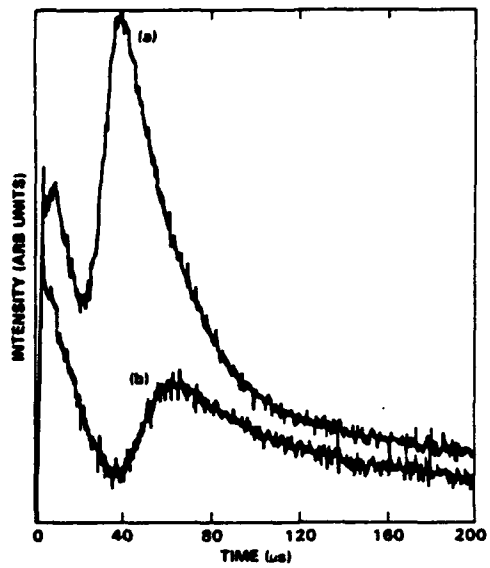

Figure 4. Time profile of 874-nm emission intensity followng pulsed HF laser excitation of FN_3/HF gas mixture (a) and effect of adding 10 Torr of SF_6 to the gas mixture (b).

stage was coincident with the delayed appearance of NF(a). The fraction of FN_3 consumed in the initial decay increased with increasing HF/DF concentration, but the amplitude of the net decay remained constant, suggesting that all the FN_3 was consumed in each case. These observations suggest that vibrationally excited HF/DF dissociates FN_3, but does not yield NF(a), and that a second mechanism is responsible for the subsequent decay of FN_3 which liberates NF(a). The largest peak NF(a) concentration was 9.7×10^{15}/cm^3, obtained with 9 Torr of DF and 2 Torr of initial FN_3, approximately 50 μs after initiation of a 20-mJ, 10-μs laser pulse. The peak NF(b) concentrations were monically 2 orders of magnitude smaller than the corresponding NF(a) yields.

By use of low HF concentrations (1 Torr) and relatively short (1–2 μs) laser pulses, it was possible to observe the free decay of the HF(Δv=3) emission. The approximate decay time of the HF(v) signal was diminished from 20 μs (in the absence of FN_3) to about 10 μs when 1 Torr of FN_3 was added. Therefore, the rate of FN_3 quenching of HF(v), which sets an upper limit on the rate of FN_3 dissociation by HF(v), is shown to approximate the V–T rate for HF self-quenching[26] or about 3×10^{-12} cm^3/s. The decays of NF(a) following its peak were also too fast to be explained by quenching due to He, HF, or N_2 resulting from FN_3 decomposition.[27] Setser[28] recently reported that NF(a) is subject to second-order decay (self-annihilation) at a rate of 2.2×10^{-12} cm^3/s, based on low-density flow tube experiments at NF(a) concentrations of 10^{12-13} cm^3. We therefore fit our decay curves to second-order kinetics and obtained an average rate constant of 3×10^{-12} cm^3/s, in good agreement with Setser's finding. Since our data were collected at NF(a) concentrations that were typically 3 orders of magnitude larger than in the Setser study, the second-order nature of the quenching is apparent.

Addition of 50 Torr of SF_6 to the photolysis cell eliminated the appearance of NF(a) completely. As shown in Figure 4b, intermediate levels of SF_6 addition reduced the peak NF(a) concentration significantly and delayed the onset of NF(a) production relative to no SF_6 addition (Figure 4a) but had little effect on the subsequent rate of NF(a) decay. This behavior is incompatible with quenching by SF_6 as an explanation for the reduction of the peak NF(a) signal, since quenching would also advance the peak

(26) Hancock, J. K.; Green, W. H. *J. Chem. Phys.* **1972**, *56*, 2474.
(27) Koffend, J. B.; Gardner, C. E.; Heidner, R. F. "Kinetics of the H_2-NF_2 System"; Technical Report 85-55; Aerospace Corporation: El Segundo, CA, Sept 1985.
(28) Quinones, E.; Habdas, J.; Setser, D. W. *J. Phys. Chem.* **1987**, *91*, 5155.

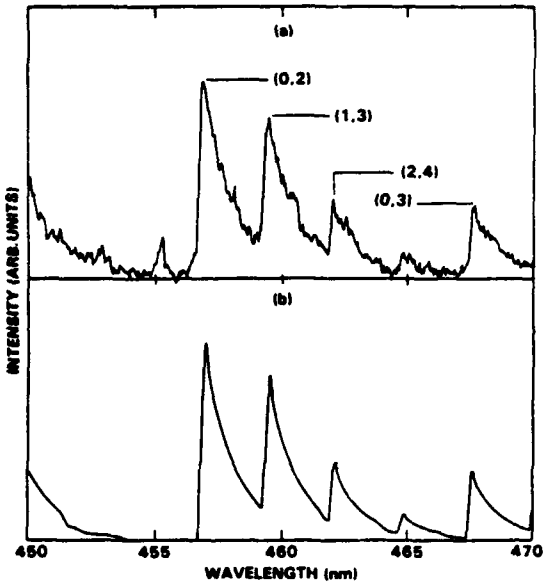

Figure 5. Comparison of (a) measured and (b) calculated BiF(A–X) emission spectra.

NF(a) concentration in time and increase the rate of NF(a) decay in proportion to the amplitude reduction, which is not observed. The result is not surprising, since SF_6 is expected to be a slow quencher of NF(a). The heat capacity[29] of SF_6, however, is substantially larger than He. Addition of SF_6 therefore tends to reduce the rise in temperature of the bath gas due to reactive heating, which is turn slows the rate of thermal dissociation of the FN_3. Consequently, the observations noted above are consistent with delayed production of NF(a) by thermal dissociation of FN_3, which begins to occur when the temperature of the bath gas had increased sufficiently due to heat released in the preceding reactions.

The gas temperature was measured spectroscopically by trace addition of $Bi(CH_3)_3$ which resulted in intense BiF(A–X) emission[11,30] that tracked the NF(a) time profile. A high-resolution (0.2-nm fwhm) spectrum of the $\Delta v = 2$ and $0 \rightarrow 3$ transitions was recorded by using the OMA with a 40-μs gate initiated at the peak of the NF(a)/BiF(A) time profile. The recorded spectrum was normalized on a relative basis by assuming that the instrument response was a smooth (linear) function of wavelength over the limited range between the $0 \rightarrow 2$ and $0 \rightarrow 3$ transitions. The slope of the instrument response function was then adjusted so that the normalized $0 \rightarrow 2$ and $0 \rightarrow 3$ intensities were in accord with the ratio of the corresponding Franck–Condon factors.[31] The vibrational and rotational temperatures were then obtained from the relative intensities and widths of the $0 \rightarrow 2$, $1 \rightarrow 3$, $2 \rightarrow 4$, and $3 \rightarrow 5$ bands, by comparison to a series of temperature-dependent synthetically calculated BiF(A–X) emission spectra that were adjusted for instrument resolution. The calculations were performed and provided to us by Koffend and Herbelin.[32] The normalized and synthetic spectra were shown in Figure 5, a and b, respectively, which demonstrate a good fit to $T = 950 \pm 50$ K for both the rotational and vibrational temperatures.

CO_2 Laser Pyrolysis. The preceding experiments provided mechanistic information on the dissociation of FN_3 but were not optimal for determining the NF(a) branching ratio, since only a fraction of the FN_3 was dissociated thermally and the second-order decay of NF(a) occurred on a time scale that was competitive with the dissociation reaction. To overcome these difficulties, as well as to verify the thermal dissociation mechanism, a CO_2 laser-induced temperature jump experiment was performed to trigger the thermal dissociation reaction directly. The incident laser radiation was absorbed by SF_6, resulting in both generation of F atoms by multiphoton processes and heating of the bath gas by V–T quenching. At the high concentrations of SF_6 used (5 Torr), thermalyzing SF_6–SF_6 collisions limit the F atom yield[33] to approximately 100 mTorr; consequently, the major effect of the laser excitation was to induce a rapid jump in gas temperature. Recall that in the flow tube experiment no visible emission resulted from admitting FN_3 to a similar environment of F atoms. Direct absorption of the incident laser radiation by FN_3 does not occur in this experiment;[4,10] therefore, appearance of NF(a) demonstrates thermal dissociation of the FN_3. Because of the higher temperatures that can be achieved by CO_2 laser pumping in relatively short times, NF(a) is expected to reach its peak concentration much more rapidly than in the HF/DF laser experiments, where the heating is due to relatively slow quenching reactions. The FN_3 concentration in these experiments was also lower than in the HF/DF experiments, since the cell design required lower pressures to promote uniform mixing. Visual observation of the NF(b–X) emission demonstrated that the Ar window purges tended to sweep the FN_3 out of the laser beam when the photolysis cell was operated at pressures greater than 25 Torr. At these lower FN_3 concentrations, less NF(a) is formed, and consequently the second-order decay of NF(a) is slower. Therefore, the peak NF(a) concentration in this experiment is much closer to the nascent yield of NF(a) produced by the dissociation of FN_3 than in the HF/DF experiments.

Excitation of the SF_6/FN_3/buffer gas mixture by the CO_2 laser generated both NF(a) and NF(b) rapidly, with no significant N_2 emission,[11] and the peak yield of NF(a) corresponded to 70% of the FN_3 molecules that were initially within the active volume of the CO_2 laser beam. As in prior experiments, the yield of NF(b) was typically 1% or less of the NF(a) concentration. The NF(a) signal peaked in approximately 2 μs, consistent with the bandwidth limitation of the high-gain preamplifier that was used to couple the filtered Si photodiode to the signal averager. The majority of the FN_3 was therefore converted to NF(a) on a submicrosecond time scale. A fit of the NF(a) decay (150-μs half-life) to second-order kinetics also yielded a rate constant of 3×10^{-12} cm^3/s, in good agreement with both Setser's data[28] and the HF/DF laser experiments, where the peak NF(a) concentrations were a factor of 2–5 higher. Addition of H_2 to the gas mixture produced $N_2(B)$ and enhanced the yield of NF(b) by the same mechanisms[23,25] that occurred in the flow tube, while addition of trace $Bi(CH_3)_3$ yielded an intense BiF(A–X) signal that followed the NF(a) time profile after an induction period of approximately 10 μs.

Since FN_3 is not consumed to heat the buffer gas in these experiments, it is more efficiently utilized to generate NF(a). Consequently, the attainable NF(a) concentrations are limited primarily by the initial FN_3 concentration, provided the dissociation reaction remains fast compared to the second-order annihilation of NF(a). To achieve the highest possible NF(a) concentrations, we therefore performed similar experiments in the redesigned high-pressure reactor which yielded peak NF(a) concentrations as large as 3×10^{16}/cm^3. The time for FN_3 consumption (10% → 90%) in this reactor was approximately 2 μs as revealed by absorption measurements at 210 nm; the temperature at the peak of the NF(a) time profile (coincident with 90% FN_3 consumption) was found to be approximately 1150 K by spectroscopic analysis with trace addition of $Bi(CH_3)_3$, and the NF(a) decayed to 50% of its peak concentration in about 5 μs. A detailed study of the performance of this reactor is in progress, and the results will be forthcoming in a future publication.

Discussion

While NF(a) production by thermal dissociation of FN_3 is clearly indicated by the above experiments, the source of the reactive heat to raise the gas temperature in the HF/DF laser

(29) Chase, M. W.; et al. JANAF Thermochemical Tables, 3rd ed.; *J. Phys. Chem. Ref. Data* **1985**, *14*, (Suppl. No. 1).
(30) Herbelin, J. M.; Klingberg, R. A. *Int. J. Chem. Kinet.* **1984**, *16*, 849.
(31) Jones, W. E.; McLean, T. D. *J. Mol. Spectrosc.* **1981**, *90*, 481.
(32) Koffend, J. B.; Herbelin, J. M. The Aerospace Corporation, El Segundo, CA, private communication.
(33) Quick, C. R.; Witting, C. *Chem. Phys. Lett.* **1977**, *48*, 420.

experiments is uncertain. Since the decay of the vibrationally excited HF/DF molecules can be separated in time from the appearance of the NF(a), it follows that reactive heating of the bath gas is controlled by the decay of metastable intermediates, at least for low HF/DF concentrations. Also, since interaction of FN_3 with vibrationally excited HF/DF dissociates the molecule, but does not yield NF(a), it is likely that NF(X) is produced instead. A potential mechanism for NF(X) generation is V → E energy transfer from vibrationally excited HF/DF molecules to FN_3, yielding the triplet state which then dissociates. Wilkins has performed a series of NEST calculations[34] that model the optical pumping of HF molecules under our experimental conditions (without FN_3). These calculations show peak $v = 1$ and $v = 2$ mole fractions of roughly 10% and 1%, respectively. Based on Michel's placement of the triplet state[9] in FN_3, only the energy levels of HF at or above $v = 2$ could dissociate FN_3 by this mechanism. If dissociation of FN_3 upon collisions with HF(v=2) occurs at a rate of 3×10^{-11} cm/s, then the apparent rate of quenching of HF(v) by FN_3 would be 3×10^{-12} cm^3/s (the HF ladder is equilibrated by rapid V–V collisions), and the initial decay of the FN_3 should occur on the 10-μs time scale, consistent with the data. The following reactions are therefore capable of heating[29] the bath gas:

$$FN_3 \rightarrow NF(X) + N_2 + 2.8\ eV \quad (1)$$

$$2NF(X) \rightarrow N_2(X) + 2F + 3.6\ eV \quad (2)$$

$$NF(X) + FN_3 \rightarrow N_2F_2^* + N_2 + 7.5\ eV \quad (3)$$

The estimated rate of quenching of vibrationally excited HF by FN_3 shows that reaction 1, induced by vibrationally excited HF/DF, is probably the rate-limiting step, as might be expected since spin is not conserved. When NF(X) is produced slowly at ambient temperature by thermal dissociation of FN_3 and subsquent quenching of the NF(a), reaction 3 is expected to dominate over reaction 2 because of the linear vs quadratic dependence on NF(X) concentration. This result is consistent with Haller's observation[1] that N_2F_2 is formed efficiently by slow thermal decomposition of FN_3. In the HF/DF laser-driven experiments, however, the NF(X) and FN_3 concentrations may be comparable which would allow reactions 2 and 3 to compete with each other. Energy released by any of these reactions can be tied up in vibrational excitation of the products, which then heat the bath gas upon V–T quenching after a time delay. Moreover, spin conservation in reaction 3 implies that electronically excited triplet $N_2F_2^*$ is formed in preference to the singlet ground state. Ab initio calculations of the N_2F_2 potential surfaces performed by Brenner[35] have indicated that the lowest triplet (metastable) state lies at 4.5 eV, within easy reach of the heat release[5,29] in reaction 3. Therefore, slow electronic quenching may also be a factor in the heating of the bath gas prior to thermal dissociation of FN_3. In any case, since vibrationally excited HF/DF initiates and controls the (first) decomposition of FN_3 (which reactively heats the bath gas), increasing the HF/DF concentration is expected to accelerate the NF(a) time profile, as observed. Thermodynamic estimates[5,29] also show that decomposing approximately two-thirds of the initial FN_3 yields the observed gas temperatures at the peak of the NF(a) time profile, in good agreement with the FN_3 absorption data in Figure 3.

To achieve the highest NF(a) concentrations in the HF/DF experiments, thermal dissociation of FN_3 must be induced as rapidly as possible to minimize the effect of the second-order decay. Since even 1 mJ of incident radiation saturates the HF/DF molecules that are exposed to the laser beam, increased laser energy has little effect. Larger HF/DF concentrations and longer laser pulses are useful, however, because only about 10% of the HF/DF rotational distribution is directly pumped by the laser, and these factors increase the number of molecules that interact with the laser beam as well as promote faster and more complete rotational redistribution during the laser pulse.[36] At 10 Torr of HF concentration, a maximum temperature rise of 100 °C due to laser absorption is estimated based on the NEST calculations,[34] adjusted for quenching of HF(v) by FN_3. This temperature rise is insufficient to drive the thermal dissociation of FN_3 by itself; however, it can have a significant effect in combination with reactions 1–3 due to the exponential dependence of the dissociation rate on temperature. Finally, since thermal dissociation of FN_3 (to yield NF(a)) and the subsequent self-quenching of NF(a) are both exothermic processes, the dissociation reaction is expected to drive to completion once it is thermally initiated, in line with our experimental observations.

Regardless of the mechanisms that heat the bath gas, the critical factors that control the NF(a) time profile are the temperature, the frequency of collisions between FN_3 and the bath gas, the activation energy for dissociation, and the second-order decay process. Since Setser's data[28] and both of our laser experiments show good agreement, the second-order decay rate of $k_q = 3 \times 10^{-12}$ cm^3/s is confirmed. As an aside, we also confirm Setser's finding that too little NF(b) is produced to account for the second-order decay rate by energy pooling of two NF(a) molecules to yield NF(X) and NF(b). On the other hand, the reaction to form a N_2 molecule and two F atoms could possibly account for the observed decay kinetics. The activation energy and collision frequency can be estimated from the value of k_q and the HF/DF data as follows.

Once a FN_3 molecule is sufficiently energized to overcome the activation barrier, dissociation will occur on the time scale of a vibrational period or 10^{-13} s, while the time between collisions is longer than 10^{-10} s at 150 Torr. Substantially (10^3 times) longer lifetimes for the activated FN_3 molecules are unlikely because of the simple structure which allows the molecule to be treated as a pseudodiatomic as discussed in the Introduction. Consequently, collisions with the buffer gas are not effective in restabilizing the activated FN_3 molecules, and the conversion of FN_3 to NF(a) is rate-limited by the production of the activated FN_3 molecules. In this (low-pressure) limit, the rate of appearance of the dissociation products is proportional to the concentration of collision partners.[37] The rate equation for NF(a) at the peak of is time profile can therefore be written as

$$d[NF(a)]/dt = k_a[C][FN_3] - k_q[NF(a)]^2 = 0 \quad (4)$$

where [C] is the concentration of collision partners (bath gas) and k_a is the apparent dissociation rate constant. Since the activation energy (E_a) is large compared to kT, the FN_3 molecule must accumulate sufficient energy to dissociate as a result of several collisions and since typically one vibrational quantum of energy (E_v) is either added to or subtracted from the azide in each of these events, the energy necessary to dissociate the molecule is acquired in random-walk fashion. Statistics also favors collisions that relax FN_3 over those that increase its internal energy. Consequently, the number of collisions required to induce dissociation is $(E_a/E_v)^2 \exp(E_a/RT)$. The collision frequency is given by the product of the cross section (σ_c) and the thermal velocity term $(8\pi RT/M)^{1/2}$ where M is the reduced mass of the colliding pair. The dissociation rate can therefore be written as

$$k_a = \sigma_c(8\pi RT^*/M)^{1/2}(E_v/E_a)^2 \exp(-E_a/RT^*) \quad (5)$$

where T^* is the temperature at the peak of the NF(a) time profile. Solving eq 4 and 5 to eliminate k_a yields

$$\sigma_c(8\pi RT^*/M)^{1/2}(E_v/E_a)^2 \exp(-E_a/RT^*) = k_q\frac{[NF(a)]^2}{[FN_3][C]} \quad (6)$$

The right-hand side of eq 6 can be evaluated from the HF/DF data (Figure 3) as 8.5×10^{-15} cm^3/s, assuming [NF(a)] ~ 10^{16}/cm^3, [FN_3] ~ 7×10^{15}/cm^3, and [C] ~ 5×10^{18} cm^3, at $T^* = 950$ K. Since the NF(a) yield drops very rapidly with

(34) Kwok, M. A.; Wilkins, R. L. *Appl. Opt.* **1983**, *22*, 2721.
(35) Brenner, N. University of Louisiana, Baton Rouge, LA, private communication.
(36) Gurev, V. I.; Vasilev, G. K.; Batovskii, O. M. *JETP Lett.* **1976**, *23*, 230.
(37) Weston, R. E.; Schwartz, H. A. *Chemical Kinetics*; Prentice-Hall: Englewood Cliffs, NJ, 1972; Section 5.2.

temperature, it is not practical to solve eq 6 for σ_c and E_a by collecting additional emission data at a significantly lower temperature. On the other hand, the slow decay of FN_3 at ambient temperature (T_0) is described by the similar relation

$$\sigma_c(8\pi RT_0/M)^{1/2}(E_v/E_a)^2 \exp(-E_a/RT_0) = 1/\tau[C_3] = k_0 \quad (7)$$

where $T_0 = 287$ K, $[C_0] \times 5 \times 10^{18}/cm^3$, and the decay time ($\tau$) is approximately 4×10^3 s, which yields $k_0 = 5 \times 10^{-23}$ cm^3/s. Taking $M \sim 4$, since He is the predominant collision partner in each case, and setting $E_v = 503$ cm^{-1} (the lowest vibrational frequency[4] of FN_3) then allows simultaneous solution of eq 6 and 7 to yield $E_a = 0.63$ eV and $\sigma_c = 34$ Å^2.

The potential errors in the preceding analysis include quenching of NF(a) by FN_3 and NF(X), catalytic dissociation of FN_3 on the walls of the holding tank, and errors in the measurement of T^*. Since the NF(a) branching ratio approaches unity and since NF(X) would be scavenged by reactions 2 and 3, it is unlikely that NF(X) achieves a concentration that is comparable to NF(a). Also, since FN_3 is not a radical species, it is not likely to quench NF(a) as rapidly as NF(a). Gholivand et al. found that the infrared absorption spectrum of gaseous FN_3 and thin films of condensed FN_3 were nearly identical, which demonstrates negligible intramolecular interaction.[10] Consequently, the Teflon-lined walls of the holding tank are not likely to catalyze FN_3 decomposition. Each of these potential errors results in an underestimation of both σ_c and E_a. Since E_a is determined from a logarithmic ratio of the decay rates, relatively large errors are required to change its value significantly. Such errors would also tend to increase σ_c to physically unrealistic values, since σ_c is already close to the gas kinetic limit. The value of E_a, however, scales much more directly with the value of T^* (which is accurate to about ±5%). The measured value of E_a therefore supports Michel's calculation of the barrier height.[9] The value of σ_c we obtained is also in good agreement with a calculated hard-sphere collision cross section of 38 Å^2 based on bond lengths[38] and van der Waals radii.[39] The agreement between our data and the above estimate should be considered as fortuitous, however, since the effects of long-range T → R collisions and steric factors have not been included in the analysis.

A computer code was assembled to numerically integrate the differential rate equations for the gas temperature and the FN_3/NF(a) concentrations in the side-pumped reactor which achieved the highest NF(a) concentrations. The optical pumping by the CO_2 laser was treated as a heat input, and the only reactions were thermal dissociation of FN_3 to yield NF(a) with unity branching ratio and NF(a) self-annihilation to form N_2 + 2F. By use of the kinetic rates discussed above and available thermodynamic data,[5,11,29] good agreement (±10%) was obtained between the model and the data for the simultaneous FN_3/NF(a) time profiles and the peak temperature/NF(a) concentration with only modest (±25%) variation of the rate parameters. These results confirm our basic understanding of the kinetics of generation and decay of NF(a) upon rapid thermal dissociation of FN_3.

It is also interesting to compare the production of NF(a) by thermal dissocation of FN_3 to the F + HN_3 reaction,[24,25] which proceeds by first generating N_3 radicals (HF abstraction) and then passing through an FN_3 intermediate (F + N_3 reaction) to generate NF(a). It therefore follows that efficient production of NF(a) in the F + HN_3 reaction tends to imply efficient production of NF(a) upon thermal dissociation of FN_3, as observed. The thermal dissociation reaction, however, is much easier to scale to large NF(a) concentrations, since it does not involve reactive intermediates (N_3) which tend to self-annihilate.[40] The very large concentrations of NF(a) that have been obtained ($\sim 10^3$ of the F + HN_3 reaction[25]) reflect this difference and the slow quenching[28] of NF(a) by the reaction byproducts (N_2). The attainable yields appear to be limited only by the self-annihilation reaction which is inherent to any scheme for generation of NF(a).

In summary, thermal dissociation of FN_3 is a process with an activation energy of approximately 0.6 eV, which yields metastable NF(a) with near-unit efficiency. Large ($>10^{16}$/cm^3) concentrations of NF(a) can be generated by this reaction; however, the gas temperature must be increased rapidly, so that the NF(a) concentration builds up on time scale that is shorter than the second-order decay, which occurs at a rate of approximately 3×10^{-12} cm^3/s. A significant application for this new source of NF(a) is the development of advanced short-wavelength chemical transfer lasers that are analogous to the oxygen–iodine system.[41] With greater than 10^{16}/cm^3 concentrations of NF(a) and transfer rates[42] approaching 10^{-10} cm^3/s, it will be possible to obtain partial inversions on molecules such as BiF which have radiative lifetimes[43] on the order of 1 μs.

Acknowledgment. This research was supported in part by a contract from the Air Force Weapons Laboratory and the Air Force Astronautics Laboratory.

Registry No. FN_3, 14986-60-8.

(38) Radimacher, P.; Bittner, A. J.; Schatte, G.; Willner, H. *Chem. Ber.* **1988**, *121*, 555.
(39) Maitland, G. C.; Rigby, M.; Smith, E. B.; Wakeman, W. A. *Intermolecular Forces*; Clarendon Press: Oxford, 1981.
(40) Piper, L. G.; Krech, R. H.; Taylor, R. L. *J. Chem. Phys.* **1979**, *71*, 2099.
(41) McDermott, W. E.; Pchelkin, N. R.; Benard, D. J.; Bousek, R. R. *Appl. Phys. Lett.* **1978**, *32*, 469.
(42) Herbelin, J. M. Electronic Energy Transfer Between NF(a) and BiF(X). *Proc. Int. Conf. Lasers* **1986**.
(43) Heidner, R. F.; Helvajian, H.; Hollaway, J. S.; Koffend, J. B. "BiF(A) Radiative Lifetimes and Rate Coefficients for V-T Transer and Electronic Quenching"; Technical Report 87-19; Aerospace Corporation; El Segundo, CA, April 1987.

PROCEEDINGS REPRINT

SPIE—The International Society for Optical Engineering

Reprinted from

High-Power Gas Lasers

15–17 January 1990
Los Angeles, California

Volume 1225

Invited Paper

Chemical pumping of potential visible laser transistions in bismuth monofluoride by thermal dissociation of fluorine azide

B.K. Winker, D.J. Benard and T.A. Seder

Rockwell International Science Center
Thousand Oaks, CA 91360

ABSTRACT

A visible chemical laser on the BiF(A-X) transistions at 430-470 nm can potentially be generated by the interaction of Bi-atoms with metastable species such as NF($a^1\Delta$). Experiments were performed in which these constituents were obtained in situ by fast pulsed CO_2 laser pyrolysis of FN_3 and $Bi(CH_3)_3$, respectively. Time-resolved optical diagnostics were used to follow the concentrations of FN_3, NF($a^1\Delta$), $Bi(CH_3)_x$, Bi(^{2}D) and BiF(A). The optimal concentrations of FN_3 and $Bi(CH_3)_3$ were limited by NF($a^1\Delta$) self-annihilation and Bi(^{2}D) quenching reactions, respectively. The $Bi(CH_3)_3$ was found to be only 20 % dissociated at the peak of the NF($a^1\Delta$) time profile and the yield of Bi-atoms from dissociated $Bi(CH_3)_3$ was determined to be approximately 5 %; however, significant recycling of the active Bi/BiF species was observed at a limiting rate of $4 - 5 \times 10^{-11}$ cm^3/s, driven by NF($a^1\Delta$). On the basis of these results, a peak BiF(A) concentration of 10^{13}/cm^3 was predicted by kinetic modeling and subsequently observed. The model also predicts an absolute population inversion of the BiF(A-X) transistion at high NF($a^1\Delta$) concentration with unsaturated gains of approximately 10^{-3}/cm. Intracavity experiments have verified that the BiF(X) ground state concentration is low enough relative to the excited state to generate at least a partial inversion, and initial evidence for an absolute population inversion has been obtained.

1. INTRODUCTION

Since chemical reactions follow the same spin-selection rules as optical transistions, it is difficult to produce electronically excited products with high efficiency unless they are optically metastable, because the reaction will preferentially populate any lower energy product state that is of the same spin. Consequently, the generation of electronic transistion chemical lasers typically involves a two-step process consisting of efficient chemical production of an optically metastable species, which acts as an energy store, followed by some form of energy transfer from the store to a more suitable radiating species. In our work, the $a^1\Delta$ state of nitrogen monofluoride (NF) is the energy store and bismuth monofluoride (BiF) is the radiating species. The transfer of energy from NF($a^1\Delta$) to BiF was initially discovered by Herbelin[1] who used the reaction of H-atoms with NF_2 radicals to generate the NF($a^1\Delta$). Recently, we have developed a new source of NF($a^1\Delta$) that is based on thermal dissociation of fluorine azide (FN_3), which is capable of achieving unusually high NF($a^1\Delta$) concentrations.[2] Large yields of NF($a^1\Delta$) are important to this application since the BiF(A) state has a radiative lifetime[3] near 1 μs and the rate of BiF excitation (which must approach 10^6/s) is controlled by the NF($a^1\Delta$) concentration. In this work, we have used the FN_3 source of NF($a^1\Delta$) to extend Herbelin's work to higher NF($a^1\Delta$) concentrations and to investigate any differences in the mechanism of BiF excitation that may occur between the two chemical sources of metastable NF.

2. EXPERIMENTAL

Figure 1 shows schematically how the experiments were performed. A variable gas mixture of FN_3, $Bi(CH_3)_3$ and SF_6 in He buffer gas was admitted to a slowly flowing reactor that was exhausted to a vacuum. The gas flow in the reactor was optically pumped by a pulsed CO_2 laser at a rate of 1-2 Hz, so that gas flow in the reactor changed the active sample between shots.

The functions of the SF_6 additive were to absorb the incident CO_2 laser radiation and to heat the gas upon subsequent collisional relaxation. The laser fluence in these experiments was well below the threshold for significant production of F-atoms by multiphoton dissociation.[4] The excited states of NF and BiF were detected in emission at 874/528 and 450 nm, respectively,[5] by an optical multichannel analyzer (OMA) for spectral analysis and by a filtered silicon photodiode interfaced to a fast preamplifier and digital signal averager for temporal analysis. The diode/filter combinations were absolutely calibrated by comparison to a standard lamp of known emissivity that is traceable to the National Bureau of Standards. Therefore, absolute $NF(a^1\Delta, b^1\Sigma)$ and BiF(A) concentrations could be inferred with knowledge of the relevant A coefficients,[3,6,7] and the gas sample / photon collection geometry. Ground state species such as $Bi(CH_3)_x$ and FN_3 were followed by time-resolved ultraviolet absorption using a D_2 lamp source and a filtered 1P28 photomultiplier tube as the detector. The absorption signals were processed in the same manner as the emission signals from the silicon detector, and absolute concentrations were inferred from these data with knowledge of the active path length and the relevant extinction coefficients.[8,9] Detection of $Bi(^2D)$ was accomplished by ultraviolet absorption since the emission signal was prone to spectroscopic interference due to overlapping HF emissions. In this case, the D_2 lamp was replaced by a Bi-hollow cathode lamp which was electronically pulsed to enhance its intensity. The lamp current was pulsed to approximately 500 ma for about 500 μs with a 200 μs lead on the CO_2 laser pulse used to initiate the chemical reactions to be monitored. Hence, the lamp intensity was essentially constant during the time of data collection. In these experiments, the 289.8 nm line was selected by the filter that was placed over the detector, and the absolute concentration of $Bi(^2D)$ was determined from the absorption data using a cross section that was calculated from the radiative rate[10] assuming a Doppler broadened line profile. The gas temperature was determined with ± 50 K accuracy by comparison of a section of the BiF(A-X) emission spectrum to a set of synthetically generated emission spectra, provided by Koffend,[11] as described in a prior publication.[2] Worst case propagation of errors in the concentration measurements suggests an accuracy of approximately ± 35 %.

The reactor was designed for wall-free operation by admitting the reactive gas flows to a central 2.5 mm × 2.5 cm rectangular duct that was surrounded by a velocity matched Ar shield flow. All gas flows were electronically monitored by mass flow meters and the reactor pressure was monitored by an inductance transducer. The $Bi(CH_3)_3$ was eluted from a cold trap at ice temperature by bubbling a flow of He carrier gas through the liquid. The mole fraction of the $Bi(CH_3)_3$ in the He flow was determined from the vapor pressure[12] of the $Bi(CH_3)_3$ and a measurement of the total pressure in the trap, assuming complete saturation of the He flow. Prior experience has shown this method to overestimate the $Bi(CH_3)_3$ mole fraction by a factor of less than two. Typical conditions in the reactive jet were 0-0.1 torr $Bi(CH_3)_3$, 1.5 torr FN_3, 13.5 torr SF_6 and balance He to a net pressure of 150 torr. The jet was side pumped by the CO_2 laser with a soft line focus (2.5 mm × 2.5 cm) at a fluence of approximately 1 joule/cm^2. The SF_6 concentration was chosen so that approximately 66 % of the incident laser energy was transmitted through the reactor to a retroreflecting cylindrical mirror that refocused and counterpropagated the beam through the reactor. This procedure was used to insure uniform excitation of the reactive flow across its short dimension. The optical measurements were taken along the 2.5 cm long axis of the reactive flow (perpendicular to the CO_2 laser beam).

The FN_3 flow was generated by reacting commercial grade sodium azide with stearic acid at 110°C to yield hydrogen azide (HN_3) gas in a He carrier stream, which subsequently reacted with a dilute F_2/He gas stream to yield HF, which was eliminated in a cold trap, and FN_3. This is a somewhat hazardous and complex operation that is described in detail in prior publications.[2,13] The mole fraction of FN_3 in the He carrier stream was determined by absorption measurements at 425 nm using the extinction data of Gholivand.[8] The materials of construction were limited to stainless steel, teflon/viton and glass/quartz to prevent undesired reaction, and care was taken to avoid even mild heating of the FN_3 flow to prevent disproportionation[14] into

N_2F_2 and N_2. The FN_3 gas flow at the laser pyrolysis reactor showed negligible decomposition as determined by mass spectroscopy.

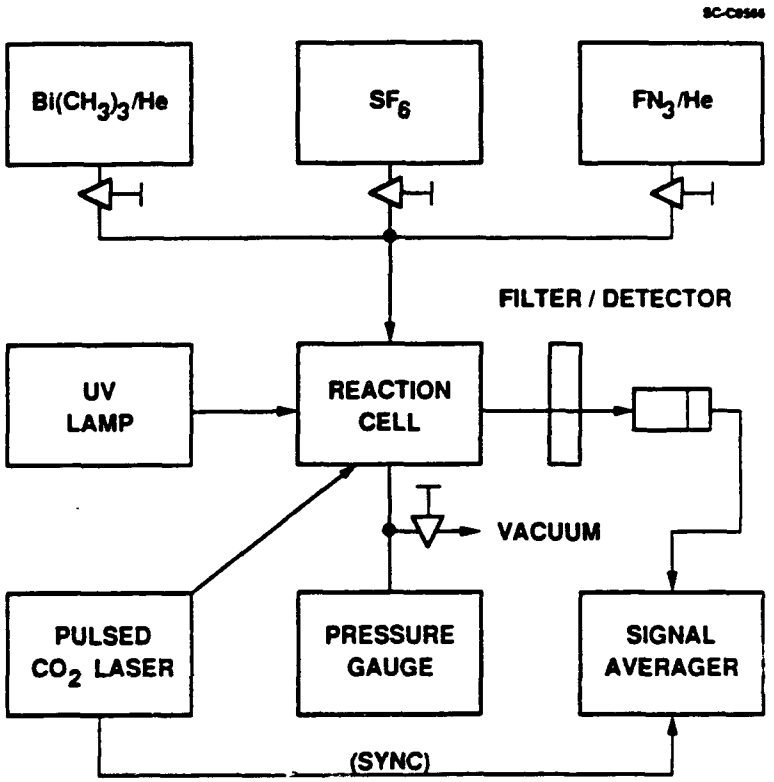

Fig. 1 Block diagram of experiment used to investigated energy transfer from NF($a^1\Delta$) to BiF.

3. GENERATION OF NF($a^1\Delta$)

Figure 2 shows the typical emission spectrum that is obtained in the vicinity of the NF(a-X) transitions at 874 nm by CO_2 laser excitation of FN_3/SF_6 gas mixtures. It is characteristically free of overlapping N_2(B-A) emissions that are common to other NF($a^1\Delta$) sources, which is consistent with the very simple mechanism of excitation just described.

Typical time profiles of the FN_3 and NF($a^1\Delta$) following the CO_2 laser pulse (in the absence of $Bi(CH_3)_3$) are shown in Fig. 3. These data were collected with 100 ns resolution; however, the NF($a^1\Delta$) time profile has been smoothed since NF($a^1\Delta$) is a weak emitter and the statistical noise is significant on the sub-μs time scale. The error bar indicates the magnitude of the peak-to-peak noise at 100 μs resolution. The FN_3 absorption data is relatively noise free but does experience some electrical interference from the CO_2 laser at early times as indicated by the error bar and the dashed portion of the line. The yield of NF($b^1\Sigma$) in these experiments was approximately 10^{-2} of the NF($a^1\Delta$), and the peak temperature was estimated at 1200 K using trace addition of $Bi(CH_3)_3$. The rise of the NF($a^1\Delta$) is seen to coincide with the decay of the FN_3 indicating a simple mechanism, namely:

$$FN_3 \xrightarrow{\Delta} NF(a^1\Delta) + N_2 \qquad (1)$$

The subsequent decay of the NF($a^1\Delta$) due to self-annihilation

$$NF(a^1) + NF(a^1\Delta) \rightarrow \text{products} \tag{2}$$

has been observed by Setser[15] in low density flowtube experiments. The products of this reaction are not known; however, the yield of NF($b^1\Sigma$) obtained in both Setser's and our experiments is too low to account for the NF($a^1\Delta$) loss due to energy pooling. Because of the self-annihilation process, high densities of NF($a^1\Delta$) can be achieved only if the FN_3 is dissociated rapidly.

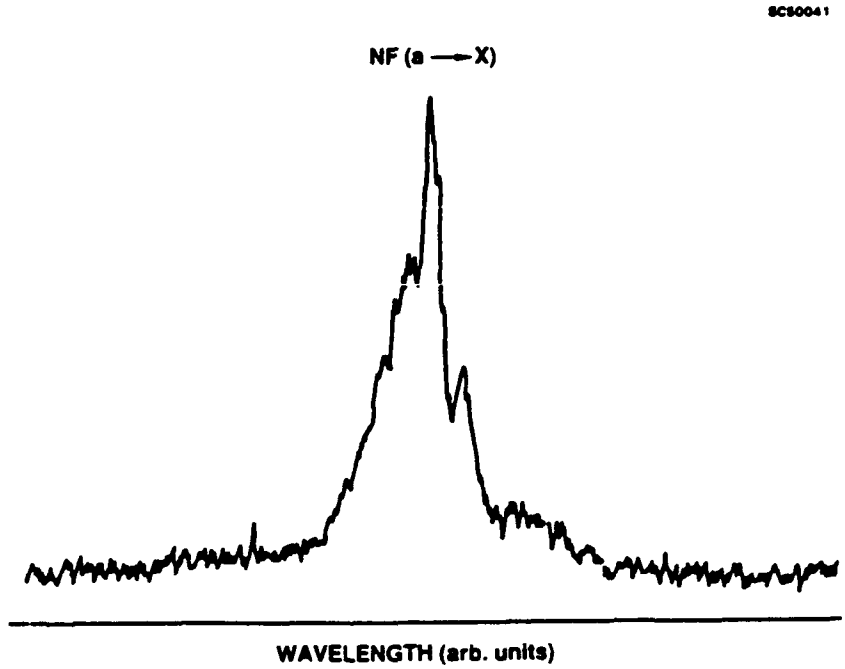

Fig. 2 Emission spectrum of NF($a^1\Delta$) obtained by thermal dissociation of FN_3.

The principal factors that govern the dissociation rate are the collision frequency, the barrier height for activation of the dissociation reaction and the gas temperature. Michels[16] has calculated the barrier to FN_3 dissociation by ab initio methods to be approximately 0.5 eV. The dissociation of FN_3 and the production and decay of the NF($a^1\Delta$) can therefore be described by the following set of coupled differential rate equations which treat temperature as a dynamic variable and assume 100 % conversion of FN_3 to NF($a^1\Delta$) upon dissociation with negligible loss of reactants or heat due to transport phenomena.

$$\frac{d}{dt}[FN_3] = -k_d\, e^{-T/T_o}\,[FN_3]\,[M] \tag{3}$$

$$\frac{d}{dt}[NF(a)] = -\frac{d}{dt}[FN_3] - k_q\,[NF(a)]^2 \tag{4}$$

$$\frac{d}{dt}T = \frac{1}{C}\left(\sigma\, I(t)\,[SF_6] - H_d\frac{d}{dt}[FN_3] + H_q\, k_q\,[NF(a)]^2\right) \tag{5}$$

The terms are defined as follows: k_d is the collision rate between FN_3 molecules and other species (M), T is temperature and T_o is the barrier height expressed in terms of temeprature, k_q is the self-annihilation rate, C is the heat capacity of the gas, I(t) is the intensity time profile of the incident CO_2 laser radiation, σ is the cross section for absorption by SF_6, and $H_{d,a}$ are the heat releases associated with the dissociation of FN_3 and the self-annihilation reactions, respectively. The thermodynamic factors are available in large part from the JANAF tables. The products of reaction (2) are assumed to be N_2 and two F-atoms. The heat of formation of FN_3 was obtained as +120 kcal/mole from prior work involving ArF photolysis of the azide at low pressure.[17] The cross section (σ) was determined by actual transmission measurements since its value is somewhat dependent on the intensity of the CO_2 laser. Finally, I(t) was modeled as the sum of two linearly decaying time profiles that correspond to the fast and slow components of the CO_2 laser output. The principal fitting parameters are k_d, which can be estimated at 10^{-11} cm^3/s by kinetic theory, T_o, which is approximately 6000 K on the basis of Michel's calculation and k_q which was measured by Setser and confirmed in our laboratory to have a value near 3×10^{-12} cm^3/s. Figure 4 shows the typical result obtained by computer integration of equations (3-5) subject to the initial values defined by the experimental conditions. Table 1 provides a more detailed comparison between theory and experiment under conditions which optimize the yield of $NF(a^1\Delta)$. These results were obtained with only modest variation of the rate parameters (± 25 %) and the activation barrier (± 10 %). Therefore, the general agreement that is obtained as well as the ability of the model to reproduce the qualitative trends that are observed with variation of laser energy and initial FN_3 concentration suggest that reactions (1) and (2) are the dominant processes and that the rate constant/barrier height estimates are approximately correct. Since our gas sample was heavily diluted, the rise in gas temperature was primarily due to laser heating rather than the induced reactions, as shown in Fig. 4. If this condition were not satisfied, the time profiles would be considerably more complex and difficult to model accurately.

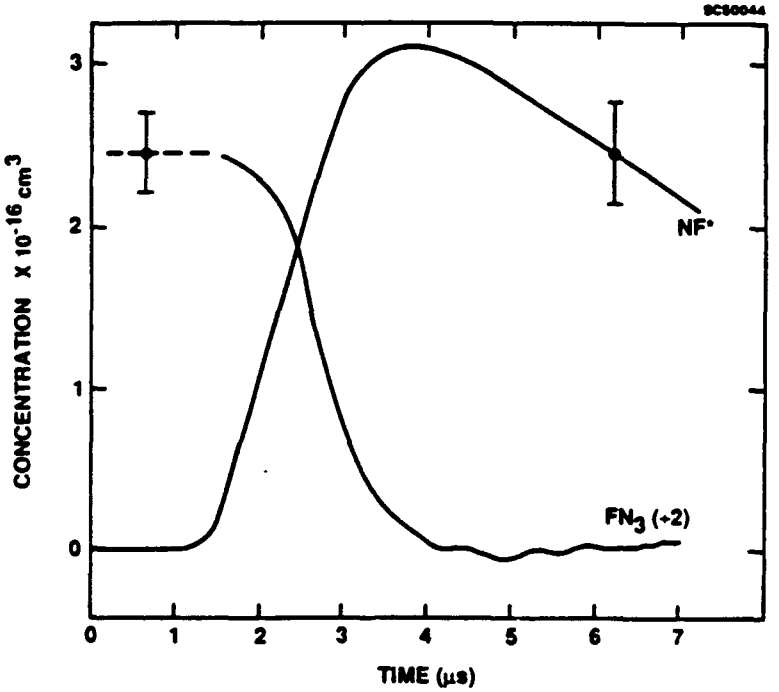

Fig. 3 Characteristic time profiles of FN_3 and $NF(a^1\Delta)$ following pulsed CO_2 laser excitation.

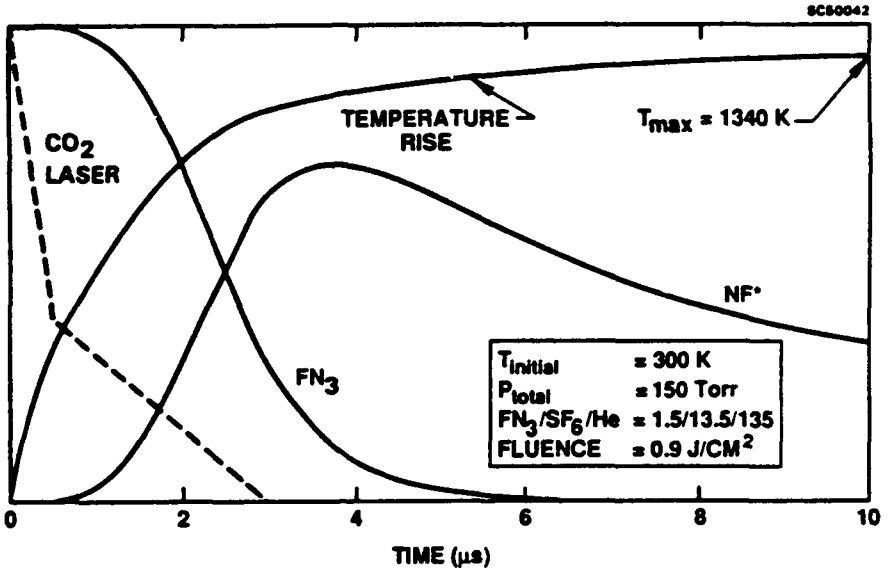

Fig. 4 Time profiles of FN_3, $NF(a^1\Delta)$ and gas temperature obtained by kinetic modeling.

Table 1
Comparison of Modeling Results to Experimental Data
for CO_2 Laser Driven Pyrolysis of FN_3

Result	Model	Data	Units
Peak [$NF(a^1\Delta)$]	4×10^{16}	3×10^{16}	cm^{-3}
Rise Time (10-90 %)	2.6	2.4	μs
Decay Time (100-50 %)	5.7	5.0	μs
Temperature at Peak	1237	1150	K

4. EXCITATION OF BiF(A)

Upon addition of $Bi(CH_3)_3$ to the FN_3 and SF_6 in the reactor very intense BiF(A-X) emission was observed. The mechanism of excitation of this species is considerably more complex than that of $NF(a^1\Delta)$, as shown by the processes indicated on the energy level diagram given as Fig. 5. Once Bi-atoms are introduced into the system, the reactions

$$NF + BiF_x \rightleftarrows N + BiF_{x+1} \quad (6)$$

$$NF + BiF_x \rightleftarrows NF_2 + BiF_{x-1} \quad (7)$$

set up a complex equilibrium between Bi-atoms, BiF, BiF_2 and BiF_3. From a strictly thermodynamic standpoint, the majority of the Bi is expected to be in the form of BiF_2 and

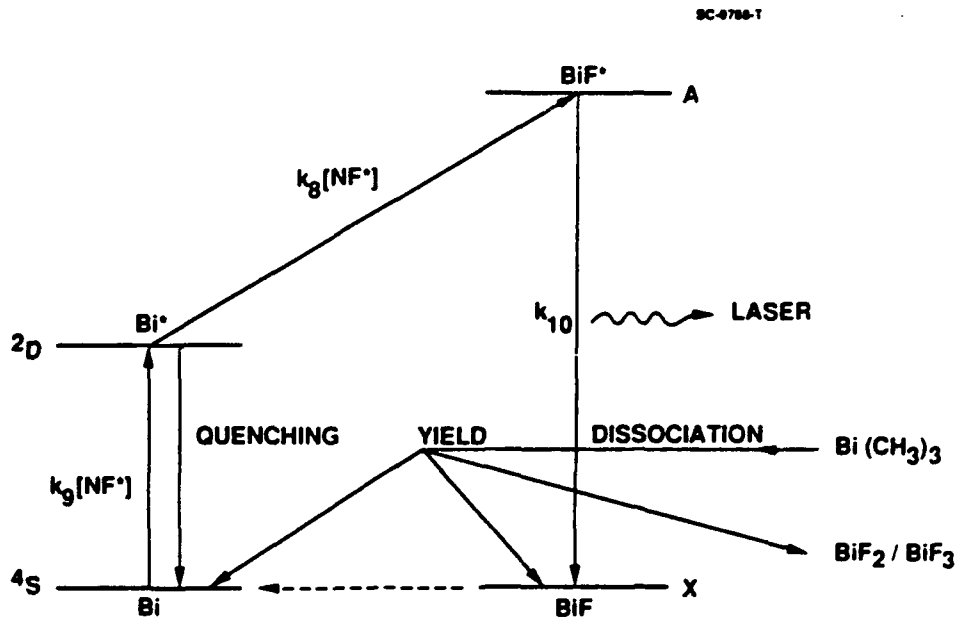

Fig. 5 Energy levels and kinetic processes involved in the excitation of the BiF(A) state. The reactions responsible for recycling active Bi/BiF are shown by the dashed line.

BiF_3 which do not participate in the observed chemiluminescence. Therefore, the efficiency of converting dissociated $Bi(CH_3)_3$ into active Bi/BiF is a key concern. Related issues are the rate and mechanism of $Bi(CH_3)_3$ dissociation and the quenching of $NF(a^1\Delta)$ and other significant electronically excited species by undissociated $Bi(CH_3)_3$ or its dissociation by-products. Herbelin[11] has suggested that the actual mechanism responsible for the BiF(A) generation is

$$NF(a^1\Delta) + Bi(^2D) \rightarrow N + BiF(A) \quad (8)$$

where the $Bi(^2D)$ is generated by the fast resonant transfer reaction

$$NF(a^1\Delta) + Bi \rightarrow NF(X^3\Sigma) + Bi(^2D) \quad (9)$$

first studied by Sutton and Capelle.[18] Once produced, BiF(A) decays radiatively

$$BiF(A) \rightarrow BiF(X) + h\nu \quad (10)$$

and there is a potential for recycling of the Bi-atoms if reactions such as (7, x = 1) or

$$N + BiF \rightarrow NF + Bi \quad (11)$$

occur at a significant rate. It is therefore important to know which step in the cyle is rate limiting and the associated rate constant. Reactions such as (7, x = 1) and (11) also help to

remove BiF(X) and thereby to maintain population inversion of the A-X transistion. Our investigation is aimed at a resolution of these issues.

5. RESULTS AND DISCUSSION

Measurements of the time profiles of $Bi(CH_3)_x$, Bi(^{2}D) and BiF(A) were collected under conditions of both high (3×10^{16}/cm^3) and low (3×10^{15}/cm^3) peak NF($a^1\Delta$) concentration to resolve the kinetic issues described above. The peak NF($a^1\Delta$) concentrations were changed by adjusting the initial FN_3 concentration. The principal reason for this alteration was to slow the self-annihilation reaction (2) which occurs at a rate comparable to the Bi/BiF kinetics for high NF($a^1\Delta$) concentrations. Since the experimental observables reflect both the time evolution of the NF($a^1\Delta$) as well as the Bi/BiF species, this condition was necessary in some cases to effect a deconvolution of these phenomena. The data are presented and analyzed in the order that yields the simplest interpretation of the results.

5.1 Production of BiF(A) from Bi(^{2}D)

The time profiles of Bi(^{2}D) and BiF(A) at high peak NF($a^1\Delta$) concentration are shown in Fig. 6. The initial $Bi(CH_3)_3$ concentration in these experiments was set to 6×10^{14}/cm^3 to optimize the Bi(^{2}D) measurement. At this concentration of $Bi(CH_3)_3$, the NF($a^1\Delta$) time profile is not significantly altered, as will be shown later. Since the BiF(A) time profile follows the Bi(^{2}D) by approximately one radiative lifetime in the vicinity of the peak emission regime, our data are compatible with reaction (8) as the principal pumping mechanism. The rate of the pumping reaction (k_8) of Bi(^{2}D) with NF($a^1\Delta$) to yield BiF(A) can be determined by applying the steady state relation

$$k_8 [NF(a^1\Delta)] [Bi(^2D)] = A [BiF(A)] \quad (12)$$

at the peak of the BiF(A) time profile. Taking $A = 7 \times 10^5$/s as measured by Koffend,[3] [NF($a^1\Delta$)] ~ 3×10^{16}/cm^3 and [BiF(A)] ~ 2 [Bi(^{2}D)] from Fig. 6 gives $k_8 \sim 4.7 \times 10^{-11}$ cm^3/s in resonable agreement with an independent determination of the same rate as measured by Herbelin[11] using the H + NF_2 reaction to generate the NF($a^1\Delta$). The sum of the Bi(^{2}D) and BiF(A) concentrations, however, is only about 1 % of the initial $Bi(CH_3)_3$ concentration. The other 99 % must therefore be accounted for by incomplete dissociation of the $Bi(CH_3)_3$, the yield of active Bi/BiF from the $Bi(CH_3)_3$ that was dissociated, and the production of ground state Bi/BiF species. The latter is believed to be negligible, however, since Sutton found complete disappearance of ground state Bi in the presence of NF($a^1\Delta$). A similar situation may also exist in regard to ground state BiF(X) at high NF($a^1\Delta$) concentrations, due to reactions (7, x = 1) and (11). Therefore, we will proceed on the assumption of negligible BiF(X) concentration and will address this point independently later.

5.2 Dissociation of $Bi(CH_3)_3$

The disappearance of the Bi-donor was tracked at 270 nm where FN_3 absorption[8,9] is weak compared to $Bi(CH_3)_3$. Background data were collected and subtracted to account for residual FN_3 absorption and ultraviolet chemiluminescence emitted by the reactor. The absorption vs time after the CO_2 laser pulse was found to increase initially and then to decline to zero as shown in Fig. 7. This behavior is attributed to sequential loss of the methyl groups and a higher absorption coefficient in the intermediate $Bi(CH_3)_2$ or $Bi(CH_3)_1$ species than in $Bi(CH_3)_3$. To deal with this complication, a simple model of the form

$$Bi(CH_3)_3 \rightarrow \text{Intermediates} \quad (13)$$

$$\text{Intermediates} \rightarrow Bi \quad (14)$$

was constructed. The rates k_{13} and k_{14} were assumed to be fixed, owing to a thermal dissociation mechanism, since the absorption data were not influenced by the presence or lack of FN_3. In other words, $NF(a^1\Delta)$ does not contribute significantly to the dissociation of $Bi(CH_3)_3$ as a result of energy transfer or chemical reactions. The absorption signal was normalized to unity at $t = 0$ and the ratio of the ultraviolet absorption cross sections (intermediates to initial $Bi(CH_3)_3$) was used as a fitting parameter along with k_{13} and k_{14}. The rate equations corresponding to reactions (13) and (14) were solved analytically, and the absorption signal was calculated and also normalized to unity at $t = 0$. The cross section ratio was analytically selected to yield an absorption time profile that peaked in time at the same point as the data. Trial values of k_{13} and k_{14} were then selected and the solutions were compared against the data for relative peak height and overall decay rate. The best fit to the absorption data shown in Fig. 6 corresponds to $k_{13} = 4.2 \times 10^5$/s and $k_{14} = 3.9 \times 10^5$/s. While the values of k_{13} and k_{14} could be co-varied somewhat without significantly affecting the agreement with the data, the yield of Bi-atoms, which was then calculated analytically, did not vary significantly. Therefore, as shown in Fig. 7, the $Bi(CH_3)_3$ is completely converted to Bi-atoms in about 10 μs. At high $NF(a^1\Delta)$ concentrations, however, the peak BiF(A) emission occurs at about 2 μs. Consequently, only about 20 % of the $Bi(CH_3)_3$ contributes to the pumping of the BiF(A) state when the $NF(a^1\Delta)$ yield is optimized. Since the overall yield of active Bi/BiF from initial $Bi(CH_3)_3$ is 1 %, it then follows that the yield of active Bi/BiF from dissociated $Bi(CH_3)_3$ is about 5 %.

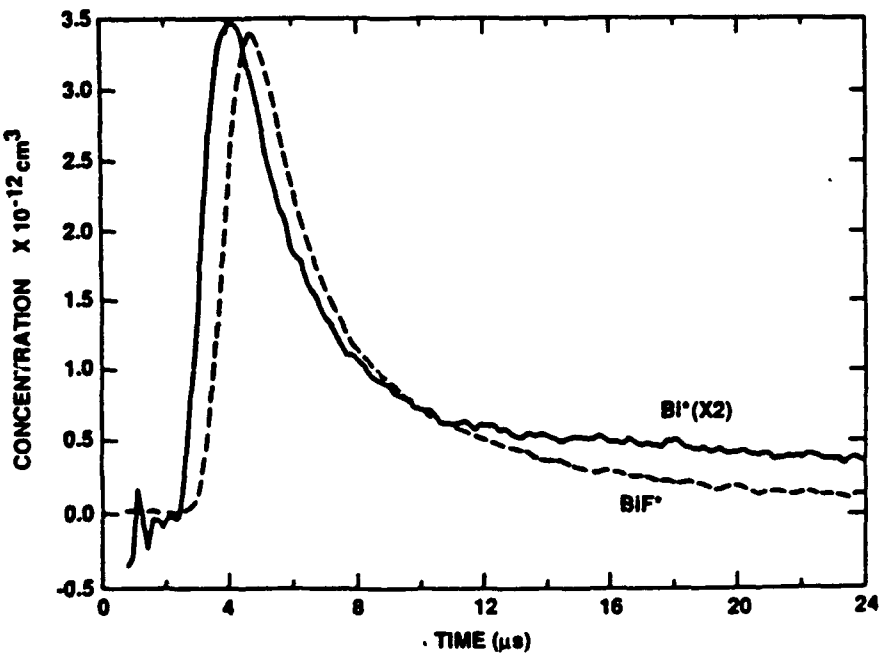

Fig. 6 Time profiles of $Bi(^2D)$ and BiF(A) following pulsed CO_2 laser excitation.

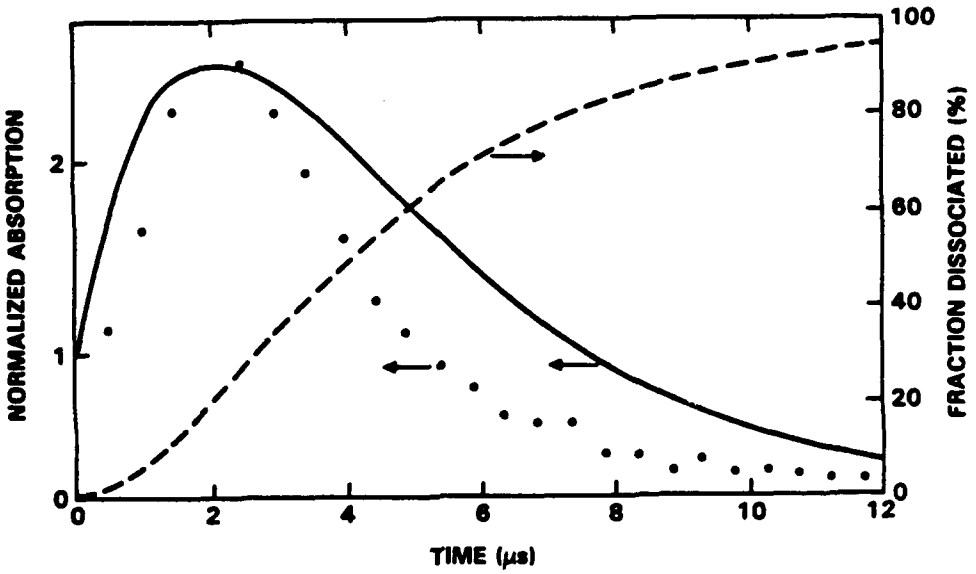

Fig. 7 Time profile of ultraviolet absorption due to $Bi(CH_3)_x$ species (dots) and related kinetic modeling results (solid and dashed lines).

5.3 Recycling of Active Bi/BiF

By reducing the initial FN_3 concentration an order of magnitude and using trace concentrations of $Bi(CH_3)_3$, essentially all of the $Bi(CH_3)_3$ is dissociated before the peak $NF(a^1\Delta)$ concentration decays significantly. When this is done, a 10 μs rise in the BiF(A) time profile is observed, which can be assigned to the dissociation of the $Bi(CH_3)_3$, as shown in Fig. 8. Following this rise, the decay of the BiF(A) essentially follows the decay of the $NF(a^1\Delta)$. Consequently, a near steady state condition is achieved, which suggests that active Bi/BiF is recycled following the emission step; otherwise a more rapid decay of the BiF(A) would be observed. By integrating the BiF(A) time profile, the net yield of BiF(A-X) photons per unit volume was found to equal 70 % of the initial $Bi(CH_3)_3$ concentration. Since all the $Bi(CH_3)_3$ dissociates in this experiment but only 5 % of the dissociated $Bi(CH_3)_3$ yields active Bi/BiF, approximately 14 photons were generated per each active Bi/BiF species, which demonstrates effective recycling. Under these conditions, the rate of photon emission is governed by the limiting rate in the cycle. The radiative step (10) is not limiting in this case as all of the other reactions are driven by low $NF(a^1\Delta)$ concentrations. The excittion of $Bi(^2D)$ by $NF(a^1\Delta)$, reaction (9), is known to be fast[18] by comparison to reaction (8). Therefore, the limiting rate is either the pumping step (8) or the conversion of BiF(X) back into Bi-atoms due to reactions (7, x = 1) and (11). Without determining which rate is limiting, the limiting rate constant (k_o) can be determined under cycling/total dissociation conditions by applying the steady state relation

$$I = k_o \, Y \, [Bi(CH_3)_3] \, [NF(a^1\Delta)] \qquad (15)$$

where I is the rate of BiF(A-X) photon emission per unit volume and Y is the dissociation yield of active Bi/BiF or about 5 %. Applying the above analysis to the data in Fig. 7 yields $k_o \sim 5 \times 10^{-11}$ cm³/s in close agreement with the measured rate of reaction (8). It therefore follows that the rates of the BiF(X) removal reactions (7, x = 1 and 11) are at least this fast or possibly faster. Consequently, at high $NF(a^1\Delta)$ concentrations, the rate of BiF(X) removal exceeds $(5 \times 10^{-11}$ cm³/s) × $(3 \times 10^{16}$/cm³) or 1.5×10^6/s, which is twice the radiative rate of

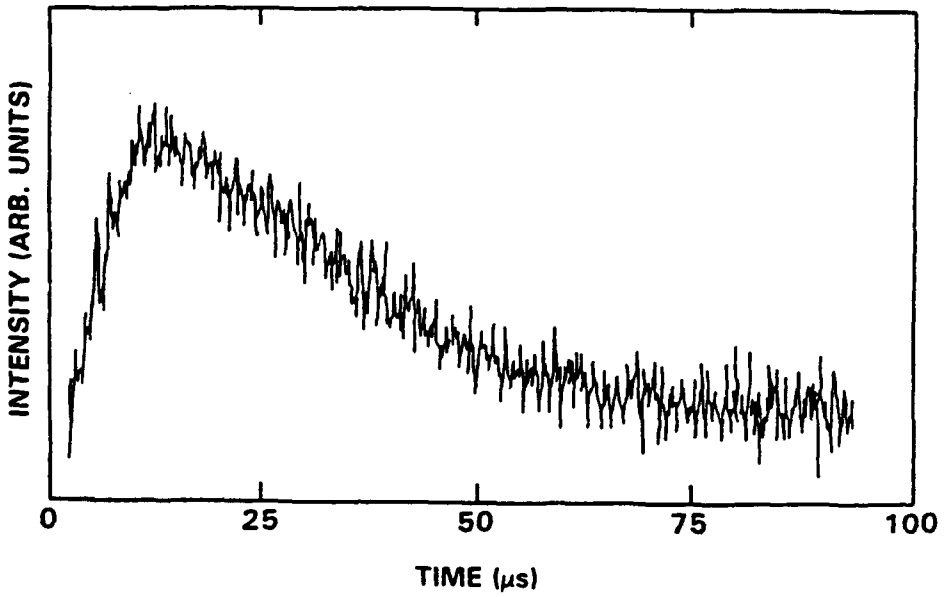

Fig. 8 Time profile of BiF(A) at reduced NF($a^1\Delta$) concentration showing a 10 μs rise due to the dissociation of $Bi(CH_3)_3$.

the BiF(A-X) transition. This result, which implies an absolute population inversion at high NF($a^1\Delta$) concentration, is consistent with the earlier assumption of negligible BiF(X) concentration.

5.4 Scaling of BiF(A)

The peak achievable yield of BiF(A) depends critically on the amount of $Bi(CH_3)_3$ that can be productively added to the FN_3. This factor is controlled primarily by the associated quenching of Bi(^{2}D) and BiF(A) by $Bi(CH_3)_3$ and its by-products. Since BiF(A) decays radiatively at a high rate, it is less subject to quenching than Bi(^{2}D) which has a much longer kinetic lifetime. Optimum addition of $Bi(CH_3)_3$ will therefore be limited by the competition between the reaction of Bi(^{2}D) with NF(a) and its quenching by $Bi(CH_3)_3$ according to the relation

$$k_8\,[NF(a^1\Delta)] = k_s\,[Bi(CH_3)_3]_{optimal} \qquad (16)$$

where k_s is the quenching rate constant that controls scaling. Taking $k_s = 3 \times 10^{-10}$ cm^3/s based on Trainor's work[19] yields 3×10^{15}/cm^3 as the optimum $Bi(CH_3)_3$ concentration for [NF($a^1\Delta$)] ~ 3×10^{16}/cm^3. Higher concentrations of $Bi(CH_3)_3$ will promote quenching at a rate that is competitive with the pumping reaction and therefore will not increase the yield of BiF(A) significantly. Consequently, the peak yield of BiF(A) is expected to be 3×10^{15}/cm^3 multiplied by 0.2 to account for the dissociation fraction, 0.05 to account for the yield of active Bi/BiF and 0.66 to account for the fraction of active Bi/BiF in the BiF(A) state. In practice, this steady-state estimate must be discounted by an additional factor of 2, since under optimal $Bi(CH_3)_3$ loading the time duration (FWHM) of the BiF(A) pulse is comparable to the radiative lifetime. The net result is an expected BiF(A) yield of 10^{13}/cm^3, which was indeed observed as shown in Fig. 9 where the rollover with initial $Bi(CH_3)_3$ concentration occurs at the predicted 3×10^{15}/cm^3 concentration.

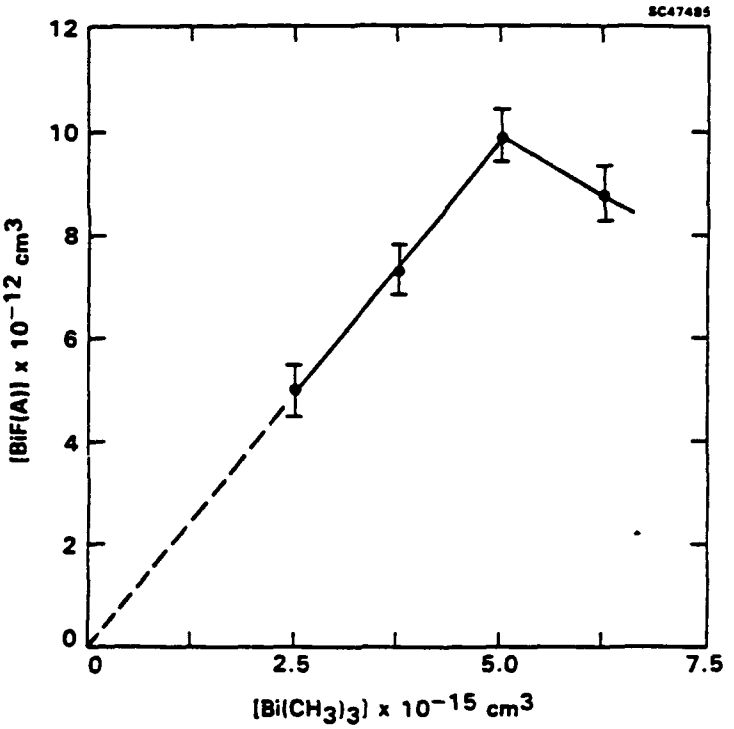

Fig. 9 Scaling of BiF(A) yield vs addition of $Bi(CH_3)_3$.

The scaling of the BiF(A) yield was also investigated at fixed $Bi(CH_3)_3$ concentration with respect to varied initial FN_3 concentration as shown in Fig. 10. Here the scaling is apparently nonlinear in [NF($a^1\Delta$)] at low concentrations because quenching dominates the decay rate of the Bi(^2D) intermediate. In this limit, [Bi(^2D)] scales proportional to [NF($a^1\Delta$)] since the metastable species drives its production, and [BiF(A)] produced via the reaction of Bi(^2D) with NF($a^1\Delta$) then scales as [NF($a^1\Delta$)]^2. As the NF($a^1\Delta$) concentration is increased, the pumping reaction (8) begins to compete with the quenching of the Bi(^2D). The Bi(^2D) concentration then saturates and the BiF(A) state begins to scale linearly with [NF($a^1\Delta$)]. At high NF($a^1\Delta$) concentrations, a saturation of the BiF(A) yield could set in if a destructive reaction between NF($a^1\Delta$) and BiF(A) were to occur with a sufficiently high rate constant to compete with the radiative decay of the BiF(A) state. No evidence of such reaction was obtained, however, up to NF($a^1\Delta$) concentrations of $3 \times 10^{16}/cm^3$.

Under optimal $Bi(CH_3)_3$ loading conditions, the BiF(A) time profile is shorter than the NF($a^1\Delta$) time profile in the absence of $Bi(CH_3)_3$ by roughly a factor of two, as shown in Fig. 11. This result indicates that $Bi(CH_3)_3$ quenching of NF($a^1\Delta$) is also a significant factor. The NF($a^1\Delta$) data has been smooth to eliminate peak-to-peak noise as indicated by the error bar. The BiF(A-X) emission is quite intense and therefore noise free. The vertical scale for the BiF emission is substantially reduced in sensitivity relative to the NF data.

The typical per BiF(A, $v' = 0$) stimulated emission cross sections for the most favored transitions are approximately 10^{-16} cm^2 at 1200 K. At this temperature, roughly 35 % of the BiF(A) state concentration is in $v' = 0$; however, this figure increases with reduced temperature as does the cross section due to the combined effects on the rotational distribution and Doppler width. Therefore, with careful optimization, $10^{13}/cm^3$ concentrations of BiF(A) are capable of generating unsaturated gain coefficients that approach 10^{-3}/cm, adequate for large scale high energy laser devices, provided the concentration of BiF(X) is not excessive.

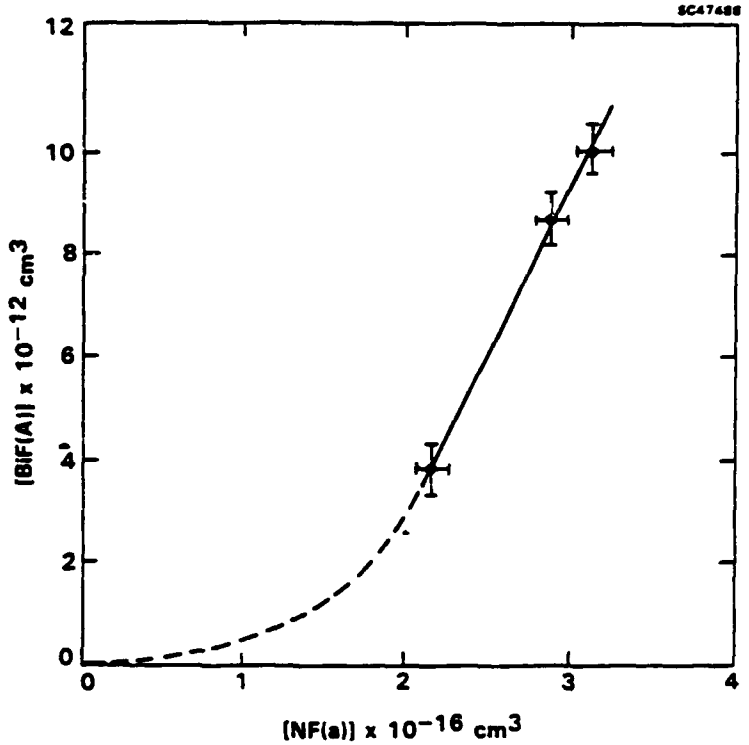

Fig. 10 Scaling of BiF(A) yield vs initial FN_3 concentration.

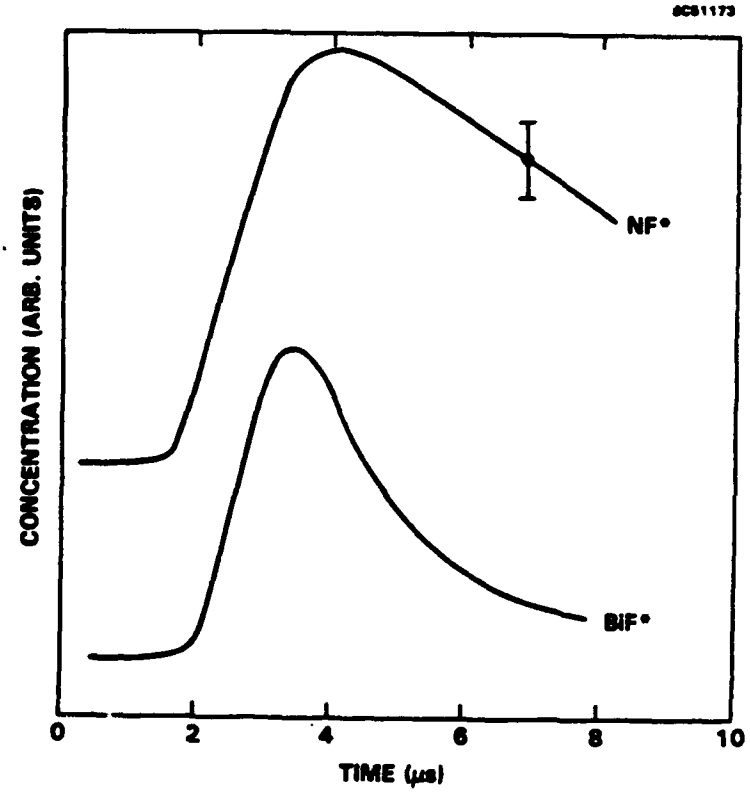

Fig. 11 Time profiles of $NF(a\,^1\Delta)$ in the absence of $Bi(CH_3)_3$ - upper curve and BiF(A) with optimal loading of $Bi(CH_3)_3$ - lower curve.

5.5 Population Inversion

To test for excess population of the BiF(X) ground state, the reactor used in the above studies was enclosed inside an optical cavity formed by a pair of concave dielectric mirrors. The mirrors were sealed to the reactor without use of intracavity windows by long, purged stainless steel bellows so that the optical axis of the resonator passed through 2.5 cm of the reacting flow. The mirror separation was set at 50 cm so that the c/2L spacing of the cavity modes was approximately 25 % of the Doppler width of the BiF(A-X) transitions to insure that a cavity mode was located near line center where the cross section is at a maximum. Mirrors were selected with constant R = 95 % reflectivity over the wavelength band of the BiF(A-X) transitions so that on the average, a photon would execute $1/(1-R^2) \sim 10$ roundtrips inside the cavity before escaping to an external detector. The effective path length through the active medium was therefore 50 cm. The OMA was used to collect on-axis radiation leaking from the cavity and to compare the spectrum of the cavity emissions to a direct chemiluminescence spectrum obtained without use of an optical cavity. The intensifier section of the OMA was gated to detect only the peak of the BiF(A) time profile in each case. The region of the $v' = 0$ to $v'' = 0$ transitions was then analyzed for signs of spectroscopic distortion due either to intracavity self-amplification or self-absorption. Band-to-band comparisons were not used because slight departures from vibrational equilibrium, which are possible due to the short duration of the experiment, would lead to erroneous results. Distortion of the shape of a single band, however, depends on the rotational distribution which is more rapidly thermalized. In the $v' = 0$ to $v'' = 0$ band, the cross section is peaked to the red of the bandhead at $J \sim 30$ (437 nm). Therefore, the presence of gain or loss in the cavity will distort the shape of the band as seen through the mirrors. Contrary to first intuition, the presence of gain initially increases the width of the band by enhancing the $J \sim 30$ radiation relative to the bandhead.

Within the signal-to-noise ratio of the experiment, which was 20 to 1 or better, no significant distortion of the band shape was observable, as shown in Figs. 12(a) and 12(b). An upper limit on the BiF(X) concentration was therefore established by assuming a trial value for [BiF(X)] and then calculating the absorption of $J \sim 30$ and bandhead radiation over a 50 cm path, assuming $[BiF(A)] = 10^{13}/cm^3$ and rotational-vibrational equilibrium at 1200 K. The cross sections were calculated from knowledge of the radiative rate[3] and the spectroscopic parameters[20] of the BiF(A-X) band system. The trial concentration of BiF(X) was then adjusted so that the differential absorption matched twice the signal-to-noise ratio of the experiment. By following this procedure, the concentration of BiF(X) was shown to be less than $4 \times 10^{13}/cm^3$. This result does not rule out an absolute inversion, but tends to suggest at least partial inversions on the $v' = 0$ to $v'' \geq 3$ transitions, assuming a near thermal vibrational distribution in the BiF(X) ground state.

More sensitive experiments have been conducted with mirrors of 99.9 % reflectivity in which the potential peak gains can actually exceed the cavity threshold. Saturated lasing is not expected in this case, however, because the peak gain lasts for only about 2 μs (Fig. 11) during which the photons can execute approximately 600 roundtrips. At a peak gain per roundtrip of $(3 \times 10^{-4}/cm)(5\ cm) \sim 0.15$ %, neglecting mirror losses, the initial spontaneous emission can only experience a net enhancement of order unity. Therefore, no significant laser output is expected, but spectroscopic distortion of the cavity output due to optical gain can be substantial. In these final experiments, the production of BiF(A) was also enhanced by using a KrF laser to partially photodissociate the $Bi(CH_3)_3$ with a variable lead in time relative to the peak of the NF(a) time profile. The best results were obtained when the KrF laser pulse was applied approximately 1 μs ahead of the peak NF(a) signal, resulting in a 50% enhancement of the peak BiF(A) concentration. The BiF(A) signal disappeared entirely, however, when the KrF laser was applied with the CO_2 laser beam blocked, confirming that NF(a) production by thermal dissociation of FN_3 was necessary to excitation of the metal fluoride. This result is not surprising since

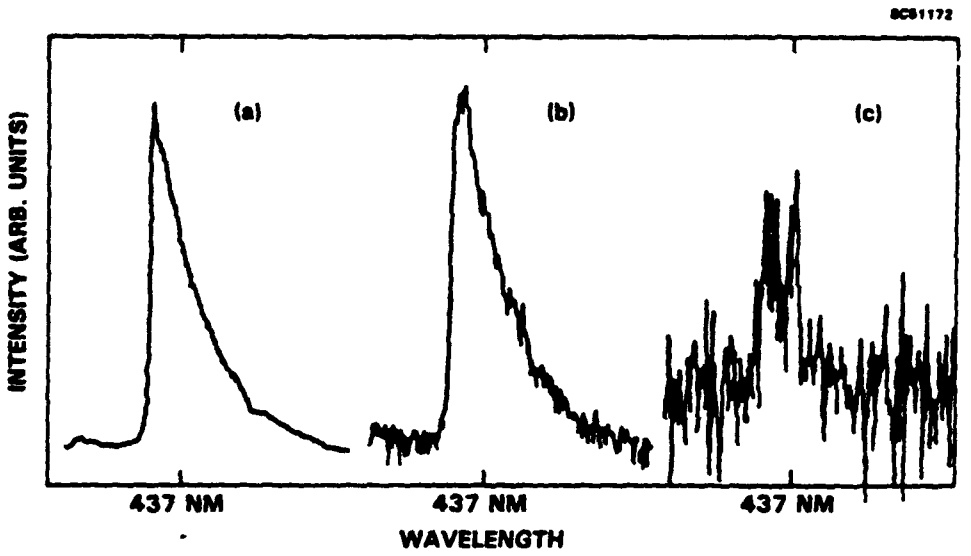

Fig. 12 Comparison of BiF(A-X, $v' = 0$ to $v'' = 0$) bands in the absence of a cavity (a) and with a cavity using mirrors of 99.5 % reflectivity (b) and 99.9 % reflectivity (c).

the KrF radiation is strongly absorbed[8,9] by $Bi(CH_3)_3$, but only very weakly by FN_3. Time profiles of $Bi(^2D)$ collected with and without use of the KrF and CO_2 lasers revealed that the KrF laser did yield a prompt source of $Bi(^2D)$ that was comparable to the $Bi(^2D)$ produced by reaction (9), which accounts for the enhanced BiF(A) production. The KrF laser, however, does not help to clear the BiF(X) ground state and since the photon lifetime in the high reflectance cavity is comparable to the radiative lifetime of BiF(A), the intracavity experiment constitutes a valid test for chemical removal of the BiF(X) ground state. The corresponding cavity emission data, shown in Fig. 12(c), is characterized by a lower signal-to-noise ratio because of the reduced transmission through the high reflectance mirrors. Nonetheless, a significant distortion of the $v' = 0$ to $v'' = 0$ band at 437 nm is evident, which is presumably the result of amplification, since it is a reproducible feature of the cavity emission spectrum and is not present in background scans taken with the CO_2 laser blocked. This result implies an absolute inversion of the BiF(A-X) transition. Work is currently proceeding to use a pulsed dye laser to charge the optical cavity with resonant photons so that amplification during the cavity ring down can be sensitively detected with a high signal-to-noise ratio. Details of this experiment will be reported in a subsequent publication.

6. CONCLUSIONS

The results we have obtained using the FN_3 source of $NF(a^1\Delta)$ to excite BiF(A) with $Bi(CH_3)_3$ as a starting material are basically compatible with Herbelin's findings in the same system driven by $NF(a^1\Delta)$ obtained from the $H + NF_2$ reaction, and support the conclusion that energy transfer from $NF(a^1\Delta)$ to BiF is a viable mechanism for the generation of a visible wavelength chemical laser. Further work will be required to develop the laser, however, in three key areas. Since the potential gains are small, larger gain lengths and gain times will be required for efficient power extraction. In a high energy system, it will also be desirable to replace the CO_2 laser heating mechanism with supersonic mixing between a preheated primary gas stream and secondary injection of FN_3 at 300 K. The nozzle design will be critical in several regards. First, due to the self-annihilation reaction, it will be necessary to accomplish mixing on the μs time scale to dissociate the FN_3 efficiently; second, careful optimization of temperature is required to tradeoff dissociation rate with gain cross section; and third, adiabatic expansion and the use of an inert diluent gas as a thermal buffer will have a strong

influence on the coupling between Mach number as influenced by reactive heat release and dissociation rate as influenced by changes in gas temperature due to pressure recovery. Finally, it will be desirable to replace the $Bi(CH_3)_3$ with superheated Bi vapor that consists primarily of Bi-atoms, to eliminate the kinetic bottleneck and by-product quenching reactions that are associated with use of the organometallic Bi donor.

7. ACKNOWLEDGEMENTS

This work was partially supported under a contract from the Air Force Weapons Laboratory and the Air Force Astronautics Laboratory.

8. REFERENCES

1. J.M. Herbelin and R.A. Klingberg, "Efficient Production of Electronically Excited BiF(A) via Collisions with $NF(a^1\Delta)$," International Journal of Chemical Kinetics, vol. 16, pp. 849-866, 1984.
2. D.J. Benard, B.K. Winker, T.A. Seder and R.H. Cohn, "Production of $NF(a^1\Delta)$ by Dissociation of Fluorine Azide," Journal of Physical Chemistry, vol. 93, pp. 4790-4796, 1989.
3. R.H. Heidner, H. Helvajian, J.S. Holloway, and J.B. Koffend, "BiF(A) Radiative Lifetimes and Rate Coefficients for V-T Transfer and Electronic Quenching," Technical Report 87-19, Aerospace Corporation, El Segundo, CA, 1987.
4. C.R. Quick and C. Wittig, "Time-Resolved HF Vibrational Fluoresence from the IR Photodissociation of SF_6/H_2 Mixtures," Chemical Physics Letters, Vol. 48, pp. 420-424, 1977.
5. B. Rosen, ***Selected Constants Relative to Diatomic Spectra***, Pergammon Press, New York, 1970.
6. R.J. Malins and D.W. Setser, "Rate Constants, Branching Ratios and Energy Disposal for NF(b,a,X) and HF(v) Formation from the $H + NF_2$ Reaction," Journal of Physical Chemistry, vol. 85, pp. 1342-1349, 1981.
7. P.H. Tennyson, A. Fontijn and M.A.A. Clyne, "Radiative Lifetimes of Metastable States of Free Radicals. I. $NF(b^1\Sigma)$," Chemical Physics, vol. 62, pp. 171-177, 1981.
8. K. Gholivand, G. Schatte and H. Willner, "Properties of Triazadienyl Fluoride, N_3F," Inorganic Chemistry, vol. 26, pp. 2137-2140, 1987.
9. J. Connor, P.J. Young and O.P. Strausz, "Flash Photolysis of Trimethylanitmony and Trimethylbismuth and the Quenching of Excited Antimony and Bismuth Atoms," Journal of the American Chemical Society, vol. 93, pp. 882-828, 1971.
10. M. Stanek, K. Musiol and S. Labuz, "Experimental Determination of Transition Probabilities in Bi I and Bi II," Acta Physics Polonica, vol. A59, pp. 239-245, 1981.
11. J.M. Herbelin and B. Koffend, Aerospace Corporation, El Segundo, CA, private communication.
12. Alfa Catalog, "Research Chemicals and Materials," pg. P-168, Morton Thiokol, Danvers, MA, 1986/87.
13. D.J. Benard and R.H. Cohn, "Model Studies of CBES Decomposition," Technical Report 87-071, Air Force Astronautics Laboratory, Edwards Air Force Base, CA, 1987.
14. J.F. Haller, "A Study of the Preparation, Structure, Properties, and Decomposition of Azine Fluoride and of Difluorodiazene," Ph.D. thesis, Cornell University, Ithaca, NY, 1942.
15. E. Quinones, J. Habdas and D.W. Setser, "Gas-Phase Chemistry of $NF(a^1\Delta)$: Quenching Rate Constants," Journal of Physical Chemistry, vol. 91, pp. 5155-5158, 1987.
16. H. Michels, United Technologies Research Laboratories, E. Hartford, CT, private communication.
17. D. Patel, A.T. Pritt, and D.J. Benard, "Photolysis of FN_3 at 193 nm," Journal of Physical Chemistry, vol. 90, pp. 1931-1934, 1986.

18. G.A. Sutton, D.G. Capelle and J.I. Steenfeld, "Near-Resonant Electronic Energy Transfer from NF($a^1\Delta$) to Bi," Journal of Chemical Physics, vol. 69, pp. 5140-5146, 1978.
19. D.W. Trainor, "Collisional Relaxation of Electronically Excited Bismuth: $6p^3(^2D^\circ_{3/2})$ and $6p^3(^2D^\circ_{5/2})$," Journal of Chemical Physics, vol. 66, pp. 3094-3099, 1977.
20. W.E. Jones and T.D. McLean, "The Electronic Spectrum of Bismuth Monofluoride: A Reinvestigation of the A-X System," Journal of Molecular Spectroscopy, vol. 90, pp. 481-506, 1981.